UPPSALA
UNIVERSITET

Digital Comprehensive Summaries of Uppsala Dissertations from the Faculty of Science and Technology 1929

Small Particles with Big Impact

Structural Studies of Viruses and Toxicological Studies of Nanodiamonds

ANNA MUNKE

ACTA
UNIVERSITATIS
UPSALIENSIS
UPPSALA
2020

ISSN 1651-6214
ISBN 978-91-513-0933-0
urn:nbn:se:uu:diva-406705

Dissertation presented at Uppsala University to be publicly examined in Room B8, Biomedicinskt centrum, Husargatan 3, Uppsala, Wednesday, 27 May 2020 at 09:15 for the degree of Doctor of Philosophy. The examination will be conducted in English. Faculty examiner: Professor Nicola Stonehouse (University of Leeds).

Abstract

Munke, A. 2020. Small Particles with Big Impact. Structural Studies of Viruses and Toxicological Studies of Nanodiamonds. *Digital Comprehensive Summaries of Uppsala Dissertations from the Faculty of Science and Technology* 1929. 93 pp. Uppsala: Acta Universitatis Upsaliensis. ISBN 978-91-513-0933-0.

Nanoparticles (NPs) can be found everywhere and their existence has both beneficial and harmful consequences for the environment and living beings. The investigations on which this thesis is based upon have contributed to an increased understanding of some of these particles and to the development of a method that could be used to study their structure.

Three different NPs have been studied by different means. In the first study, I describe how single-particle cryo-electron microscopy was used to determine the atomic structure of an algal virus; *Chaetoceros tenuissimus* RNA virus type II. This virus is taxonomically classified in the order *Picornavirales*, which includes viruses that infect a wide range of organisms, including humans, plants and insects. By comparing the algal virus structure to structures of related viruses in the order, we could identify a number of traits that were likely acquired or lost among these viruses during the course of evolution. In the second study, rice dwarf virus was utilised as a test sample to develop a new structural biology method, single-particle coherent diffractive imaging (CDI). The method aims to study macromolecules in a single-particle fashion at room temperature with the help of an X-ray free-electron laser, thus enabling studies of fast dynamics without the need to crystallize or freeze the sample. The study was the first of several within a large international collaboration and the first single-particle CDI experiment reported using femtosecond hard X-ray pulses. Despite several advances by the team, many challenges remain for the method to reach its full potential. In the third study, I describe *in vitro* and *in vivo* toxicological studies of detonation nanodiamonds (DNDs). I could demonstrate that some DNDs are toxic and that the toxicity is dependent both on the core and surface of the particles. DNDs are suggested for numerous different biomedical applications that alternately utilise their toxic properties or require biocompatibility. The results presented show that these contrasting properties can be exhibited by similar DNDs and that thorough characterisation and close control of the manufacturing process is essential for biomedical applications.

This thesis explores how studies of some of nature's nanoparticles - viruses - can lead to biological insight, how virus NPs can play a role in developing new technologies that may enable an even deeper understanding and explores issues that need to be considered for NPs to reach their potential in biomedical applications.

Keywords: Chaetenuissarnavirus II, cryo-EM, CtenRNAV-II, Escherichia coli, Danio rerio, flash X-ray imaging, Marnaviridae, single-particle analysis, single-particle imaging, Sogarnavirus, virus evolution, virus structure, XFEL, zebrafish embryo

Anna Munke, Department of Cell and Molecular Biology, Molecular biophysics, Box 596, Uppsala University, SE-75124 Uppsala, Sweden.

ISSN 1651-6214
ISBN 978-91-513-0933-0
urn:nbn:se:uu:diva-406705 (http://urn.kb.se/resolve?urn=urn:nbn:se:uu:diva-406705)

Till Astrid

List of papers

This thesis is based on the following papers, which are referred to in the text by their Roman numerals.

I **Munke, A.**, Kimura, K., Tomaru, Y., and Okamoto, K. (2020) Capsid structure of a marine algal virus of the order *Picornavirales*. *Journal of Virology*, 94(9):e01855-19

II **Munke, A.**, Andreasson, J., Aquila, A., Awel, S., Ayyer, K., Barty, A., Bean, R.J., Berntsen, P., Bielecki, J., Boutet, S., Bucher, M., Chapman, H.N., Daurer, B.J., DeMirci, H., Elser, V., Fromme, P., Hajdu, J., Hantke, M.F., Higashiura, A., Hogue, B.G., Hosseinizadeh, A., Kim, Y., Kirian, R.A., Kumar, H., Lan, T.Y., Larsson, D.S.D., Liu, H., Loh, N.D., Maia, F.R.N.C., Mancuso, A.P., Mühlig, K., Nakagawa, A., Nam, D., Nelson, G., Nettelblad, C., Okamoto, K., Ourmazd, A., Rose, M., van der Schot, G., Schwander, P., Seibert, M.M., Sellberg, J.A., Sierra, R.G., Song, C., Svenda, M., N. Timneanu, Vartanyants, I.A., Westphal, D., Wiedorn, M.O., Williams, G.J., Xavier, P.L., Yoon, C.H. and Zook J. (2016) Coherent diffraction of single Rice Dwarf Virus particles using hard X-rays at the Linac Coherent Light Source. *Scientific Data*, 3:160064

III **Munke, A.**, Fang, H., Sahlberg, M. and Seibert, M.M., Detonation nanodiamond toxicity is core and surface dependent. *Manuscript*

List of additional publications

Bielecki, J.*, Hantke, M.F.*, Daurer, B.J.*, *et al*. (2019) Electrospray sample injection for single-particle imaging with X-ray lasers. *Science Advances*, 5:eaav8801

Wiedorn, M.O., *et al.* (2018) Megahertz serial crystallography, *Nature Communications,* 9:4025

Kurta, R.P., *et al.* (2017) Correlations in scattered x-ray laser pulses reveal nanoscale structural features of viruses, *Physical Review Letters*, 119:158102

Reddy, H.K.N., *et al.* (2017) Coherent Soft X-ray Diffraction Imaging of Coliphage PR772 at the Linac Coherent Light Source, *Scientific Data,* 4:170079

Munke, A., *et al*. (2017) Phage display and kinetic selection of antibodies that specifically inhibit amyloid self-replication, *Proceedings of the National Academy of Sciences,* 114:6444-9

Munke, A. (2016) Structural studies of small viruses using an X-ray Free Electron Laser, Licentiate thesis

* Authors contributed equally to the work.

Contents

1. Introduction 15
1.1. Outline of the thesis 18

2. Background on nanoparticles 19
2.1. Viruses 19
2.1.1. The virus life cycle 20
2.1.2. Classification 21
2.1.3. Host cells and organisms 23
2.1.4. Virus evolution and origin 23
2.1.5. Friend or foe? 24
2.1.6. Structural virology 25
2.2. Engineered nanoparticles 29
2.2.1. Nanotoxicity 29
2.2.2. Applications 31

3. Single-particle cryo-EM of CtenRNAV-II 33
3.1. CtenRNAV-II 34
3.2. Single-particle cryo-EM 36
3.2.1. Microscopes and image formation 37
3.2.2. Sample preparation and data collection 39
3.2.3. Single-particle analysis 39
3.3. Present investigation – **Paper I** 40
3.3.1. Aim 41
3.3.2. Methodology 41
3.3.3. Results 42
3.3.4. Discussion 45

4. Single-particle coherent diffractive imaging of rice dwarf virus 47
4.1. Rice dwarf virus 48
4.2. Single-particle imaging with an X-ray laser 49
4.2.1. X-ray free-electron lasers 49
4.2.2. Diffraction before destruction 50
4.2.3. Single-particle coherent diffractive imaging 51

4.3. Present investigation – **Paper II** 53
4.3.1. Aim 54
4.3.2. Methodology 55
4.3.3. Results 56
4.3.4. Discussion 57

5. Toxicity of detonation nanodiamonds 59
5.1. Detonation nanodiamonds 60
5.2. Toxicity 60
5.3. Present investigation – **Paper III** 61
5.3.1. Aim 61
5.3.2. Methodology 62
5.3.3. Results 63
5.3.4. Discussion 63

6. Concluding remarks and future perspectives 67

Author's contribution 71

Populärvetenskaplig sammanfattning 73

Acknowledgements 77

References 79

Abbreviations

CCD	charge-coupled device
CDI	coherent diffractive imaging
CFU	colony-forming unit
CMOS	complementary metal-oxide semiconductor
cryo-EM	cryo-electron microscopy
CSPAD	Cornell–SLAC Pixel Array Detector
CtenRNAV-II	*Chaetoceros tenuissimus* RNA virus type II
CTF	contrast transfer function
DLS	dynamic light scattering
DMA	differential mobility analysis
DNA	deoxyribonucleic acid
DND	detonation nanodiamond
dsDNA	double-stranded deoxyribonucleic acid
dsDNA-RT	double-stranded deoxyribonucleic acid-reverse transcriptase
dsRNA	double-stranded ribonucleic acid
E.coli	*Escherichia coli*
EM	electron microscopy
FEL	free-electron laser
FET	fish embryo toxicity
fs	femtosecond
FSC	Fourier shell correlation
FT	Fourier transform
FT-IR	Fourier transform infrared spectroscopy
GDVN	gas dynamic virtual nozzle
HPHT	high-pressure high-temperature
ICTV	International Committee on Taxonomy of Viruses
keV	kiloelectron-volts
LCLS	Linac Coherent Light Source
mRNA	messenger ribonucleic acid
ND	nanodiamond
NP	nanoparticle
NTA	nanoparticle tracking analysis
PDB	Protein Data Bank
RDV	rice dwarf virus
RNA	ribonucleic acid
SFX	serial femtosecond crystallography

SPA	single-particle analysis
SPI	single-particle imaging
ssDNA	single-stranded deoxyribonucleic acid
ssRNA	single-stranded ribonucleic acid
ssRNA-RT	single-stranded ribonucleic acid-reverse transcriptase
TEM	transmission electron microscopy
TDS	thermal desorption (mass) spectrometry
TNT	trinitrotoluene
XFEL	X-ray free-electron laser

1. Introduction

A ‘particle’ can be defined as “an extremely small piece of matter” [1] and classified based on size as *subatomic*, which are particles smaller than atoms; *microscopic*, which are particles of sizes ranging from atoms to molecules and includes objects that can only be observed using a magnifying instrument; and *macroscopic* particles, which include particles that are visible with the naked eye. *Figure 1.1* illustrates a scale ranging from subatomic particles (such as the electron), to microscopic particles (such as the nanodiamond), to macroscopic particles (such as the zebrafish embryo). Within the microscopic scale resides another scale, the nanoscopic scale (or nanoscale) that covers the range 1-100 nm, and whose particles are typically called nanoparticles (NP). The simplest definition of a nanoparticle is a microscopic particle with at least one dimension less than 100 nm. However, this topic is highly debated within the nanotechnology field and between governments, industry and standards organisations [2].

NPs are all around us and have great impact on our everyday life. Good and bad. They can be classified into one of two categories: natural or anthropogenic (man-made). Natural NPs include for example viruses, ocean spray, and volcanic ash, and have for a long time contributed in shaping the world in which we live in and will continue to do so. Anthropogenic NPs can in turn be divided into incidental, which are those that have no predetermined size and undefined chemistry and are by-products of human activities, such as operating diesel engines and mining, and those that are engineered and typically have more defined characteristics, which include for example nanodiamonds (NDs) and silver nanoparticles. Anthropogenic NPs have a relatively recent history compared to natural NPs. The effect of incidental NPs on our lives increased as a consequence of the industrial revolution in the 18th century and the majority of engineered NPs were introduced later towards the end of the 20th century. Engineered particles can be found in many consumer products, such as hairstyling tools, lotions, clothing, cosmetics and car lubricant, and their use is constantly increasing [3]–[6].

Nanoparticles are often put in a negative limelight. Viruses for example, are often described as pathogens that cause disease and suffering for humans and domesticated plants and animals. As a result, those viruses affecting human health and economy have historically been extensively studied. However, viruses are also being described with a positive attitude: as “major players in the global ecosystem” [7], “one of the most dominant drivers of

evolutionary change across mammalian and human proteomes" [8], for having "a critical role in maintaining the proper function of a healthy gut microbiome" [9], and a "mutualistic relationships with their host" [10]. In addition, there are many possible benefits of utilizing viruses for medical and technological applications, such as for drug delivery [11], phage therapy [12], and phage display [13]. Anthropogenic NPs are likewise often described to have a negative impact on humans and the environment, especially in the public arena (e.g. microplastics [14], [15] and pollution). However, engineered NPs have a range of attractive properties that are being explored for several applications in diverse industrial sectors, including medicine, environment, renewable energies, construction, and agriculture [16]. These opposite aspects of NPs are further addressed throughout this thesis.

Another concept in the context of NPs is aerosol, which is a particle suspension in a gas or gas mixture. Likewise, aerosols can either be natural or anthropogenic. On one hand, aerosols formed in combustion or when sneezing greatly affect our climate and health. On the other hand, aerosols are utilized in several technological applications, such as in medical applications (treating persons with respiratory illness) and in the natural and technology sciences where aerosols have been developed e.g. for mass spectrometry and, as will be further described in *Chapter 4*, to introduce particles into an X-ray beam.

Because of their small size, specific instruments are required to visualize and characterize NPs. A conventional light microscope is not sufficient to characterise the structure of NPs as they have a size below the wavelength of visible light. Instead, different types of electron microscopy (EM) and X-ray techniques are required (Fig. 1.1). Basic characteristics such as count and size can be determined using for example optical sizing techniques, such as dynamic light scattering (DLS) and nanoparticle tracking analysis (NTA), or a differential mobility analyser (DMA). All of these techniques are further described in the following chapters.

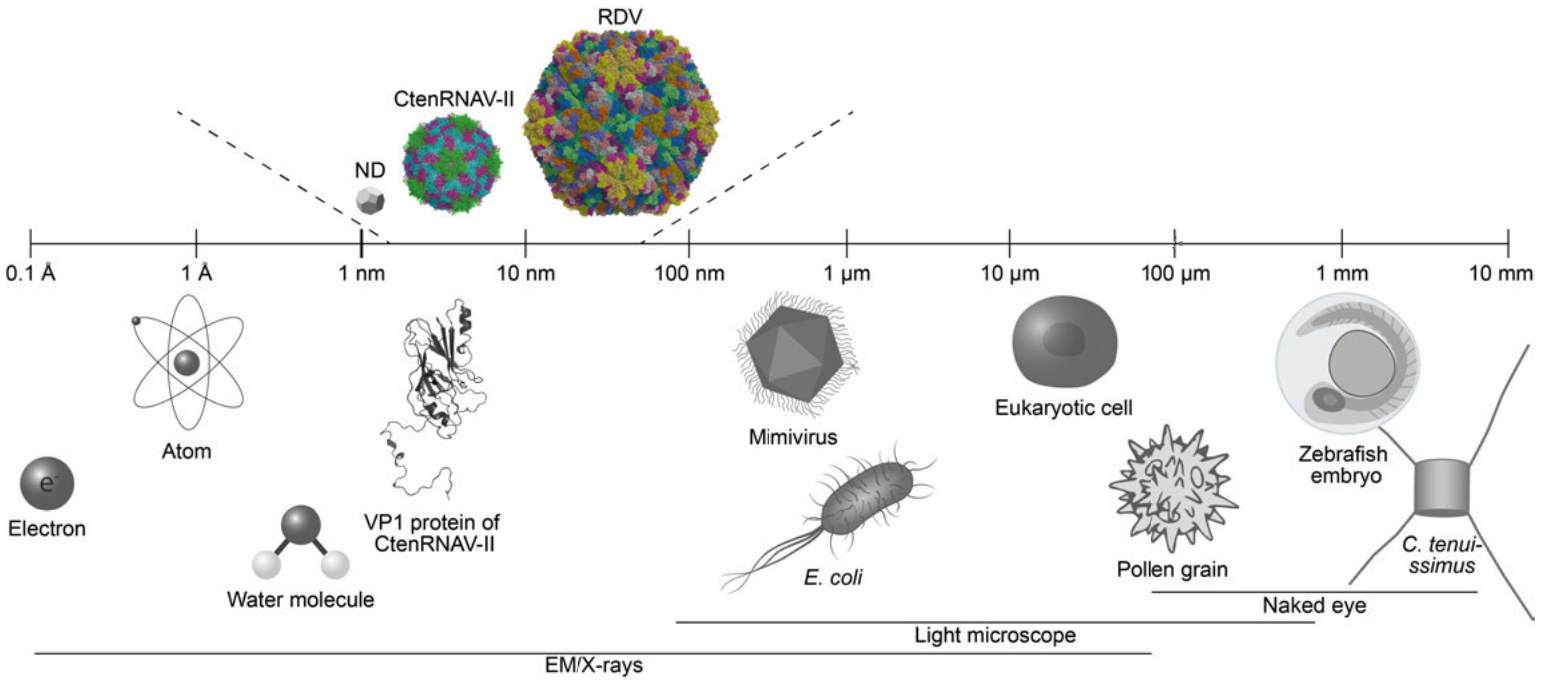

Figure 1.1. Examples of particles and other biological elements on a logarithmic scale. The smallest particle on the scale is the electron, which is classified as a subatomic particle. The microscopic scale ranges from the atom to eukaryotic cell, whereas the pollen grain and beyond reside on the macroscopic scale. Present investigations described in this thesis have studied particles residing on the nanoscale (1-100 nm), and consists of the nanodiamond (ND) and the viruses *Chaetoceros tenuissimus* RNA virus type II (CtenRNAV-II) and rice dwarf virus (RDV) (illustrated in the upper half of the figure). The figure also includes other particles and biological samples that have played important roles in the investigations. These include the electron, essential for the structural studies; *Escherichia coli* and zebrafish embryo, used as model organisms in toxicity experiments; and *Chaetoceros tenuissimus*, the diatom that is infected by CtenRNAV-II.

1.1. Outline of the thesis

In the investigations on which this thesis is based upon, particles ranging from subatomic to macroscopic have played important roles (Fig. 1.1). Viruses and engineered NPs are however the main subjects of this thesis, for which a background is given in *Chapter 2*. The following chapters (*Chapter 3-5*) describe the specific NPs studied, the theoretical background to methods used, and outlines of present investigations. *Chapter 6* summarises the accomplished achievements and elaborate on future prospects. All chapters address the dual impact that nanoparticles can have.

The thesis is based on three papers. In **Paper I** and **II** (*Chapter 3* and *4*, respectively), structural work was carried out on viruses, namely *Chaetoceros tenuissimus* RNA virus type II (CtenRNAV-II) and rice dwarf virus (RDV). In **Paper I**, a comparably well-established method, cryo-electron microscopy (cryo-EM), was used to determine the atomic structure of CtenRNAV-II, whereas the work described in **Paper II** contributed to the development of a new method, namely single-particle coherent diffractive imaging (single-particle CDI), for which RDV was utilized as a model sample. **Paper III** (Chapter 5) instead focused on engineered NPs, specifically detonation nanodiamonds (DNDs), which were subjected to toxicity testing on *Escherichia coli* (*E. coli*) and zebrafish embryos.

2. Background on nanoparticles

2.1. Viruses

A virus is an infectious agent that can only replicate inside a living cell. The common building blocks of a virus are the genome and outer shell of proteins, the capsid. Viruses are however genetically and structurally extremely diverse, which is further described throughout this chapter.

As for many important discoveries, the discovery of viruses can be credited to several people. Dimitri Ivanofsky and Martinus Beijerinck were two of several scientists that played immense roles in elucidating the novel infectious agent that caused the tobacco mosaic disease in the late 19th century. Ivanofsky demonstrated that crushed leaf extracts from infected tobacco plants remained infectious even after filtration to remove bacteria [17], whereas Beijerinck demonstrated that the agent could reproduce in living tissue [18], and thereby disproving Ivanofsky's claim that the disease causing agent was a toxin. Beijerinck called it a *contagium vivum fluidum* [18], or a contagious living liquid, and it took another couple of years to show that the infectious agent was particles.

The circumstances under which viruses were discovered shaped for a long time the definition of a virus and how viruses were perceived. Until the beginning of the 21st century, viruses were described as small and simple parasitic particles that do not serve any essential function for their host [10], [19]. One of the discoveries that contributed to changing this view was the finding of the first so-called giant virus, the Mimivirus, in 2003 [19]. Since then, several other giant viruses have been discovered, some which are even larger than the Mimivirus [20]. Not only have these giant viruses changed the view of viruses being something small and simple, they have also initiated a debate about the evolution of viruses and cells [21]–[23]. The tobacco mosaic virus was discovered as a result of elucidating the cause of a disease, and that was how all viruses were discovered during that time. As a consequence, viruses are well known for being pathogenic and have historically been studied mainly due to public health and economic reasons. However, most viruses probably coexist peacefully with their host [24] and the numbers of studies that describe the beneficial aspects of viruses are constantly increasing [7]–[10].

Regardless of how viruses are defined and from where they originate, it is evident that they play significant beneficial roles on Earth, for example as

key components in evolution [25]–[28] and as influencers of biogeochemical and ecological processes [7], [29]. Wanik and Turner even describe viruses as "the most successful inhabitants of the biosphere", a statement that is based on several lines of evidence, including the fact that viruses are the most abundant biological entities (10^{31} viruses on Earth [30]) that probably occupy all organisms and thus all sorts of environments (deserts, hot springs, Antarctica). Most importantly, viruses are successful due to their ability to adapt to environmental changes [31].

2.1.1. The virus life cycle

The virus life cycle consists of a number of steps that a virus undergoes to infect an organism. The exact mechanisms and events taking place during the life cycle differs greatly between viruses, but the general principles can be explained in five steps. *Figure 2.1* illustrates the five steps of a lytic cycle, however some viruses can also have a lysogenic cycle, in which their genome stays within the host and transmits to daughter cells upon cell division. The first step of the lytic cycle is the *attachment* to the cell. The capsids of different viruses have evolved to recognize only specific cell types. Next, the cell is *penetrated* by the virus – either by injecting the genome alone (common for prokaryotic viruses), or by internalization of the entire virion (as in Fig. 2.1). In the latter case, the capsid has to disassemble inside the cell to release its genome content, which for example can be initiated by a pH drop. Plant viruses (such as RDV in **Paper II**) are unique in that they require a vector organism, e.g. insect, to mechanically penetrate the robust cell wall. In the *biosynthesis* step the cell is hijacked to produce new viral components, such as capsid proteins, genome, and enzymes. The exact processes behind this differ between viruses, which is further described in *Section 2.1.2*. The new viral components are then *assembled* into new virions, which take place either by self-assembly or by assistance of other proteins. Finally, the cell lyses and *releases* the newly synthesized virus particles that can infect other cells.

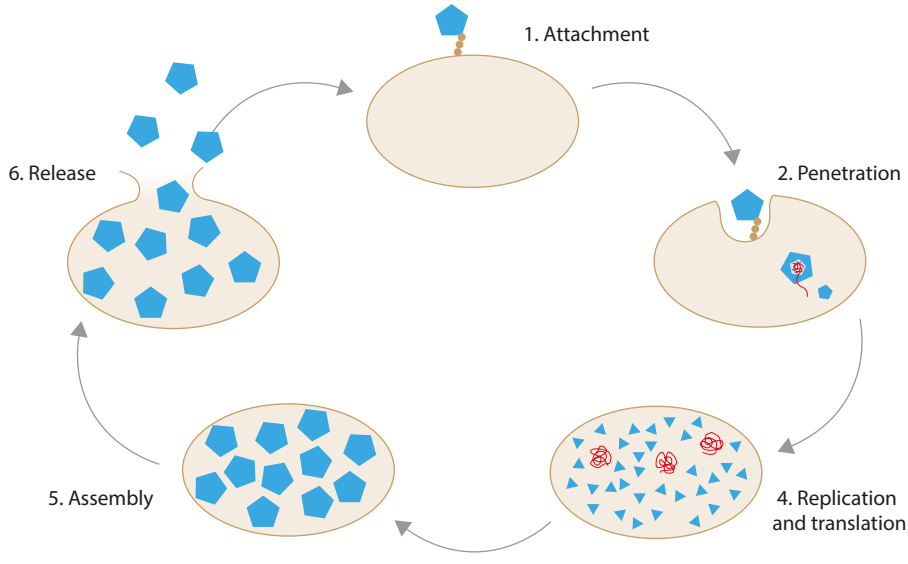

Figure 2.1. A general view of the lytic life cycle of a virus. The life cycle can be explained in five steps: 1. Attachment of the virus to the host; 2. Penetration, where the genome (red) enters the host; 3. Biosynthesis of viral components, e.g. capsid proteins (blue) and genome (red); 4. New virus particles are assembled; and 5. The cell lyses and releases the virus particles, which can infect other cells.

2.1.2. Classification

Viruses can be classified based on different characteristics, commonly according to morphology, nucleic acid type, replication strategy, and host organism. In addition, an approach of structure-based classification has been proposed to identify distant relationships between viruses [32], [33], a topic further described in *Section 2.1.6*.

The Baltimore classification system [34], one of the most widely used systems, organises viruses into seven groups based on their type of genome and replication-expression strategy (Fig. 2.2). In Group I, III and V, mRNA (defined as a positive (+) strand) can be produced directly by either using the host cell's DNA-dependent RNA polymerase (Group I) or an RNA-dependent RNA polymerase encoded by the virus (Group III and V). Viruses in Group II first have to convert their ssDNA to dsDNA. The (+)ssRNA in Group IV viruses can either be used directly to make proteins or be copied into (-)ssRNA. Group VI and VII viruses instead encode a reverse transcriptase that is used to produce DNA from an RNA strand, which in turn is used to make the mRNA. The viruses studied in **Paper I** and **II** are of (+)ssRNA (CtenRNAV-II) and dsRNA (RDV) type.

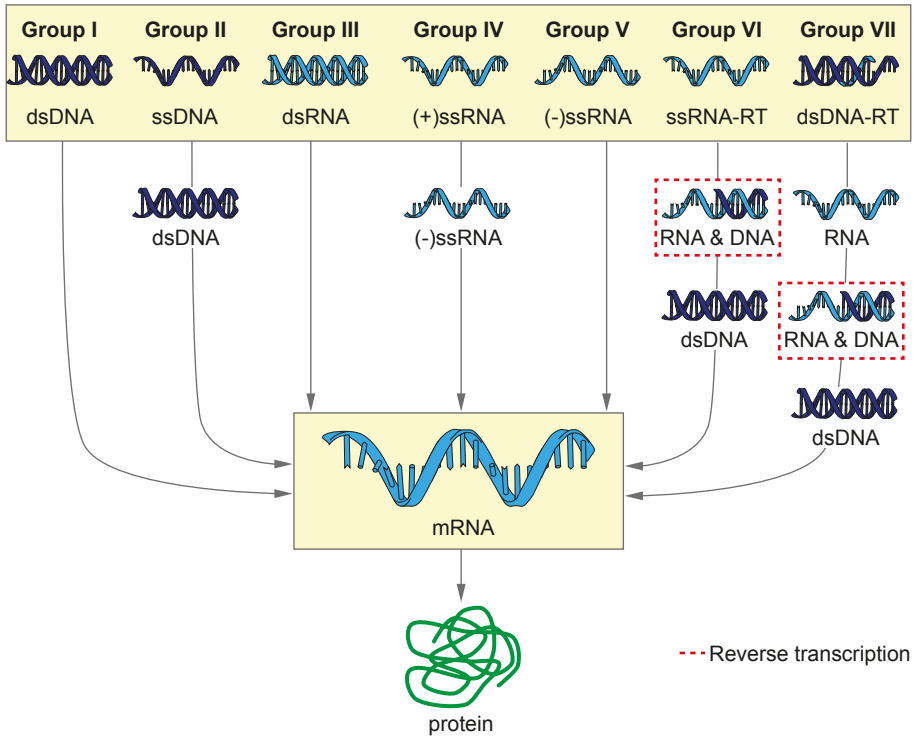

Figure 2.2. The Baltimore classification system. The classification scheme is based on the type of genome and replication strategy. The virus protein synthesis is dependent on the translational machinery of the cell, which requires mRNA for protein synthesis. The arrows show the different pathways for mRNA synthesis that are used by viruses from the different groups.

Viruses from the different Baltimore classes are unevenly distributed between prokaryotes and eukaryotes. In bacteria and archaea, the majority of viruses are of DNA types, in particular dsDNA, while in eukaryotes the majority are of RNA type, in particular (+)ssRNA. The cause of this uneven distribution is however unknown [35].

The International Committee on Taxonomy of Viruses (ICTV) conducts the formal taxonomical classification, and takes both genetic and biological characteristics into account when grouping [36]. *Table 2.1* lists the current taxonomic ranks.

Table 2.1. The current ranks in virus taxonomy and their respective specific suffix. The taxon name of the viruses (CtenRNAV-II and RDV) studied in **Paper I** and **II** are also listed.

Taxa	Suffix	Paper I	Paper II
Realm	*-viria*	*Riboviria*	*Riboviria*
Subrealm	*-vira*		
Kingdom	*-virae*		
Subkingdom	*-virites*		
Phylum	*-viricota*		
Subphylum	*-viricotina*		
Class	*-viricetes*		
Subclass	*-viricetidae*		
Order	*-virales*	*Picornavirales*	
Suborder	*-virinae*		
Family	*-viridae*	*Marnaviridae*	*Reoviridae*
Subfamily	*-virinae*		
Genus	*-virus*	*Sogarnavirus*	*Phytoreovirus*
Subgenus	*-virus*		
Species		*Chaetenuissarnavirus II*	*Rice dwarf virus*

The current ICTV taxonomy release (2018b) includes 1 realm, 1 phylum, 2 subphyla, 6 classes, 14 orders, 7 suborders, 151 families, 79 subfamilies, 1,022 genera, 59 subgenera and 5,561 species. Classification of viruses must include species and genus, whereas higher-level taxa are not mandatory. Viral families belonging to the same order have likely diverged from a common ancestral virus [37].

2.1.3. Host cells and organisms

Viruses can also be grouped based on the kind of cell they infect, namely eukaryotic, prokaryotic and archaeal. Eukaryotic viruses are further divided into animal viruses (which in turn can be either vertebrate or invertebrate viruses), fungal viruses, plant viruses and protist viruses. A particular virus can only infect certain species of hosts and only certain cells within that host. This selectivity is a result of the structural and functional adaptations that a virus has derived during the course of evolution. Animal and plant viruses are among the most well studied viruses due to their biomedical and economical importance. Prokaryotic viruses, or bacteriophages as they are called, are another group of viruses that have been extensively studied due to their ease of handling. Viruses probably infect all living organisms.

2.1.4. Virus evolution and origin

Studying virus evolution is important both for understanding the fundamental processes in virus evolution (which is intertwined with their hosts evolution), but also for understanding newly emerging pathogens (epidemiology).

The same processes that are responsible for the cellular evolution, such as mutations, natural selection and recombination, also apply for viruses. Cells are however monophyletic, i.e. they have one universal common ancestor and phylogenetic trees can be constructed by comparing gene regions (e.g. the 16S rRNA of the small ribosome subunit) that are common in all living organisms. No such gene exists among all viruses, suggesting that viruses are polyphyletic and have evolved on several independent occasions, an assumption also supported by studies on the folds of capsid proteins [23], [38], a topic further described in S*ection 2.1.6*.

Because of their short generation times, large population sizes and high mutation rates, viruses can evolve rapidly and it is therefore a difficult task to determine how and when viruses first evolved. Historically, two main theories have been discussed regarding the origin of viruses, namely the escaped gene hypothesis and the virus-first hypothesis. As the names suggest, these theories propose either that genes escaped from cells and acquired a protein coat and the ability to self-replicate, or that viruses antedate cellular life and are descendants of replicating elements from an RNA world [39, Ch. 11]. With the discovery of giant viruses, a third old hypothesis was revisited, the reduction hypothesis, which also led to a debate about the definition of viruses, whether or not they are alive and constitute a fourth domain of life [20], [22], [40]–[42]. While the reduction hypothesis states that viruses originated from small cells that lost their autonomy and transitioned into obligate intracellular parasites [20], [39, Ch. 11], others have suggested an expansion model for the evolution of giant viruses where smaller ancestral viruses through gene duplications and horizontal gene transfer gave rise to the giant viruses of today [42]. All of these theories have arguments for and against, and different kinds of viruses can be more easily explained by some theories, and thus it is possible that some viruses evolved before cells appeared on earth, while others appeared more recently [39, Ch. 11]. Yet another and more recent theory on the origin of viruses exist, a chimeric scenario, in which capsid-less genetic elements emerged before the first cellular lives (as in the virus-first hypothesis), which in a later stage captured capsid protein genes from primitive cells. As a result of the continued evolution into modern cells, new viruses emerged [23]. The theory is based on the revelation that the capsid proteins are derived from cellular proteins [38], a topic further touched upon in *Section 2.1.6*. Regardless of origin, viruses have for sure played an immense part in cellular evolution [43], [44].

2.1.5. Friend or foe?

The word “virus” is derived from Latin “poison”, and that is often how viruses are perceived. This is understandable considering the extensive disease and suffering for humans and domesticated plants and animals that viruses cause. However, the beneficial impact of viruses on other organisms is sub-

stantial and there are several examples of why viruses deserve more appreciation. Viruses can affect cellular life on many levels – from genome composition to ecosystem. Humans might not have existed on this planet unless long ago our ancient ancestor had undergone retrovirus infections. The mammalian placenta contains a retroviral gene that encodes a protein crucial for the ability to transfer nutrients and gases from the maternal blood. Moreover, the protein might even help the mammal mother not to reject their babies from the placenta [28]. The importance of the microbiome for human health has been heavily studied the last two decades, but the possible contribution of viruses is less explored [45]. However, the few studies conducted suggest that animals and phages that adhere to their mucosal surfaces coexist in a beneficial relationship [46] and that a healthy gut phagome exists [9]. In addition, there are several other examples of virus-host mutualism in a range of hosts [10], [47]. For example, viruses improve draught and cold tolerance in plants [48], are required for developing wings on aphids [49], and some viruses can suppress other more severe virus infections in humans [10], such as HIV [50]. A last example of beneficial impacts of viruses is their importance for maintaining functional ecosystems. Microorganisms (primarily prokaryotes) represent more than 90% of the oceans' biomass. However, viruses are the most abundant biological entity and are estimated to kill about 20% of the microorganism biomass every day [7]. This, in turn, affects several biogeochemical and ecological processes such as nutrient cycling, climate, and microorganism diversity and distribution [7], [29], [51].

Another aspect is the many viral-derived applications that are either in use or under development [52]. Despite their role in causing disease, viruses have been investigated also for treating disease, so-called virotherapy, which includes gene therapy [53], cancer therapy using oncolytic viruses [54], and phage therapy [55]. While the first two therapeutic strategies have undergone several clinical trials [53], [54], phage therapy have been less evaluated (at least in the Western countries) [52] with a limited number of clinical trials completed in Europe and US until now [55], [56]. In addition to the medical applications, viruses have proved themselves useful in molecular biology, with applications including for example phage display and a source of enzymes (e.g. reverse transcriptase from retroviruses and RNA polymerases from phages) and gene vectors for protein production.

2.1.6. Structural virology

Virus shapes, symmetry and folds

Viruses display a wide diversity of shapes, where spherical (or icosahedral) and helical are the two most extensively described in literature. There are however a large number of other varieties with more complex morphology, including for example the T4 bacteriophage that has a head and a tail. Unusual and complex virus shapes are especially found among archaea viruses. The greatest morphological diversity has been observed among viruses in-

fecting thermophilic archaeal organisms, and as a consequence it has been proposed that a wider diversity might have existed during the earlier steps of cellular evolution [57].

Virus capsids are built up by a number of identical protein subunits, which is justified by the requirement of genetic economy as it enables viruses to enclose their genomes in small compartments. As a consequence, virus particles are usually highly symmetric. Many viruses, including the ones studied in this thesis, have capsids with icosahedral symmetry. An icosahedron is composed of 60 subunits having five-, three- and twofold symmetry axes. One-sixtieth of an icosahedron is therefore called the icosahedral asymmetric unit, as it can make up the complete structure when all the different rotations are applied [39, Ch. 3]. However, spherical viruses can be composed of more than 60 identical subunits, and it was described by Caspar and Klug [58] that also these viruses can conform to icosahedrally symmetric organization by allowing small distortions from the strict equivalence. This is achieved by dividing the subunits into smaller pieces or triangles. The number of triangles, and thus the complexity of the capsid, in the subunit is defined by the triangulation (T) number, which is defined by the equation $T=h^2+hk+k^2$, where *h* and *k* are 0 or positive integers. The equation can be explained as follows: An icosahedron consists of 20 triangular faces (red triangles in Fig. 2.3). The unfolded faces are mapped onto a two-dimensional hexagonal lattice that consists of hexagons (light blue in Fig. 2.3), except at each vertex of the triangular faces that instead has a pentagon (dark blue in Fig. 2.3) that curves the hexagonal matrix into a sphere (Fig. 2.3B). The values of *h* and *k* are obtained by taking *h* steps from one pentagon in a straight line toward the next pentagon, and *k* is the number of steps shifted to the side to reach the next pentagon [39, Ch. 3], [58] (Fig. 2.3C). Several exceptions exist, for example CtenRNAV-II in **Paper I** that has a pseudo-T=3 capsid, which is organized in a T=3 lattice with different capsid proteins in the subunit in contrast to T=3 viruses that have the same protein at all three positions.

There is likely a defined number of different capsid protein folds existing in the virosphere [33]. Both experimental and computational investigations suggest that these folds can be used to organize viruses into linages [33], [59], which in turn can aid the current classification system by ICTV [32], [33], and provide insights about virus origin and evolution [23]. The members within a specific linage can differ both in genome type, and which host they infect, where the latter indicates that viruses predate the separation of the three cellular domains of life [60], [61]. Capsid proteins are presumably derived from cellular proteins (as described in *Section 2.1.4*), and the existence of a limited number of protein folds likely represents the number of independent occasions on which the capsids have evolved [23], [38].

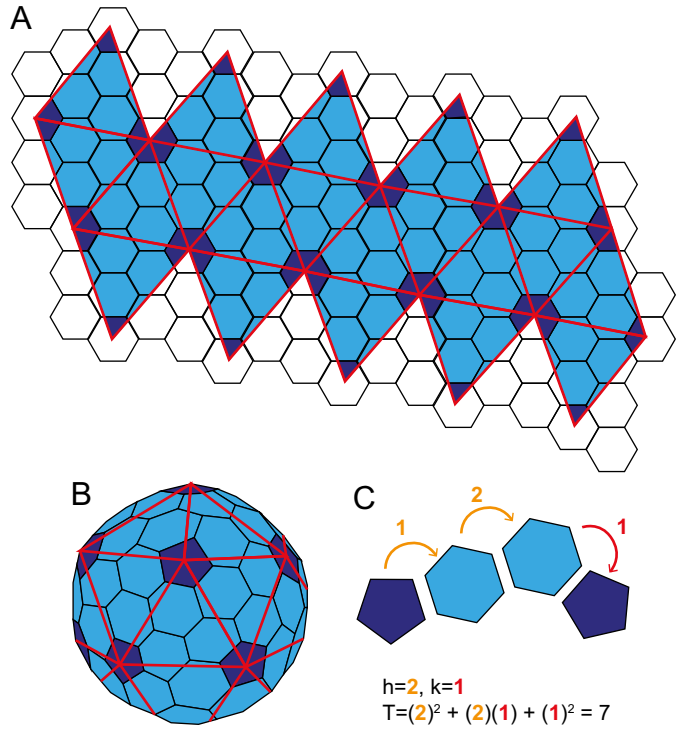

Figure 2.3. Illustration of the Caspar and Klug triangulation number system exemplified by a capsid with T=7 symmetry. (**A**) A flat view of a T=7 capsid. The 20 triangular faces in red are mapped onto a two-dimensional hexagonal lattice that consists of hexagons (light blue), with a pentagon (dark blue) at each vertex of the triangular faces. (**B**) The pentagons curve the hexagonal matrice into a sphere. (**C**) Illustration of how the T-number is calculated for a T=7 capsid using the equation $T=h^2+hk+k^2$.

Why structural virology?

The capsid serves several important functions in viral infection, including attachment to the cell, cell entry, release of its content that has been protected in the extracellular environment, and assembly of new virus particles. Thus, studying virus structures is essential for understanding these events, and such one of the keys for preventing diseases associated with them. To design anti-viral agents, knowledge about surface structures and interaction with the host is one component. Another component is the genome. As the genome often plays a large role in capsid formation, a deeper understanding of its structure could be crucial for designing drugs that interfere with the virus assembly.

Metagenomic analysis is an important tool in evolutionary studies. However, to understand deeper evolutionary connections where the genomic information has been erased, structural comparison is crucial. As such, structural studies of viruses are also important for understanding virus evolution. An important point in regard to this is that more efforts should be put into

structural studies of certain underrepresented viruses, such as those infecting single cell eukaryotes and archaea, to address the enormous knowledge gap about viruses.

Overview of methods

The main methods for studying the atomic structure of macromolecules are X-ray crystallography, three-dimensional (3D) electron microscopy (EM) and nuclear magnetic resonance (NMR) spectroscopy. 3D electron microscopy comprises three approaches: tomography, single particle analysis (SPA) and crystallography. In turn, tomography and SPA goes under the common name cryo-EM, which are also the approaches that are currently the best-established EM methods and most relevant for viruses.

Accounting for about 90% of the total number of deposits in the Protein Data Bank (PDB), X-ray crystallography has historically been the most successful technique; this is also true for virus structural studies. However, recent developments on the microscopes (foremost on new detectors), more efficient data collection routines, and on the image processing have turned cryo-EM into a highly competitive technique, especially for large samples such as viruses. This advancement is obvious from the data deposited in the PDB, where electron microscopy currently accounts for about 3% of the total number of deposits, but 7% of the depositions the last five (2015-2019) and 13 % of the last two years (2018-2019).

Several other techniques exist that can complement the information obtained from X-ray or electron data. These include for example neutron crystallography, conventional transmission electron microscopy using negative stain, atomic force microscopy, and mass spectrometry.

Furthermore, other more recent techniques, or variants of already established methods, have emerged for studying biological structures. With the construction of X-ray Free-Electron Lasers (XFELs), two new techniques became realizable, single-particle coherent diffractive imaging (CDI) and serial femtosecond crystallography (SFX). The main advantage of these XFEL based methods is the possibility to visualize biological processes on very short timescales. Electron crystallography is an old technique, developed by Aron Klug (who also invented the T-number theory), an achievement for which he was awarded the Nobel Prize in 1982. It has historically been successfully used for studies on very small two-dimensional (2D) crystals especially inorganic ones. It was not until a couple of years ago that the technique was extended to 3D crystals as a new method called microcrystal electron diffraction (MicroED) [62], leading to an expansion of electron crystallography to also accommodate macromolecular structure determination.

2.2. Engineered nanoparticles

Engineered nanoparticles (NPs) are commonly classified based on physical and chemical characteristics into carbon-based NPs, metal NPs, ceramics NPs, semiconductor NPs, polymeric NPs, and lipid-based NPs. What they all have in common is that they have unique physiochemical properties (e.g. optical, electronic, thermal, mechanical, and magnetic), owing mainly to their high surface to volume ratio, compared to their bulk counterparts (>500 nm) [63]. Due to these properties, engineered NPs have attracted attention from multidisciplinary research fields and various industry sectors the last couple of years. Nanotechnology have a relatively short academic history that has indeed accelerated recently: about half of the publications in Scopus that include the word "nanoparticle" were published the last 5 years (Fig. 2.4). The interest for engineered NPs is also obvious from the wide-spread application areas, such as in biomedicine, environmental remediation, healthcare, electronics and textiles. However, concerns exist that the pace of nanoparticle commercialization is much faster than the assessment of their safety [64].

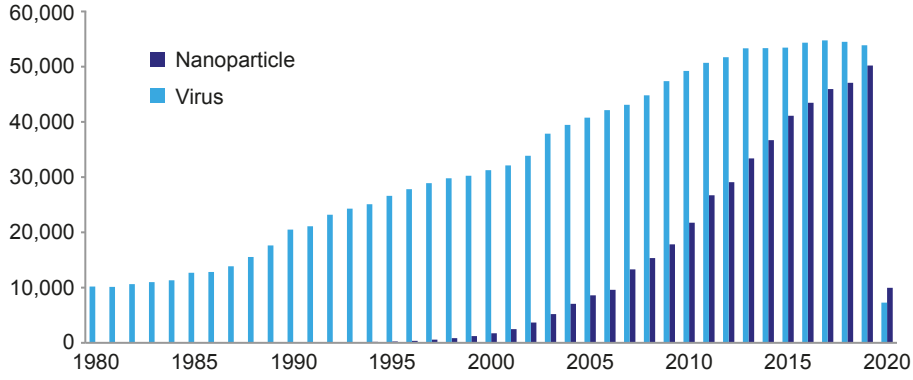

Figure 2.4. Increase in nanotechnology research. Number of publications each year that include the word "nanoparticle" (dark blue bars) in contrast to publications that include the word "virus" (light blue bars). Note: viruses are by definition also nanoparticles, however in publications the word "nanoparticle" typically referrers to engineered nanoparticles. Data obtained from Scopus until February 20, 2020.

2.2.1. Nanotoxicity

A new branch of toxicology, called nanotoxicology, has evolved alongside the many studies on various applications of NPs. The exposure to nanoparticles is not as recent as the field of nanotechnology since the production of particles from for example forest fires, volcanic eruptions, combustion and traffic dates back longer in the human history. Nevertheless, the increasingly wide-spread use of engineered NPs requires toxicological studies to ensure appropriate risk assessments [64].

The growing interest for nanomaterials (nanoparticles as well as nanostructured materials) and, as a consequence, the concerns about potential risks have resulted in demands for nano-specific regulations. Currently, no internationally accepted definition of nanomaterial for legislation purposes exists. Instead, different definitions are used by various governments and organizations [2], [65]. How and whether or not nanomaterials should be defined at all is a matter of discussion [66]–[71]. The purpose of the regulations is to protect human health and the environment. Several challenges do exist. Legislations have to be on an appropriate level so that materials that potentially could pose a risk are being evaluated, while all other materials are left out in order to not complicate more than necessary for producers of nanomaterials and products containing them [2]. Maynard also reminds us that too strict definitions can lead to some materials slipping through the regulatory net [68]. A solid framework for lawmakers is required, as having methods that can detect nanomaterials in products according to the regulations. Among the various definitions of a nanomaterial that currently exist, size is the common element. However, other properties, such as functional groups, surface charge and surface structure, can also influence toxicity. In terms of size, an inverse relationship with toxicity is often reported. For example, bulk gold is regarded as a safe and inert material, while its nanoparticle counterpart can have toxic effects [72]. Engineered NPs with a cationic surface also appear more toxic than their neutral and anionic counterparts [73]. The large number of variables makes it difficult to make general assumptions about their risks and to formulate legislations [69]. As of July 2013 (No 655/2013) and December 2014 (No 1169/2011), EU regulations require cosmetic products and food/food contact materials, respectively, to have nano-ingredients labelled.

There are four main possible exposure routes for engineered NPs: inhalation, dermal, ingestion and injection. The respiratory system is the primary route of exposure in the occupational environment, whereas for consumers the primary exposure route is currently dermal [74]. The faith of NPs that enters the body through inhalation is dependent on their size [75], but have been shown to cause effects such as inflammation and fibrosis of the lungs [76], [77]. Current research is inconclusive whether or not engineered NPs can penetrate skin and what, if any, the effects are [78]. A large number of different toxicity studies have been performed both *in vivo* and *in vitro*, and have revealed effects such as immunotoxicity, genotoxicity, carcinogenicity and toxicity to reproduction. In the majority of experimental studies conducted to date the acute effects of short-term exposure have been investigated. All types of engineered NPs, such as metal and carbon-based, have shown toxicity to some degree in numerous experiments, but the results are sometimes contradictory, and have as a consequence been criticized [79]. However, variables such as aging effects of NPs and batch-to-batch variations make nanotoxicity experiments challenging.

2.2.2. Applications

Depending on inclusion criteria and frequency of updates, different databases report 1,800 to 3,300 commercial products that currently contain nanomaterials [3]–[6]. In the Consumer Product Inventory [3] released in 2013 the majority (42%) of products belong to the health and fitness category, which includes for example clothing, cosmetics and sporting goods and the most frequently used nanomaterial in all categories is silver (24%). Regarding the nanomaterial location, about 29% are suspended in fluids (e.g. skin lotion, car lubricant) and the second largest group (17%) were solid products with surface-bound nanoparticles [6]. The exact numbers reported by Vance and co-workers are today out-dated; however the overall pattern is still valid when searching databases such as StatNano [4] and The Nanodatabase [5]. The purpose of including nanomaterial in commercial products are likely everything on a scale from a marketing gimmick, to giving products unique properties. Of the products listed in the Consumer Product Inventory the function of NPs were primarily to add antimicrobial protection (31%), which was followed by providing protective coating (15%), environmental treatment (15%), cosmetic (12%) and health promotion (e.g. dietary supplements) (11%) [3], [6].

Biomedicine is one of the fields where nanomaterials have great potential. The Food and Drug Administration (FDA) already approved the first nanoparticle-based drug-delivery system for clinical use in 1995. The drug, Doxil®, is a chemotherapy formulation delivered via liposomes. Since then several other therapy and diagnostic products based on nanoparticles have been approved or have entered into clinical trials and the list has especially increased during the last 5 years. Many of them are organic-based nanoparticles, such as liposomes, but there are also several inorganic compounds, such as iron oxide, which is used in anemia therapies and imaging applications. The majority of applications of nano-drugs are for cancer medicines, but vaccines, anaesthetics and fungal treatment are other areas of use [80]. The application areas imaging, drug delivery and diagnosis will continue to expand and advance, but other areas such as antimicrobials and implants will likely make an entrance as well [81].

Other current and future application areas for nanomaterials include the environmental sector (e.g. waste water treatment and filtration), renewable energies (e.g. solar cells and batteries), automotive (e.g. improving engine efficiency and fuel consumption), electronics (e.g. better transistors), and construction (e.g. in building materials) [16], [63].

3. Single-particle cryo-EM of CtenRNAV-II

Algae are a diverse group of eukaryotic organisms that range from unicellular microalgae of 1 μm (e.g. *Micromonas pusilla*) to multicellular forms, such as the giant kelp that can reach up to 60 m. Most of them are aquatic and autotrophic. The algae diversity is reflected on the viruses that they host, which can be of RNA or DNA type (linear, circular, double-stranded, single-stranded, segmented) and in the size range of 4.4 to 638kb [82].

An algal bloom is defined by a rapid increase of an algal population, commonly during spring and summer, as a consequence of favourable environmental conditions, such as nutrient level, light availability, pH and temperature, and are recognised by the discoloration of the water caused by their pigments. Most algal blooms are not harmful to people and the environment, however, some species do cause harm, and are thus called Harmful Algal Blooms (HABs). Some HABs produce toxins, while others are harmful due to mechanical properties. That changes in the environmental conditions affect the algae growth dynamics is a well-established knowledge. However, more recent studies suggest that the rapid disappearance of an algal bloom that sometimes occur, can be attributed to host specific algal viruses [83]. Apart from the direct effects of regulating the HABs, viruses killing eukaryotic algae also contribute to several biogeochemical and ecological processes, such as carbon and nutrient cycling, and genetic exchange and evolution [7], [29], [51]. Algae viruses could potentially be used as algaecides, which would have the advantage of specificity over current chemical products as these viruses typically only affect one or a limited number of algae [84]. This is not an unlikely future scenario since virus pesticides have been used for a long time to combat insects (e.g. baculovirus).

Diatoms are microalgae with very ancient origin, dating back about 150-200 million years. Together with other types of phytoplankton, diatoms are major players in aquatic ecosystems, by converting CO_2 to organic carbon, and thereby releasing O_2 into the atmosphere, and as base of the aquatic food web. A unique feature of the diatom is that they are surrounded by a cell wall made of silica (also known as frustule), and such, diatoms are key participants of the ocean's silicon cycle [85].

To date, about 20 diatom viruses have been described. They are either single-stranded RNA (ssRNA) viruses [86]–[88] or single-stranded DNA (ssDNA) viruses [87], [89]. Most diatom viruses are highly specific to their host, with species specificity or even strain specificity. Viruses infecting

marine unicellular organisms and their ecological significance are comparably recent discoveries, which combined with the historical interest of studying viruses that are of public-health and economical concern, contributes to the enormous knowledge bias about viruses. Little is therefore known about the infection mechanisms of algae viruses, and diatom viruses in particular. The diatom's frustule serves to protect the cell, however, the frustule has pores that allow uptake of nutrients, gas exchange and secretion of cellular products, and may thus also facilitate viral infections [85, pp. 211–225]. Recent discoveries have shown that infection strategies such as hijacking autophagy pathways and sialic acid interactions, which were previously thought to be exclusive to vertebrate viruses, are possible infection routes also for algae viruses [90], [91].

This chapter describes CtenRNAV-II and how the capsid structure was determined using single-particle cryo-EM. **Paper I** describes the structure and the extensive comparison to related viruses.

3.1. CtenRNAV-II

Chaetoceros tenuissimus is a HAB species commonly found in brackish water layers of fiords and inlets. To date, four viruses that infect it have been isolated and characterized: *C. tenuissimus* RNA virus type I [92] and type II [87] (CtenRNAV-I and CtenRNAV-II), and *C. tenuissimus* DNA virus type I [93] and type II [87] (CtenDNAV-I and CtenDNAV-II). CtenRNAV-II was isolated from sediment samples collected from the Hiroshima Bay, Japan, and distinguishes itself from other diatom viruses in that it infects different *Chaetoceros* species. The virus particles are spherical with a diameter of about 35 nm and were found randomly distributed throughout the cytoplasm in host cells, sometimes exhibited as crystalline arrays (Fig. 3.1B-D) [87].

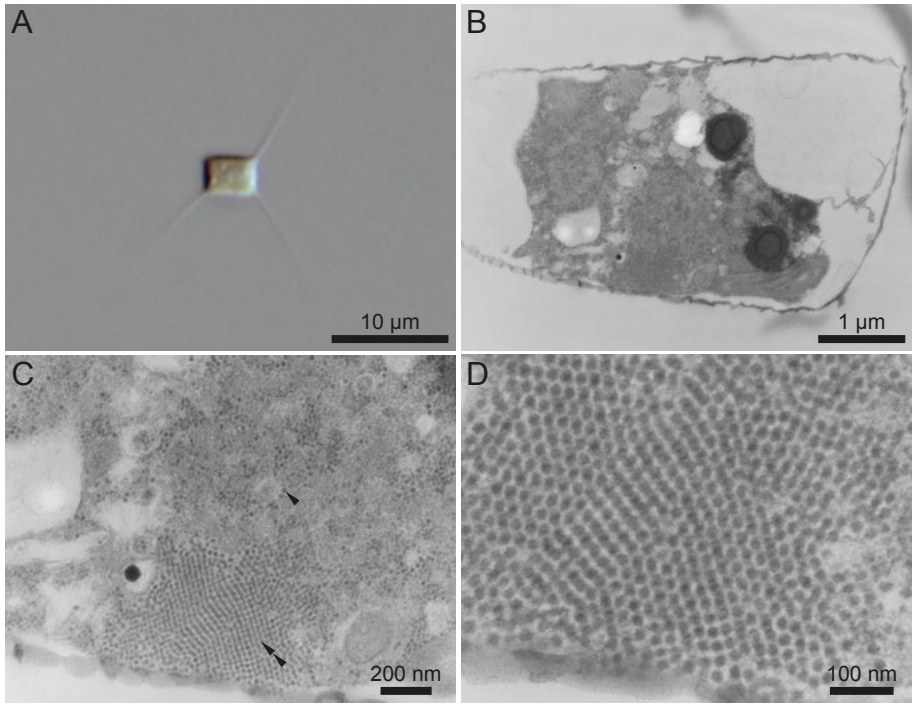

Figure 3.1. Optical (**A**) and transmission electron micrographs (**B**-**D**) of *C. tenuissimus*. (**A**) An intact *C.tenuissimus* cell, strain NIES-3715. (**B**) Ultrathin section of a cell infected with CtenRNAV-II. (**C**) Higher magnification of the cell in (**B**) displays the distribution of CtenRNAV-II particles throughout the cytoplasm (arrowhead) as well as in crystalline arrays (double arrowhead). (**D**) CtenRNAV-II forming crystalline arrays in the cytoplasm at higher magnification than (**C**). The micrographs were prepared by Yuji Tomaru and Kei Kimura.

CtenRNAV-II (species *Chaetenuissarnavirus II*) is taxonomically classified as a *Sogarnavirus* of the family *Marnaviridae*. The *Marnaviridae* family currently consists of 20 members and belongs to the order *Picornavirales* (https://talk.ictvonline.org/taxonomy/), which include viruses that are evolutionary related but infect a wide range of hosts (Table 3.1). The *Picornavirales* members share a number of common features, including morphological properties, such as being non-enveloped, spherical, and about 30 nm in diameter, and genomic properties, such as a common helicase-proteinase-polymerase replication block [94]. The capsid proteins have similar folds as several other viruses of the higher-order Picornavirus-like lineage, which include families such as *Polyomaviridae*, *Parvoviridae* and *Birnaviridae* [33], [59]. Viruses of this lineage have different genome strategies (RNA, DNA, ss and ds) and capsid complexity (from T=1 to T=13 symmetry), but are nevertheless likely distantly evolutionary related.

Table 3.1. *List of current families of the order Picornavirales, their respective host and type species, and whether any capsid structure has been determined.*

Family	Host	Type species	Structure
Marnaviridae	Protists	*Heterosigma akashiwo RNA virus*	Yes (CtenRNAV-II)
Iflaviridae	Invertebrate	*Infectious flacherie virus*	Yes
Dicistroviridae	Invertebrate	*Cricket paralysis virus*	Yes
Polycipiviridae	Arthropods	*Solenopsis invicta virus 2*	No
Secoviridae	Plant	*Cowpea mosaic virus*	Yes
Picornaviridae	Vertebrate	*Human enterovirus C*	Yes

CtenRNAV-II, as well the other members of the order, has a (+)ssRNA genome. The genome organization nevertheless varies between families as well as between species within the same family. In the majority of members, each virus RNA encodes one polyprotein. The *Dicistroviridae* family and some members of the *Marnaviridae* family, including CtenRNAV-II, are exceptions (Fig. 3.2). The order in which the structural proteins are encoded in CtenRNAV-II, VP2-VP4-VP3-VP1, is the same as for members of the invertebrate virus families. VP0 is a precursor protein that is cleaved upon assembly of the virus particles. Among the invertebrate viruses the cleavage has been suggested to take place through autocatalysis involving an Asp-Asp-Phe (DDF) motif located in a loop immediately following strand βI of VP1 [95], [96].

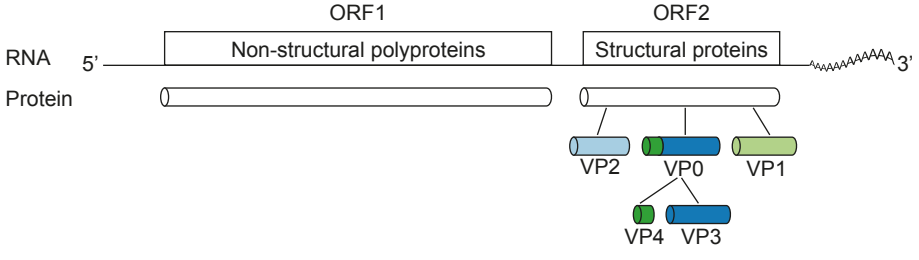

Figure 3.2. Genome organization of CtenRNAV-II. The CtenRNAV-II capsid encloses a (+)ssRNA genome that has two open reading frames (ORF). ORF2 encodes the structural proteins in the order VP2, VP4, VP3 and VP1. VP0 is a precursor protein that is cleaved upon assembly.

3.2. Single-particle cryo-EM

The impact of cryo-EM, especially single-particle cryo-EM, in structural biology during the last couple of years has not gone unnoticed. The first model based on cryo-EM was deposited in the PDB in 1997, and since then both the total number of depositions as well as the depositions with high-resolution have grown exponentially. The importance of the method was acknowledged in 2017 when the Nobel Price in chemistry was awarded to

Jacques Dubochet, Joachim Frank and Richard Henderson for their contributions.

One of the advantages with single-particle cryo-EM over X-ray crystallography and NMR is the relatively easy sample preparation: small amount of sample, no crystallisation, and forgiving on sample purity. This makes it especially suitable to study large, complex and flexible structures such as viruses, membrane proteins and ribosomes. The possibility to perform asymmetric reconstructions in the SPA workflow allows, in terms of viruses, visualization of their genomes and other structural components that do not adhere to the icosahedral symmetry, which has been demonstrated for example using bacteriophages MS2 [97] and ϕ6 [98].

3.2.1. Microscopes and image formation

Conceptually, a transmission electron microscope (TEM) is similar to an optical microscope. Both microscopes contain a number of lenses whose purpose are to focus either the electrons or photons on the sample and produce a magnified image of it. However, several important differences exist, which can be simplified as follows. One difference is that the electron microscope has to be operated in vacuum conditions to limit scattering of the electrons by air molecules. Another is the resolving power of the two microscopes, since the resolution is dependent on the wavelength of the imaging radiation source. The lenses in an electron microscope are also more complex as the microscope requires so-called lens systems, which apart from the actual lenses also host deflectors, stigmators and apertures that serve to correct for imperfections of the microscope so that the electrons can stay focused and pass through the microscope along the optical axis. Finally, when the electrons have passed through the column of the microscope they hit a detector that transform the signal into an image, which is another difference to a light microscope where the image can be observed directly by the eye through the ocular lens.

The improvements seen in resolution from cryo-EM in the last couple of years are greatly owed to the developments of new detectors, the direct electron detectors. As the name implies, these detectors have the advantage that each incoming electron is directly converted into charge. In the precursor charge-coupled device (CCD) cameras, the electrons first have to be converted to photons by a scintillator before being detected by the CCD sensor and since each electron can scatter in different directions and produce a variable number of photons, both the spread and number of counts in the CCD will vary. In the direct electron detectors, a complementary metal-oxide semiconductor (CMOS) sensor directly detects electrons, and thus the counts produced by one electron will be more localized. In addition, the readout of the image can be carried out hundreds of times per second, which makes it possible to count the incident electrons. This, in turn, gives every electron the same weight independently of the number of counts it produced. In addi-

tion, the fast readout is beneficial as there will be motion created during the exposure and this movement can be tracked because of the fast readout, and corrected for by shifting individual frames.

In X-ray crystallography, the traditionally most frequently used method in structural biology, the photons scattered by the sample are recorded on a detector as a diffraction pattern (according to Bragg's law) (Fig. 4.3A). Together with phase information, these recorded intensities can then be Fourier transformed to generate an electron density map (Fig. 3.3A). As opposed to X-rays, electrons can be focused and as a result the objective lens instead produces a diffraction pattern on its back focal plane, which in turn can be inverse Fourier transformed to form an image on the detector (Fig. 3.3B).

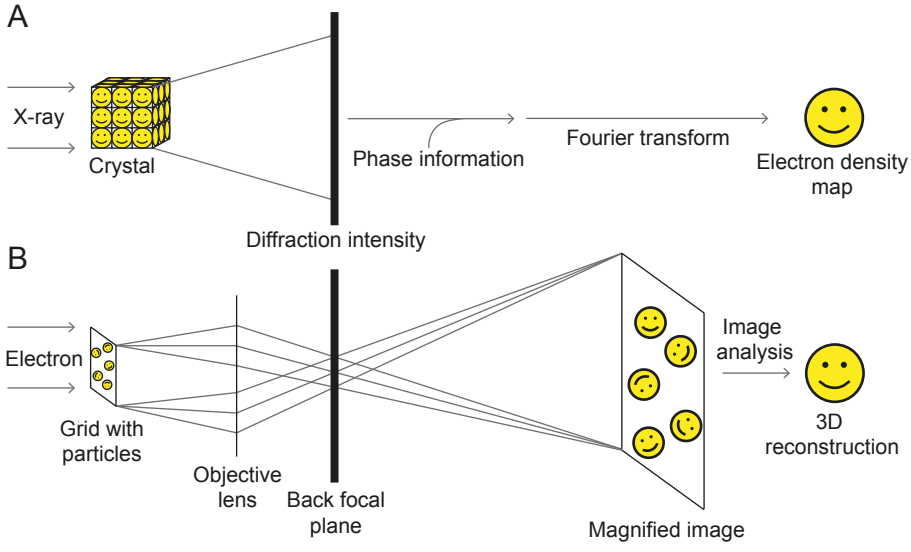

Figure 3.3. Comparison between X-ray crystallography and single-particle cryo-EM. (**A**) X-rays produce a diffraction pattern (illustrated in Fig 4.3A) of a crystal that can be converted to an electron density map by adding phase information (**B**) In an EM, lenses are used to form a magnified image on a detector. The image is noisy, but by using information from several particles (smiley faces) imaged in different orientations a 3D reconstruction can be obtained.

Because the electron microscope and imaging procedure are not perfect, not all Fourier transform (FT) components are fully present in the final image. When an electron interacts with a sample, some of it will be scattered while some will be unscattered and its contribution to the final image depends on how these processes interfere with each other. The scattered parts of the electron will be phase shifted compared to the unscattered part. Depending on the extent of the phase shift, the amplitude/contrast will be affected either positively or negatively. The amplitude/contrast contribution from different scattering events will oscillate as a function of spatial frequency (Fig. 3.4). This process is mathematically described by the contrast transfer function

(CTF), which merely describes how much the different FT components contribute to the final image. Because of the oscillations, the maximal information will be transferred to the image only at some specific spatial frequencies (purple star in Fig. 3.4), whereas zero (red star in Fig. 3.4) or partial information will be transferred at all other spatial frequencies. To correct for the loss of information, images are recorded at different defocus. By changing the defocus the CTF will be shifted and thus information from other spatial frequencies can be retrieved (orange stars in Fig. 3.4). Because of the CTF an EM image is not a true representative of the imaged object, and so it has to be corrected by performing a so-called CTF correction.

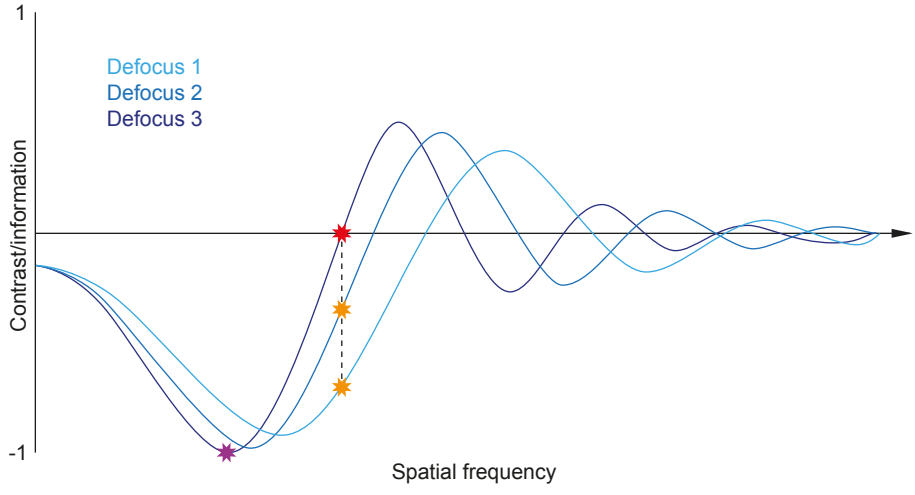

Figure 3.4. CTF. At a particular defocus value (e.g. "defocus 3") the maximal information will only be transferred to the image at some specific spatial frequencies (purple star). At other spatial frequencies, the information is completely lost (red star), but can be recovered by changing the defocus (orange stars). The CTF is dampened at high spatial frequencies due to defects of the electron gun that produces electrons at different directions and of different energy.

3.2.2. Sample preparation and data collection

In cryo-EM the sample is frozen in a layer of vitreous ice, i.e. non-crystalline ice that is formed by rapid cooling to very low temperatures (<-160°C). This is accomplished by a method called plunge freezing. A small amount of sample is placed on an EM-grid that is rapidly plunged in to a reservoir of liquid ethane or propane cooled by liquid nitrogen. Ideally, the sample is well distributed within the hole of the grid in all different orientations.

3.2.3. Single-particle analysis

The SPA workflow typically starts by correcting the recorded images, which includes motion correction, where beam-induced motion can be corrected for

by summing the individual sub-frames to a motion-corrected image, and CTF correction. In the next step, the particle picking, individual particles are selected from the micrographs, which can be performed manually and automatically. The selected particles are then classified to create class averages, an important step for obtaining an overall view of the particle, identifying heterogeneity in the sample and removing those particles that do not adhere to 'good' class averages. Next follows the reconstruction, where a 3D model of the particle is obtained by combining the different 2D projections of the particle in a 3D volume. The obtained reconstruction can be further improved by additional procedures such as masking and correcting for other aberrations [99] caused by the microscope. A flowchart of the data analysis performed in **Paper I** is shown in *Figure 3.5*. Several different software packages exits, which can perform either all or a subset of the image processing and 3D reconstruction steps (http://en.wikibooks.org/wiki/Software_Tools_For_Molecular_Microscopy). The reconstruction is conducted by splitting the dataset into two halves and performing independent refinements of each. Upon convergence, the datasets are combined and the resolution estimated by the so-called Fourier shell correlation (FSC). Basically, the FSC compares the similarity between the two reconstructions as a function of spatial resolution. A typical FSC curve therefore displays high correlation/similarity at low resolutions, and drops at high resolution (see Fig. 1C in **Paper I**). The resolution of a reconstruction is commonly reported as FSC = 0.143.

3.3. Present investigation – **Paper I**

If unicellular protists were the earliest eukaryotes on Earth they were presumably hosts of the most ancient groups of viruses. As a consequence, the capsid proteins of viruses in the *Picornavirales* order that infect unicellular organisms, such as algae, might possess certain characteristics that have changed little over the course of evolution compared to the related viruses that infect multicellular organisms. Thus, these viruses may resemble the *Picornavirales* ancestor in some respects. Sequence similarity between viral proteins that serve homologous functions is important for inferring evolutionary relationships. Nevertheless, structural information is necessary to investigate the molecular details and for elucidating distant relationships where sequence similarity is low or non-existing.

The intensive studies on viruses that infect humans, domestic animals and crops have resulted in a biased knowledge of our virosphere. The oceans hold the greatest number of viruses on the Earth where they make an enormous ecological contribution; still comparably little is known about these viruses.

3.3.1. Aim

The aim of the study presented in **Paper I** was to determine the structure of the CtenRNAV-II capsid and compare it to other *Picornavirales* viruses with the intention of elucidating the acquired and lost structural traits among viruses of the order.

3.3.2. Methodology

In summary, 3,505 images were collected using a Titan Krios microscope (Thermo Fisher Scientific) and a K2 Summit (Gatan) direct electron detector with a pixel size of 1.06 Å. *Figure 3.5* shows the data processing workflow for which the Relion 2.1 [100] package was used. Initially, 11,206 particles were picked from the images, and were further reduced to a final number of 8,315 particles by performing a number of classification steps and a manual-picking step. An atomic model was manually built into the density map.

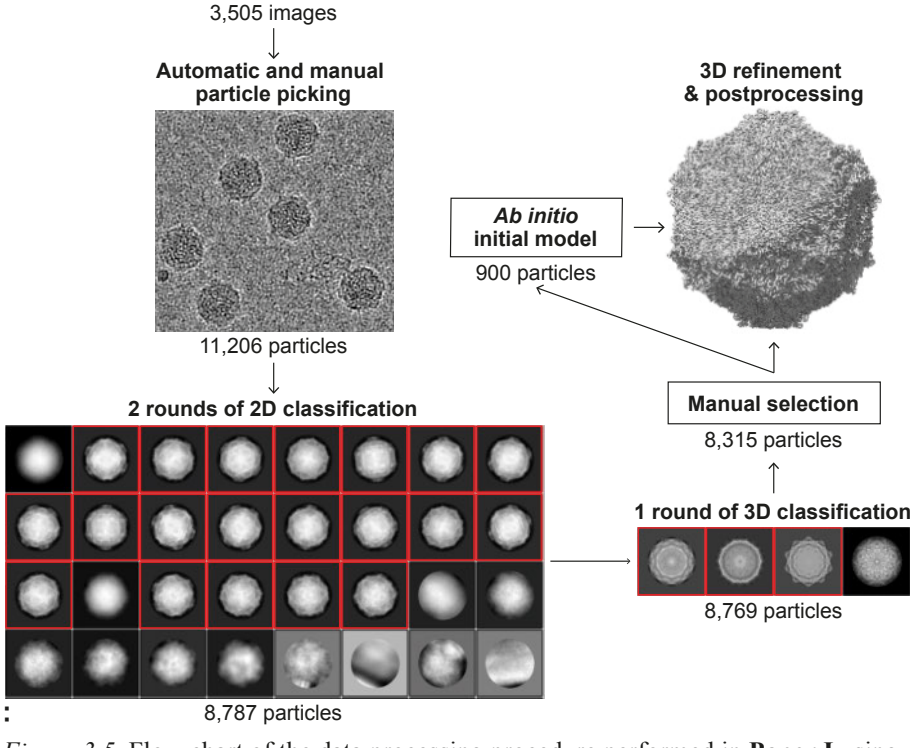

Figure 3.5. Flow chart of the data processing procedure performed in **Paper I** using Relion 2.1. The initial particle picking resulted in 11,206 particles, which was further reduced by a number of classification steps and a manual particle-picking step. The classes marked in red were selected for the next step. 8,315 particles were used for the final 3D reconstruction.

The resulting CtenRNAV-II capsid structure was compared with members of families *Picornaviridae*, *Dicistroviridae*, *Iflaviridae and Secoviridae* as no structure has been determined yet of any member of the *Polycipiviridae* family.

3.3.3. Results

Paper I describes the CtenRNAV-II structure determined using single-particle cryo-EM at a resolution of 3.1 Å (FSC = 0.143). The overall structure of CtenRNAV-II is similar to other viruses of the *Picornavirales* order that infect multicellular organisms. The major capsid proteins adopt a jelly-roll fold where VP1 surrounds the five-fold axes and VP2 and VP3 alternate around the three-fold axes (Fig. 3.6)

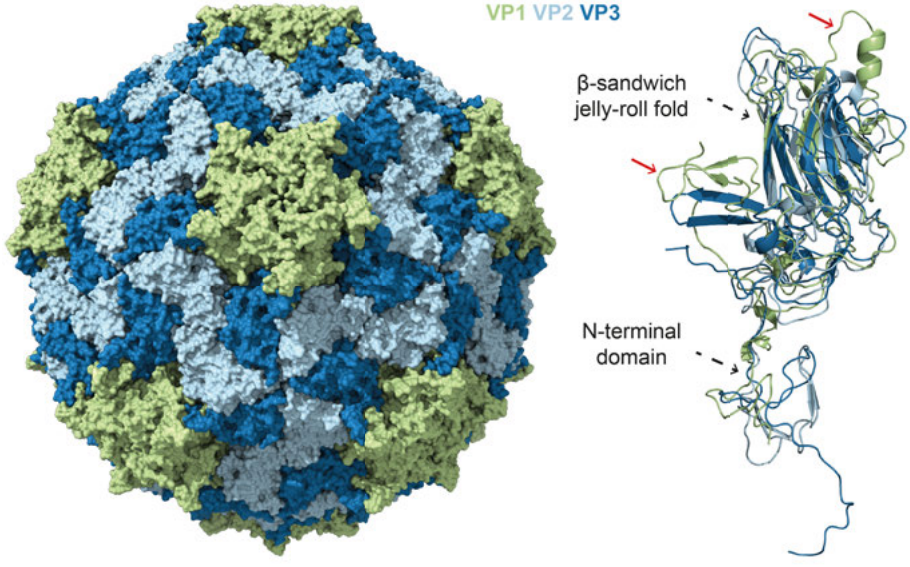

Figure 3.6. Structure of CtenRNAV-II. The complete capsid is displayed to the left in surface representation. VP1 (green) is located at the five-fold axes and VP2 (light blue) and VP3 (dark blue) alternate around the three-fold axes. VP4 is located on the inside of the capsid and thus not visible. The major capsid proteins VP1-3 are superimposed to the right, visualizing the common β-sandwich jelly-roll folds and N-terminal tails. The protruding EF- and CD-loop in VP1 described below are indicated with red arrows. Figure adopted from **Paper I**.

Paper I describes four main structural traits in CtenRNAV-II. These are summarised on the following pages and in *Figure 3.7*, which shows a structure based phylogenetic tree of viruses in the order *Picornavirales* and which of the structural traits that are present among viruses from the different families. Exceptions exist within families and Table 2 in **Paper I** gives a more detailed list.

A surface protruding EF-loop in VP1 – ⭕

CtenRNAV-II has a unique loop in VP1 formed between the E_2 and F strand (Fig. 3.6 herein and Fig. 4 in **Paper I**), and which to date is unperceived in any other virus from the order *Picornavirales* (Fig. 3.7). The loop is highly accessible on the capsid surface and positioned around the five-fold axis. Due to the unique position of the EF-loop and the fact that VP1 appears to be the most important protein for receptor binding among picornaviruses [101], [102], we hypothesise in **Paper I** that this loop is an important host recognition site for CtenRNAV-II or marnaviruses in general.

A surface protruding CD-loop in VP1 – ⭕

CtenRNAV-II has another protruding surface loop in VP1 formed between strands C and D (Fig 3.6 in here and Fig. 4 in **Paper I**), a characteristic shared with viruses of the order *Picornavirales* that infect invertebrates (Fig. 3.7). The CD-loop obscures the so-called "canyon", which is a depression around the five-fold axis in enteroviruses (family *Picornaviridae*) that serves as a host receptor-binding site. The canyon is inaccessible to immunoglobulins, and enteroviruses can thus prevent an attack by the host's immune system [103]. In **Paper I** we therefore hypothesise that the surface loops that obstruct the canyon in CtenRNAV-II and invertebrate viruses have been shortened in vertebrate viruses as an adaptation to the host immune system.

A domain swap in VP2 – ⭕

All three major capsid proteins in CtenRNAV-II have an N-terminal tail, as shown in *Figure 3.6*. This is a rather unusual characteristic among viruses of the order *Picornavirales*, but is found also in viruses of the *Dicistroviridae* family (Fig. 3.7). A few members of the *Picornaviridae* family (called 'primordial' *Picornaviridae* viruses) also posses an N-terminal tail in VP2 (Fig. 3.7), which was one of the reasons why Wang and co-workers proposed that these vertebrate viruses are evolutionary intermediates between the invertebrate and other vertebrate viruses of the order [104]. The N-terminal tail in VP2 exchanges with its two-fold symmetry related neighbour, resulting in a domain swap relative to those viruses who's VP2 proteins do not have a tail (Fig. 7A in **Paper I**). A number of partially conserved residues could be important for the domain swap (Fig. 7B in **Paper I**).

Potential autocatalytic sites in VP1 and VP3 – ⭕

As described in 3.1, the cleavage of the precursor protein VP0 is likely an autocatalytic process among the invertebrate viruses that involves a DDF motif located in a loop immediately following strand βI in VP1 [95], [96]. The order in which the structural proteins are encoded in CtenRNAV-II (Fig. 3.2) is the same as for members of the invertebrate virus families. In **Paper I** we could show from a sequence alignment (Fig. 8C in **Paper I**) that the

VP4/VP3 cleavage point in CtenRNAV-II and other marnaviruses was similar to viruses of the *Dicistroviridae* family, but that VP1 instead had an EDF motif. A second DDF motif, currently of unknown function, has been reported in some dicistroviruses and this was also found in marnaviruses, including CtenRNAV-II. Superimpositions of VP1 and VP3 proteins (Fig. 8A in **Paper I**) of CtenRNAV-II and the invertebrate viruses also demonstrated that the motifs were located at the exact same position in the structure. That, and the fact that the glutamic acid of the EDF motif is pointing towards a gap between the C-terminus of VP4 and N-terminus of VP3 (Fig. 8B in **Paper I**), led us to propose that the motif has the same function in CtenRNAV-II as in the invertebrate viruses.

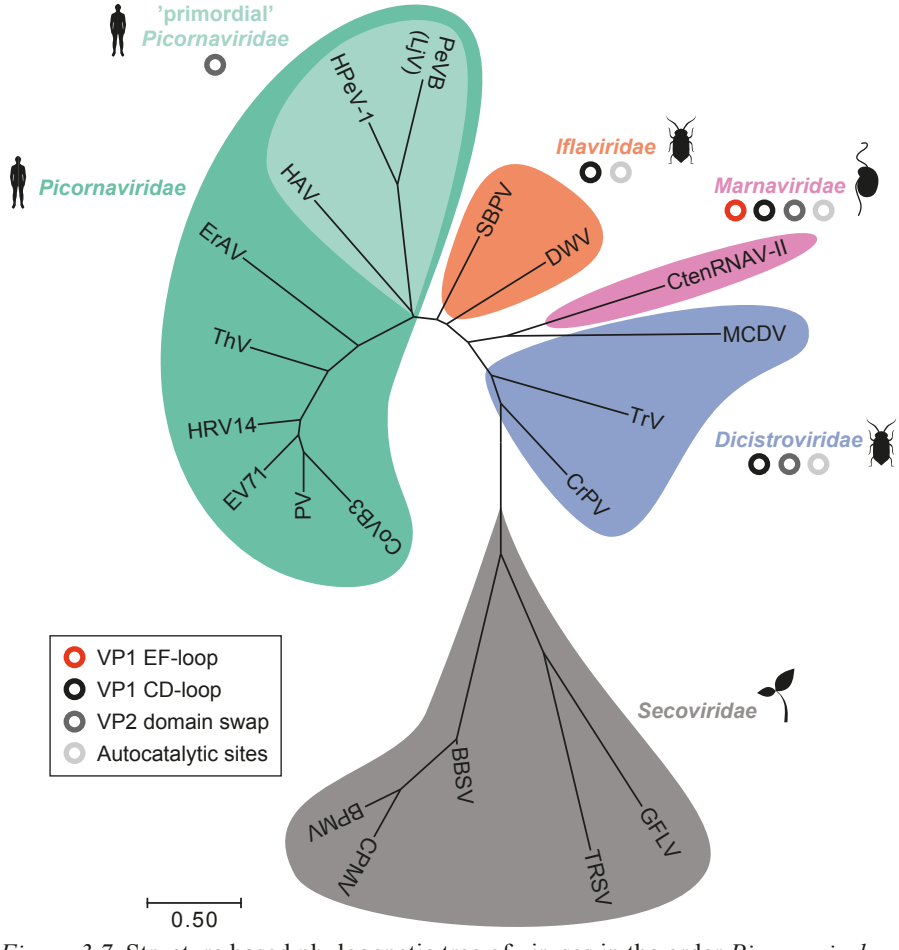

Figure 3.7. Structure based phylogenetic tree of viruses in the order *Picornavirales*. Presence of the structural traits among members of the different families is indicated with circles, the red circle highlighting the unique EF-loop in CtenRNAV-II. Figure adapted from **Paper I**.

3.3.4. Discussion

Paper I describes the first structure of a virus from the family *Marnaviridae* of the order *Picornavirales*. To my knowledge it is furthermore the first diatom virus structure. Thus, this study contributes to even out the biased knowledge of the virosphere. Since the transmission mechanisms of algae viruses are poorly understood on a molecular level, the CtenRNAV-II structure could be an important step towards filling that knowledge gap as well.

The four main structural traits described and their distribution among other viruses of the order *Picornavirales* (Fig. 3.7) suggest that viruses of the order infecting unicellular organisms indeed could share characteristics with the *Picornavirales* ancestor. With more *Picornavirales* structures determined in the future, especially from underrepresented families (e.g. *Marnaviridae*), conclusions on different structural traits can be drawn with greater certainty.

A striking and interesting revelation is that although subtle, but significant, differences exist between viruses that infect a diverse range of eukaryotic cells, the overall architecture is very similar. From studies on the infection mechanism of the invertebrate and vertebrate *Picornavirales* viruses it is evident that several details, such as the genome release [105], [106] and function of the minor capsid protein VP4 [107], [108], are shared between these viruses. Supposedly, same mechanisms also exist in unicellular viruses of the order, and perhaps only the receptor recognition has been adapted during the eukaryotic evolution.

The study described in **Paper I** also exemplifies the benefit of including structural information when inferring evolutionary relationships between viruses. In **Paper I**, the structural information obtained was used to elucidate which structural traits among related viruses that had likely been acquired or lost during the course of evolution. However, as described previously, structural comparison is also useful to infer more distant relationships between viruses (grouping into so-called lineages), including viruses that infect different domains of life [59].

4. Single-particle coherent diffractive imaging of rice dwarf virus

Plant viruses have been part of several milestones in the history of virology. Two of the most important include the tobacco mosaic virus as the very first virus to be discovered in the end of the 19th century [109] and tomato bushy stunt virus as the first atomic structure of a virus, determined about a century later [110]. Plant viruses have throughout the history been and continue to be extensively studied since they are great model systems for understanding virus structure and function due to the advantage of the relatively ease of obtaining large quantities by simply infecting host plants. In addition, an economical and environmental interest has driven the research forward due to serious crop losses caused by the viruses, with an annual worldwide estimated cost of more than $30 billion [111]. Compared to viruses that infect hosts from other kingdoms, plant viruses have additional challenges in the transmission process. Plants do not move and their cells have a robust cell wall that cannot be penetrated unaided, hence plant viruses are dependent on a vector organism (such as insects) for plant-to-plant transmission and for penetrating the cell wall. Plant viruses cause a range of macroscopic (such as leaf yellowing, leaf distortion and stunting of the plant) and microscopic symptoms (such as histological changes and structural changes in chloroplasts) in plants that they infect and often lead to yield loss in crop [112]. Since the discovery of the tobacco mosaic virus about 120 years ago [109], virus research has mainly focused on the role of viruses as pathogens. However, as described in Chapter 1, there are several recent reports on the beneficial effects of virus infections [47], a concept that has been particularly explored in plant virology. Roossnick and Bazán have described viruses as symbionts that range from mutualists to antagonists, including the commensal viruses in between. The antagonists are the ones often described in the literature and which cause severe symptoms in plants [24]. An example of a plant virus with a mutualistic relationship to its host is cucumber mosaic virus that helps its host when under abiotic stress (cold and draught) [48]. However, the majority of viruses are likely commensal, which are viruses that do not cause any evident effects on their host [24].

This chapter describes rice dwarf virus (RDV), an antagonistic virus, and its use as a model sample in single-particle CDI experiments using an XFEL. The experiments were conducted as part of the so-called single particle im-

aging initiative collaboration [113]. **Paper II** is the outcome of the very first beamtime within the collaboration and describes the data, which were collected using hard X-rays.

4.1. Rice dwarf virus

Most plant virus names describe an important symptom in the host from which the virus was first isolated. RDV, as the name suggest, causes stunted growth of rice, but also wheat, barley and other gramineae (grass) plants. Other symptoms include chlorotic flecks and inhibited root growth. Leafhoppers acquire RDV particles after feeding on infected plants. Intracellular spread between insect cells is accommodated by tubules formed by non-structural viral proteins and actin-based filopodia [114]. They spread through the digestive system and finally infect the salivary glands.

The fact that some parasites have the ability to alter the behaviour of their hosts with the purpose of enhancing transmission is a well-known characteristic [115], with *Toxoplasma gondii* as a commonly known example. However, viruses that change the behaviour of their host are a more recent revelation. In terms of RDV, Wang and co-workers demonstrated that RDV is capable of changing the preference and feeding behaviour of green rice leafhopper, for example non-viruliferous leafhoppers prefer RDV-infected plants over RDV-free plants, while viruliferous leafhoppers preferred RDV-free plants over RDV-infected plants [116].

Rice dwarf disease, first recorded in Japan 1883, is one of the earliest described plant virus diseases [117]. From the first electron micrographs of RDV in 1960, the virus were described as "spherical or hexagonal particles, approximately 70 mμ in diameter ... These particles possess central darker bodies, 40-50 mμ in diameter which are surrounded by relatively transparent regions and outer membranes …" [118]. What was then observed as one smaller body and one larger outer membrane is probably what we today know as the inner and outer capsids, which are typical to viruses of the *Reoviridae* family. RDV is further classified to the genera *Phytoreovirus*, whose members contain 12-segmented dsRNA genomes. RDV belongs to the so-called BTV-like lineage based on the capsid protein folds, which suggests a more distant evolutionary relationship to viruses that infect a diverse range of eukaryotes as well as prokaryotes [59]. The genome of RDV encodes seven structural proteins: P8, P2 and P9 build up the outer capsid in a T = 13 symmetry while P3 alone form a thin inner capsid in a T = 2 symmetry. The remaining three proteins (P1, P5 and P7) are involved in the transcription and found in the core together with the genome [119].

The first atomic structure of RDV was determined by X-ray crystallography at 3.5 Å (PDB 1UF2) and consists of a model containing P3 protein, P8 protein and some P7 protein [119]. The initial electron density map did however show a few layers of RNA density and a density mass at each 5-

fold vertex. The minor capsid protein P2 had been removed by CCl_4 treatment to limit vector transmission to direct injection. A more recent study of RDV using cryo-EM revealed the location of P2 on the viral surface around the five-fold axes and its importance for connecting the viral particles to the insect host cells [120]. Amazingly, the capsid, with its two shells and a total of 900 proteins, can self-assemble [121]. A hierarchical assembly mechanism was recently proposed when an intermediate structure could be revealed by cryo-EM [122], [123]. The function of P9 remains unknown. These recent structural studies demonstrate the advantage and potential of cryo-EM over X-ray crystallography.

4.2. Single-particle imaging with an X-ray laser

4.2.1. X-ray free-electron lasers

The discovery of X-rays in 1895 by Wilhelm Conrad Röntgen [124] was an important breakthrough, for medicine of course but also for science in general and structural biology in particular. For several decades, bombarding an anode with electrons was the only procedure for producing X-rays (a technique still used in medical X-ray equipment). Another major breakthrough was made half a century later. Scientists found that when charged particles, e.g. electrons, are accelerated they emit light. *Synchrotron radiation*, as it was named after its discovery in a General Electric synchrotron accelerator [125], is utilized in today's many synchrotron facilities around the world.

When the PDB was founded in the early 1970's only a handful of structures were deposited. The construction of X-ray synchrotron facilities around the same time contributed largely to the following acceleration in the number of determined structures (other important developments were protein engineering, computer capacity, detector improvements and developments of cryo-techniques).

Producing coherent light in the infrared and ultraviolet region using free-electron laser (FEL) technology was introduced already in the 70's. Still, facilities producing light in the X-ray regime have only been a reality for about 15 years where Free electron LASer in Hamburg (FLASH) (DESY, Germany) was the first facility, available for the user community since 2005. FLASH served as a pilot facility for the latest addition, the European XFEL, which performed its first experiments in 2017 [126], [127]. Apart from the Hamburg facilities, another five XFEL instruments are operational: the Linac Coherent Light Source (LCLS) in Stanford, California, that went online in 2009 as the first XFEL producing hard X-rays with energies of up to 9.5 keV; Free Electron laser radiation for Multidisciplinary Investigations (FERMI) in Italy; SPring-8 Angstrom Compact free electron LAser (SACLA) in Japan; Swiss X-ray Free Electron Laser (SwissFEL) in Switzerland;

and Pohang Accelerator Laboratory X-ray Free Electron Laser (PAL-XFEL) in South Korea.

As in modern synchrotron sources, an XFEL utilizes undulators to create the radiation. However, making electrons radiate in phase instead of, as in synchrotrons, independently of each other requires the XFEL undulators to be much longer. The emitted photons travel slightly faster than the electrons and interact with them, which cause the electrons to organise into micro bunches separated by a distance of the X-ray wavelength. As the relativistic electrons proceed through the undulator they get more and more bunched until saturation is reached and almost all electrons have accumulated in these bunches. At the exit stage of the undulator system a bunch of electrons will therefore radiate in phase (or *coherently*).

Another difference between XFELs and most synchrotron beamlines is the X-ray pulse duration, which generally is much shorter for XFELs. A typical macromolecular crystallography beamline operates in the time scale of picoseconds, while XFELs can work in the femtosecond range. The repetition rate (Hz) states how many pulses are generated per second, which for the LCLS, where the experiment in **Paper II** was carried out, is 120 Hz, whereas the newly built European XFEL will emit 27,000 pulses per second.

Brilliance is a measure used to compare the quality of X-ray sources. The unit (photons/s/mrad^2/mm^2/0.1%BW) states that the greater the brilliance, the more photons of a given bandwidth (0.1%BW) and direction (mrad^2) are concentrated on a spot (mm^2) per unit of time (s). The *peak brilliance* describes the brilliance for a single pulse; hence a property that is greatly improved for XFELs compared to conventional synchrotron sources. The peak brilliance of for example the European XFEL is 5×10^{33} photons/s/mrad^2/mm^2/0.1%BW, which is about a billion times higher than that produced by synchrotrons. The short pulses and high brilliance has enabled experiments that previously were impossible.

4.2.2. Diffraction before destruction

Exposing biological samples to X-rays will lead to radiation damage, processes which can be limited to some extent by cryo-cooling the sample. Femtosecond pulses from XFELs are able to outrun these damages by giving rise to a diffraction pattern before the sample is damaged. The phenomenon is known as ‘diffraction before destruction’ and was initially theoretically predicted about 20 years ago [128], but has since the construction of the first XFELs also been experimentally demonstrated on both crystalline [27], [129]–[131] and non-crystalline samples [132]–[136].

Serial Femtosecond X-ray crystallography (SFX) is an X-ray crystallography method that collects diffraction data in a *serial* manner, typically from a series of small crystals, as opposed to conventional crystallography where a single (relatively large) crystal is rotated to collect a complete data set. SFX is advantageous for two reasons: small crystals can be used, commonly

200 nm-10 μm, radiation damage can be eliminated, and time-resolved studies can be performed [137]. Several sample delivery systems that can introduce crystals in a stream across the X-ray beam [138]–[141] and data collection and analysis software that can process individual diffraction patterns [142]–[145] have been developed. The advancement of serial crystallography was a consequence of the newly constructed XFELs, however nowadays the method is also available at synchrotrons [146]. The XFEL community is still relatively small and several challenges remain, nevertheless SFX is today an established method that have a huge impact on structural biology by answering questions that were previously not possible to study. Diffraction before destruction on non-crystalline samples, by means of single-particle CDI on which **Paper II** is based on, is not yet as mature, because it needs higher pulse intensities than currently available.

4.2.3. Single-particle coherent diffractive imaging

CDI is a technique in which an object is probed with a coherent photon beam or electrons and the scattering detected downstream. The technique was originally demonstrated on nanomaterials [147], but the advent of XFELs made the technique feasible also for single biological particles.

Similarly to SFX, the sample has to be delivered into the X-ray beam in a serial fashion, which is typically managed by introducing particles one by one in a container-free manner (illustrated in Fig. 4.1), however so-called fixed-targets have been attempted as well where the sample is attached to some type of support, such as silicon nitride [148], [149].

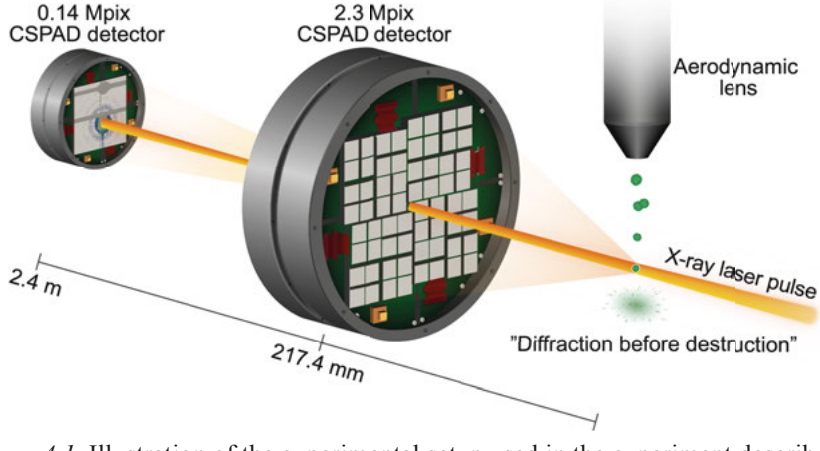

Figure 4.1. Illustration of the experimental setup used in the experiment described in **Paper II**. The aerodynamic lens focuses the aerosolized particles into the pulse train of the X-ray laser. Diffraction was recorded on two Cornell–SLAC Pixel Array Detectors (CSPADs) [150], [151], located 217.4 mm and 2.4 m downstream of the interaction region to capture high-angle and low-angle scattering, respectively.

The container-free sample delivery is achieved by aerosolising the particles into an aerodynamic lens stack (Fig. 4.2A) that serves to focuses the particle stream, and it has the advantages over the fixed-target approach that the efficiency increases and background decreases. The sample can be aerosolised either by using a gas dynamic virtual nozzle (GDVN) [139], [152] (Fig. 4.2B) (used in **Paper II**), a sample delivery method also explored in SFX, or by an electrospray unit [153]. Regardless of approach, the crucial requirement is to obtain a small initial droplet size as it increases the chance of introducing single particles into the X-ray beam and limits the amount of contaminants on the particles when the droplets evaporate [154]. As the sample emerges from the aerodynamic lens tip, the X-ray beam hits the particles in random orientation in high vacuum conditions a few hundred μm to mm below the tip of the lens. Single photons from the diffraction are detected using pixel area detectors (Fig. 4.1).

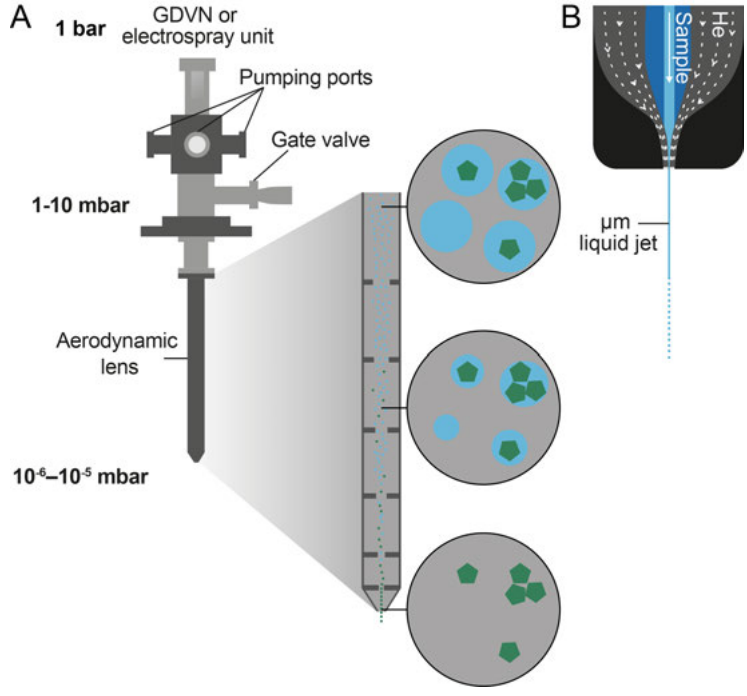

Figure 4.2. Illustration of the sample injector and GDVN (**A**) The Uppsala sample injector [155] where the GDVN (**B**) or electrospray unit is coupled on the top function to aerosolise the particles. Excess gas is pumped away, which reduces the pressure to 1-10 mbar. An enlarged inside view of the aerodynamic lens shows the cylindrical cavities that are connected by co-aligned orifaces, which serve to focus the particles into a narrow stream. The experimental chamber has a pressure of 10^{-6}-10^{-5} mbar. The evaporation process of the droplets is illustrated to the right. (**B**) Illustration of the GDVN where helium gas (He) reduces the diameter of the liquid jet, leading to breakage of the jet into droplets due to the surface tension.

As in crystallography, the intensity information from a diffraction pattern is insufficient to reconstitute an image of the object. Unlike crystallography, where a periodic sample (the crystal) produces Bragg diffraction (Fig. 4.3A), CDI of a single non-periodic object (such as a single virus particle) produces a so-called continuous diffraction pattern (Fig. 4.3B) from which phases can be recovered directly in an iterative process moving between real and reciprocal space. A reconstruction starts from random phases, which are continuously improved as the number of iterations increases by using two constraints: intensities and limited real-space volume. Comparably to cryo-EM, CDI data are 2D projections of unknown orientation that can be assembled to a 3D reconstruction, which have been demonstrated by Ekeberg *et al* [156], Kurta *et al* [134] and Lundholm *et al* [157]. Likewise, the resolution can be estimated using the FSC, or alternatively the phase retrieval transfer function (PRTF). Several different software packages have been developed to handle single-particle CDI data [144].

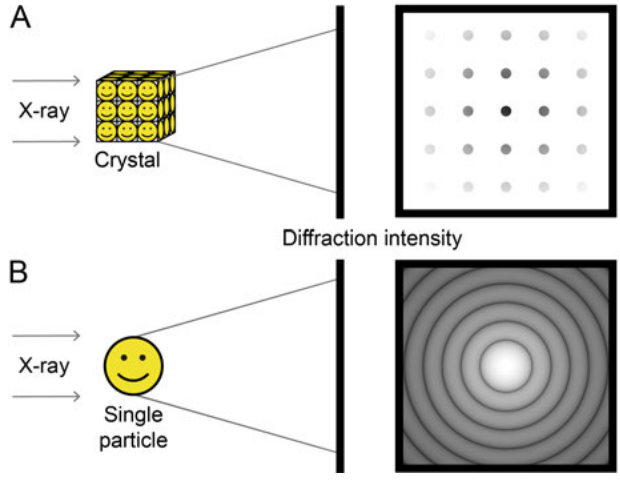

Figure 4.3. Comparison between Bragg and continuous diffraction. (**A**) X-ray diffraction pattern from a crystal. (**B**) A continuous diffraction pattern of a single particle.

4.3. Present investigation – **Paper II**

Early single-particle CDI experiments successfully imaged biological samples of hundred to several hundreds of nm in size and at resolutions in the order of tens of nm [135], [136], [155], [156]. To investigate the limits and solve the challenges for reaching near-atomic resolution, a large international collaboration was formed in 2014, which identified a number of technical and scientific issues [113]. Using samples with well-known characteristics is advantageous during the development of a new method. The aerosol injector

transfers the particles into the vacuum chamber at velocities of tens to hundreds of meters per second and a large fraction will pass the interaction region between shots, hence the sample had to be accessible in high concentrations, up to 10^{14} particles per millilitre. Further, a sample with known structure was considered advantageous, as it would help verifying reconstruction work. Other requirements were monodispersity and compatibility with the sample injection procedure. In addition, an icosahedral-like shape was considered an advantage, at least initially, as it produces a well-known diffraction pattern. Team members within the collaboration initially suggested eight candidate samples (Table 4.1).

Table 4.1. *Candidate samples suggested for experiments performed by the SPI initiative, listed in order of descending size.*

Sample	**Approximate size in diameter (nm)**
Gold octahedra	105
RNA polymerase II	75
RDV	70
PR772 bacteriophage	69
DNA origami pointer	45
Tomato bushy stunt virus (TBSV)	35
Keyhole limpet hemocyanin 1	35
MS2 bacteriophage	27

The investigation described in **Paper II** involved three steps: sample pre-characterisation, XFEL experiment, and data processing and validation (Fig. 4.4 and Fig. 1 in **Paper II**).

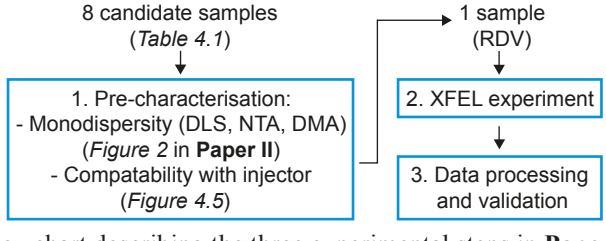

Figure 4.4. Flowchart describing the three experimental steps in **Paper II**. Eight candidate samples (Table 4.1) were initially suggested, from which one candidate sample (RDV) were selected for the XFEL experiment based on the pre-characterisation results. The third step involved e.g. file conversion and technical validation of the data collected at the XFEL.

4.3.1. Aim

The aim of the study presented in **Paper II** was to perform the first single-particle CDI experiment within the SPI initiative collaboration. Additionally, this work included finding an appropriate sample with certain characteristics and to establish a procedure for determining these.

4.3.2. Methodology

All candidate samples listed in *Table 4.1* were pre-characterised in terms of monodispersity and compatibility with the sample injection procedure prior to the XFEL experiment (Fig. 4.4).

Sample pre-characterisation

The combined results from three different particle analysis methods, namely Dynamic Light Scattering (DLS), Nanoparticle Tracking Analysis (NTA), and Differential Mobility Analysis (DMA), were used to evaluate the samples monodispersity. While DLS and NTA were used for measurements in the liquid phase, DMA was used for measurements in the gas phase. Both DLS and NTA have advantages and limitations depending on the sample. In both techniques the Brownian motion is measured using a laser and is matched to an equivalent hydrodynamic diameter. DLS measures a time dependent scattering intensity and an average particle size is calculated. All particles within the tested sample are measured at the same time and the result is therefore skewed towards larger samples as they scatter more intensely. In contrast, NTA tracks the movement of individual particles and therefore does not give an average particle size. Hence, NTA is better at resolving particle populations of similar size and is preferred for polydisperse samples, while DLS, since much more particles are measured, statistically can give more accurate results if the sample is highly monodisperse. Additionally, too small samples can be difficult to measure using NTA and for example the size of the MS2 virus could not be determined using this technique. The purpose of using DMA in addition to the other two techniques is that the gas environment resembles the injection at the XFEL experiment better. As during a single-particle CDI experiment at the XFEL, the sample is aerosolized, which for DMA is achieved through electrospray. The charged droplets are dried and the particles are separated according to their mobility in an electric field, which is related to their size, and a coupled particle counter gives the size distribution.

The second requirement that had to be tested before the XFEL experiment was the compatibility with the sample injection procedure. A similar experimental setup as at the following XFEL experiment was used. Either a glass slide with a gel piece or an EM grid was placed below the injector tip at a distance similar to the X-ray interaction region. The purpose was to confirm that the particles were able to transverse the injector by observing the formation of a sample deposit on the gel piece and that they appeared intact when examined with the EM (Fig. 4.4).

XFEL experiment

The XFEL experiment was carried out at the Coherent X-ray Imaging (CXI) end station [158], [159] at the Linac Coherent Light Source (LCLS) using a photon energy of 7 keV. RDV particles were transferred to a volatile buffer (250 mM ammonium acetate, pH 7.5) at a concentration of 10^{12} particles ml^{-1} and aerosolised into the sample injector using a GDVN (Fig. 4.2B). Diffraction patterns were recorded at a rate of 120 Hz using two Cornell-SLAC Pixel Array Detectors (CSPAD), a large 2.3 Mpix detector located close to the sample for wide angle scattering and another smaller 0.14 Mpix detector located further downstream to detect small angle scattering (Fig. 4.1).

4.3.3. Results

Paper II describes the first experiment performed within the SPI initiative collaboration. We identified a number of desirable sample characteristics (described in *Section 4.3*) and established a procedure for determining these. Several candidate samples fulfilled the requirements, however the results from the pre-characterisation leaned in the favour for RDV and thus, it was selected for the first experiment within the collaboration. We demonstrated that RDV was highly monodisperse (Fig. 2 in **Paper II**) and was compatible with the sample injection procedure (Fig. 4.5).

Paper II is reporting for the first time a single-particle CDI experiment where hard X-rays are used. The high intensity of the beam allowed the recording of diffraction patterns from single RDV particles to a resolution of 5.9 Å (Fig. 6 in **Paper II**). That is the highest resolution detected from a biological sample using this technique.

Beamtime at XFELs is scarce. **Paper II** is a data descriptor that includes a description of the data, the experimental details used to collect the data, and analyses performed to validate the data. The publication was accompanied with depositing the data online on the Coherent X-ray Imaging Data Bank (CXIDB) [160]. These actions enable a wider community to make use of the collected data for algorithm developments, thereby contributing to advance the field further.

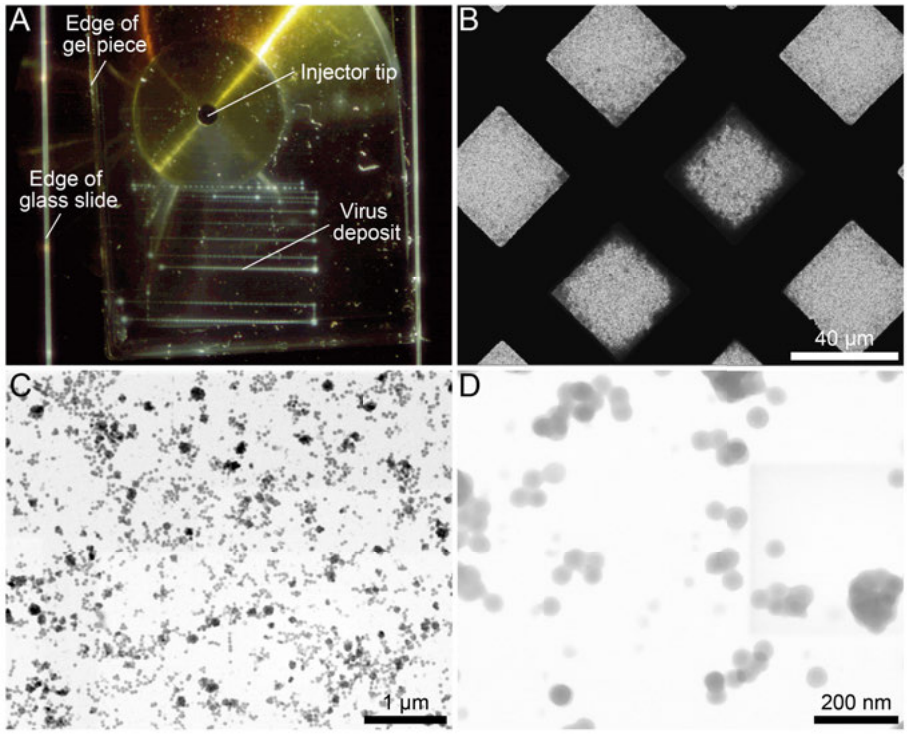

Figure 4.5. Injection testing of RDV. Either a glass slide with a gel piece or an electron microscopy grid was placed below the injector tip. (**A**) The picture shows the injector tip viewed from below. A sample deposit is visible on the gel piece, confirming that RDV particles were able to transverse the injector. (**B**-**D**) An EM grid showing RDV particles at magnifications of (**B**) ~2,000×, (**C**) ~40,000×, and (**D**) ~250,000×. The virus particles appeared intact after transversing the injector.

4.3.4. Discussion

Since the first experiment within the SPI initiative in 2015, described in **Paper II**, the collaboration has had several beamtimes, which have resulted in additional datasets on RDV [161], but also on bacteriophages PR772 [162] and MS2 (*unpublished*). In turn, this have led to that various reconstruction approaches have been explored [134], [163], [164]. However, the many advancements made in the field during the last couple of years, in terms of software [165], [166], reconstruction algorithms [134], [163], [164] and injection methods [153], have to some extent been hampered by the limitations of the past XFEL instruments [157]. The European XFEL, with its high-repetition rate and high-data rate has the chance to take single-particle CDI to the next level. The first SFX [126], [127], [167] and single-particle [168] experiments have successfully been carried out.

In terms of viruses, single-particle CDI has a future potential for studies on large viruses, as they are problematic to study in cryo-EM due to the poor

penetration depth of the electrons and the limited number of particles that can be imaged at a time. However, it is in the category of fast dynamic studies where XFELs have their true potential, and thus the ultimate goal for single-particle CDI is to be able to study biological process at room temperature on a single molecule level at ultrashort (ps-fs) timescales. This will require better algorithms and innovative sample injection methods [169] that also need to be evaluated quantitatively [170].

5. Toxicity of detonation nanodiamonds

Carbon is one of the most important elements as it is essential for life on Earth. Carbon alone can form many different crystal structures, which in turn provide materials with different properties. Diamond is one of the carbon allotropes and is particularly famous for its hardness and thermal conductivity, consequently leading to a major industrial interest. Naturally, diamonds are formed in the Earth's mantle where high temperature and pressure reign.

Nanodiamonds (NDs) are diamonds below 1 μm in size. They can be synthetically produced using several different methods [171], but are also naturally formed in space and have for example been found in meteorites [172] and in protoplanetary disks of certain starts [173]. Originally, they were produced in former Soviet Union in early 1960s from the carbon contained in high-energy explosives. This was however unknown to the rest of the world for another 20-30 years [174]. In fact, the 2012 Ig Nobel Peace Prize was awarded to the SKN Company (Russia) for converting old Russian ammunition into diamonds (https://www.improbable.com/). The so-called detonation synthesis is still one of the most common methods as it produces the smallest NDs (4-5 nm in diameter) in large quantities. While detonation synthesis is a bottom up approach, the second most common method for commercial production of NDs has a top down approach where diamond microcrystals grown at high static pressure and high-temperature (HPHT) are subjected to high-energy ball milling, resulting in particle sizes of 10-20 nm. A unique characteristic of HPHT NDs is the presence of so-called nitrogen-vacancy centres, a point defect in diamond where a nitrogen atom has replaced a carbon atom, creating a vacant site in the lattice. Under blue or green light excitation, photoluminescence appears in the red and near infrared regions. Although DNDs also contain nitrogen impurities (up to 2-3 %), they are primarily in the form of aggregates [175, Ch. 2]. A ND particle consists of a diamond core of sp^3 carbon that is stabilized by terminating the dangling bonds, either by graphitic sp^2 carbon or by various functional groups [176]. Due to their versatile properties, such as hardness, chemical stability, fluorescence and variable surface chemistry, nanodiamonds are attractive for several applications. The current applications of NDs include plating, polishing and as additive in oils and lubricants by taking advantage of the diamonds mechanical properties [176]. The biomedical sector accounts for many of the future applications and includes for example imaging, drug delivery, and tissue engineering and regenerative medicine [177]. Several patents have been

granted for various biological applications, from cosmetics to drug delivery (see examples in review by Mitev *et al.* [178]).

This chapter describes DNDs, and *in vitro* and *in vivo* toxicity experiments performed on the two model systems *E.coli* and zebrafish embryos. **Paper III** describes the results from these tests and the variables that were found decisive for toxicity.

5.1. Detonation nanodiamonds

The detonation synthesis includes two steps. In the first step, carbon-containing explosives, such as trinitrotoluene (TNT) and hexogen, is detonated in a metallic chamber. This produces a diamond-carbon soot mixture that typically contains about 20% nanodiamonds. A second post-synthesis step is then required to purify the soot from heavy metals and graphite. This is usually carried out by oxidation using strong acids like H_2SO_4, HCl and HNO_3. Several parameters of the detonation synthesis can be varied, including the choice of explosives and purification method. Further, the synthesis can be either "dry" or "wet", meaning that the explosion takes place in either gas (e.g. N2, CO2, Ar) or water. Detonation nanodiamond (DND) grains have an average diameter of 4-5 nm, but tend to form aggregates of several hundred nanometres that to a large extent withstand ultrasonication [175, Ch. 2]. Commercial DNDs can contain a large number of elemental impurities, ranging from alkali metals (e.g. Na and K) and alkaline earth metals (e.g. Ca and Mg), to transition metals (e.g. Fe and Cr) and post-transition metals (e.g. Pb and Al), to non-metals (e.g. Cl and S). The impurities are a result of the production process and can be inferred to the materials of e.g. the explosion chamber, coolant and detonator [179].

5.2. Toxicity

Several different toxicity experiments have been performed on DNDs to evaluate both *in vitro* and *in vivo* effects (a comprehensive list can be found in a review by Turcheniuk and Mochalin [177]). However, the reported results are contradictory, which to large extent can be explained by variables such as different experimental designs, concentrations, ND treatments, and time of exposure. The parameters evaluated in the conducted *in vitro* experiments are for example cell viability, oxidative stress, membrane permeability, morphology, and genetic effects [180]–[182] on a range of human cells (lymphocytes [180], blood cells [181], neuroblastoma cells, and macrophages [182]) and bacterial cells [183], [184]. *In vivo* tests have been performed on classical embryo systems, such as *Xenopus laevis* [185], the invertebrate

Caenorhabditis elegans [186], and mammalian models such as mice [187], [188]. The majority of cellular and *in vivo* tests were conducted as so-called acute toxicity tests where DNDs were given in high concentrations for a short period of time. These types of test have been criticized for using unreasonably high ND concentrations [177], however toxic effects have been observed also in tests with longer exposure times at lower concentrations [180], [189]. A possible scenario is that even small amounts of NDs could accumulate in the body, since it has been demonstrated that NDs (of HPHT type) can be entrapped in organs several days after injection [190]. Apart from DND concentration, other parameters affecting toxicity include ND surface functionalizations [182], [184], [185], ND size [180], [183] and purity [177].

5.3. Present investigation – **Paper III**

As described above, a range of toxicity experiments have been performed on DNDs where some concluded no toxicity [182], [186], [187] and others concluded toxicity [180], [183], [188] (see also review by Turcheniuk and Mochalin [177]. Several experiments with toxic outcome have been criticized for being irrelevant due to being performed on impure DNDs at too high concentrations [177], which has led to that NDs are still being described as non-toxic and biocompatible in recent literature [178], [191], [192], with basis of the earliest reports (e.g. ref. [182]). The discrepancy of these tests as well as the increased interest for NDs require more investigations on biocompatibility, a necessary property for realizing the increasing number of suggested biomedical applications, which include for example: root canal filling material [193]–[195]; bioimaging [186]; and cancer medicine [196]. The commercial interest also increases the chance of NDs entering our environment. Experimental design, concentrations, and exposure time have already been mentioned; in addition the contradictory results can also be explained by the various production procedures used by different manufacturers, and the many options for internal and external modifications. Further investigations are needed to understand what characteristics of NDs are decisive for toxicological effects and the underlying mechanisms causing them.

5.3.1. Aim

In **Paper III** the toxicity of a range of different DNDs from different manufacturers were investigated with the aim of elucidating some of the characteristics that could affect ND toxicity. An embryo model system from zebrafish was used to test whether the outcome of the initial *in vitro* experiments on *E. coli* could be correlated with *in vivo* observations.

5.3.2. Methodology

In total, 10 DND products were tested for toxicity (see Table 1 in **Paper III**). These were of various purity grades and from different manufacturers. Two batches were purchased from two products, namely PlasmaChem's ND grade G01 and G02, herein abbreviated *G01-1* and *G02-1* for batch 1 and *G01-2* and *G02-2* for batch 2. All products were tested as received without any additional treatments. A few products, namely *G01-1*, *G02-1* and *S* (the latter from Sigma-Aldrich) were additionally further treated before toxicity testing either by annealing in air and hydrogen gas (*G01-1*, *G02-1* and *S*), ammonia treatment (*G01-1*, *G02-1* and *S*) or modified by polyelectrolyte electrostatic adsorption (*S*+). All products were subjected to antibacterial testing by means of counting colony-forming units (CFU) (Fig. 5.1A), and a smaller number of products (*G01-1*, *G02-1* and *G01*+) that were considered the most important were subjected to fish embryo toxicity (FET) test, which was carried out in a 24-well plate in volumes of 1 mL (Fig. 5.1B). The effect of DNDs on *E. coli* and zebrafish embryos were evaluated based on viability and survival, respectively. In addition, hatching rate and deformities were documented for the zebrafish embryos. The NDs were also characterised by visual appearance of powder and suspension, Fourier transform infrared spectroscopy (FT-IR), Raman spectroscopy, thermal desorption (mass) spectrometry (TDS) and fluorescence.

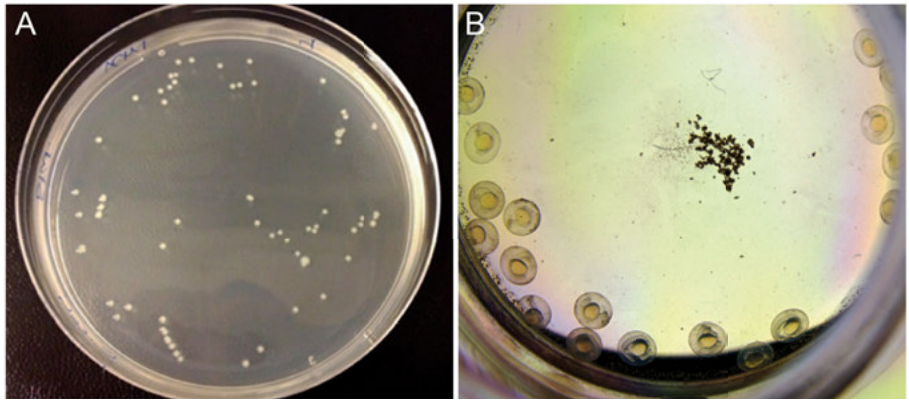

Figure 5.1. Toxicity tests. (**A**) The antibacterial test was carried out by incubating *E.coli* at a cell concentration of ~2×10^8 cells/mL with NDs for 15 minutes. The bacteria/ND suspension was then appropriately diluted (to give a colony count of 30-300) before plating 100 µL on a LB plate. Colonies were counted after incubation at 37°C for 24-48 h and CFU were calculated. (**B**) The fish embryo toxicity test was carried out in a 24-well plate in volumes of 1 mL (image shows one well from above). The embryos were exposed for 96 hours post fertilization (hpf) and their development was monitored every 24 hpf until 120 hpf. The image shows embryos after 24 hpf incubated with *G01-1* at a concentration of 0.1 g/L.

5.3.3. Results

Paper III describes the results from a number of toxicity experiments, from which several conclusions could be inferred. Some ND products were found to be toxic, the majority was however found to be non-toxic even at highly elevated concentrations of 100 g/L (Fig. 1 and 2 in **Paper III**). The results further indicate that the toxicity cannot be correlated with the purity of the product (i.e. graphite and metal content) as suggested by Turcheniuk and Mochalin [177], since a range of ND products of various purity grades were tested from a single manufacturer (PlasmaChem) (Fig. 1 in **Paper III**). Importantly, the *in vitro* results could be correlated with *in vivo* observations on survival, hatching and deformity effects on zebrafish embryos (Fig. 3 and 5 in **Paper III**). Both surface and ND interior were found to be important for toxicity. Surface layers of the nanodiamonds were peeled off with the purpose of investigating the importance of the core for toxicity. The surface peeling was carried out by performing a cyclic annealing procedure, alternating between H_2 at 500°C and air at 450°C [197]. After each annealing step a sample was removed and used in an antibacterial test. The results (Fig. 6 in **Paper III**) demonstrated that the toxicity was inherent in the core. The potency of G02 could be changed by altering the surface groups, both through annealing in hydrogen gas at elevated temperature (Fig. 6 in **Paper III**) and by ammonia treatment (Fig. 7 in **Paper III**). Positively charged NDs (*G01+* and *S+*), which had been subjected to polyelectrolyte electrostatic adsorption by PlasmaChem, were also found to be toxic (Fig. 1, 3, 4 and 5 in **Paper III**). The effect of *G01+* was likely due to the polyelectrolyte treatment as the possible bias of the manufacturer could be ruled out since a ND product from SigmaAldrich (*S*) underwent the same treatment (the ND type named *S+*). One problem when comparing the outcome from previous toxicity tests is the different experimental designs. As such, by testing this range of nanodiamonds we were able to demonstrate that the results from the antibacterial tests varied between manufacturers as well as within the same manufacturer (under otherwise same experimental conditions). This was obvious from our results where different effects were observed between ND types from different manufacturers (Fig. 1 in **Paper III**) and even for the same product from different batches (Fig. 1 **Paper III**). The second batch of G02 (*G02-2*) required addition of much higher concentrations (100 g/L) to obtain the same effect, which was also the same concentration where another ND grade (*G*) exhibited toxicity (Fig. 2 in **Paper III**). In addition, a previous study [184] on bacterial viability of G01 and G02 from PlasmaChem reported opposite effects where G01 instead of G02 were toxic.

5.3.4. Discussion

The numerous toxicity investigations performed by us and others are contradictory [177]. However, several parameters, such as experimental designs,

concentrations, ND treatments, and time of exposure, can explain these variations. In addition, it is clear from the results presented in **Paper III** that toxicity effects are highly dependent on the manufacturing process. The detonation synthesis is uncontrolled and there are several variables that can affect the end product, including the choice of explosives and purification method. Several investigations reporting toxic effects of NDs have been criticised for being conducted on ND powders as received from the manufacturer (which can contain graphite and metal impurities) without further purification at irrelevant concentrations [177]. Metal impurities, mainly originating from the metallic chamber used for the detonation, do exist [179], however, our experiments show that toxicity could not be correlated with impurities such as graphite and metals since not even PlasmaChem's most native ND products (*G/ND raw* and *G/ND pur*) caused toxicity (Fig. 1 in **Paper III**). The concentrations used are likely higher than what humans and aquatic life would ever encounter, nevertheless acute toxicity testing is a widely accepted approach to assess the safety of chemicals, pharmaceuticals, food ingredients and cosmetics. NDs (of HPHT type) have shown to be entrapped in organs several days after injection [190], hence a possible scenario is that even small amounts of NDs could potentially be accumulated in the body.

In **Paper III** we could demonstrate that some DNDs are toxic. Nevertheless the majority of ND products were not, not even at very high concentrations. As such, these results also suggest that many of the suggested biomedical applications [177] could become a reality, although, under the provision that the exact causes of toxicity can be determined and that the parameters of the detonation synthesis can be controlled. Several studies have previously shown that the toxicity is highly dependent on the ND surface chemistry [182], [184], [185], which we also demonstrate in **Paper III**. However, to our knowledge, this is the first study that also indicate that toxicity is inherent also to the ND core, which we showed by peeling of surface layers of a selection of ND products (Fig. 6 in **Paper III**). The effect of the core and surface again demonstrate the importance of having a controlled production procedure. The observed effect by positively charged NDs can possibly be related to how cationic agents used routinely for antimicrobial purposes, for example at hospitals, are functioning. These agents interact with the negatively charged cell surface by displacing the cations that stabilize the cell wall and membrane. It is therefore likely that the positively charged NDs function in a similar manner. In fact, one of the suggested applications of NDs is to be used as a bactericidal agent [184]. To my knowledge, this is also the first study where both *in vitro* and *in vivo* experiments are performed on the same ND products. It is important to notice that the results from both tests correlate; hence cautions should be taken before suggesting the use of NDs as bactericidal agents. Wehling and co-workers do however show that the toxicity effect is decreased with the addition of fetal bovine serum [184].

How the protein corona of NPs in turn can impact the toxicity is a topic on its own [198].

Despite several attempts in trying to characterise the DNDs used in this study (Fig. S1-S9 in **Paper III**), no definite conclusion could be drawn on the exact cause of toxicity observed for G02. Nitrogen is one of the most common impurities in NDs though, and in DNDs it primarily originates from the explosives [175, Ch. 2]. Nitrogen in the form of nitrogen oxide species are formed at high temperatures e.g. inside combustion engines, and are well known to have environmental effects. For these reasons, we wanted to investigate whether toxic nitrogen species could be deliberately incorporated into or attached to non-toxic NDs, such as *G01-1*, by treating with ammonia. This hypothesis turned out to be false. The treatment did however turn the toxic *G02-1* non-toxic (Fig. 7 in **Paper III**). Moreover, the Fourier Transform Infrared Spectroscopy (FT-IR) spectra displayed sharp peaks for the toxic *G* and *G02-1* (Fig. S1 in **Paper III**) at 1380 cm^{-1}. In **Paper III**, we postulated that nitrogen groups could cause these peaks. Nitrogen related features in a FTIR spectra are found in the region of 1000 – 4000 cm^{-1} [199], [200] and some groups, such as NO_2 and NO_3, give rise to sharp peaks similar to the ones seen for *G* and *G02-1*. Several nitrogen oxide species are well known to be toxic. The presence of such groups on *G02-1* could perhaps explain the effect of the ammonium hydroxide treatment since nitrogen oxide surface species could create the harmless products N_2 and H_2O in a reaction with NH_4OH.

NDs have great potential in several areas of biomedicine, where drug delivery and diagnostics are the most heavily researched applications [177]. However, the many studies on the toxicological effects of NDs cannot be disregarded, despite the discrepancies and criticism. One of the future challenges is to better understand the detonation synthesis and the effect various parameters have on toxicity. The toxicity tests do require refinement as well. The acute toxicity tests performed to date could for example be accompanied with studies that address the long-term effects by using lower ND concentrations. Understanding the underlying mechanisms of ND toxicity is also a subject where efforts should be invested.

6. Concluding remarks and future perspectives

NPs have for a long time contributed to shaping the world in which we live in and will continue to do so. Studying these particles is important for understanding their impact on living beings and the environment. In this thesis, both natural and anthropogenic NPs have been studied by different means. In **Paper I,** single-particle cryo-EM was used to determine the atomic structure of an algal virus. As this is one of the few atomic models of an algal virus this study contributed to new knowledge about algal viruses, which is a category of viruses that historically has been underexplored. The investigation also provided insights on *Picornavirales* evolution by identifying structural traits that possibly have been acquired or lost among viruses of the order that infect different hosts. **Paper II** contributed to the development of single-particle CDI, which has the potential of revolutionizing structural biology and unravel many biological mysteries impossible to uncover with any other method. **Paper III** contributed to the rapidly expanding field of nanomaterial research by providing new insights on DND toxicity. The results highlighted the limitations with the existing detonation synthesis for producing NDs for biomedical applications. More research is required for understanding the toxicity mechanisms and for improving existing methods or developing new ND production procedures.

Since the discovery of the infectious power of viruses in late 19th century, virology research has made several ground-breaking discoveries [201] and it is impossible to foresee where this science is heading in the future. Animal viruses, including the vaccines and therapeutics against them, are certainly going to continue to occupy a large part of future research. Due to the present COVID-19 outbreak, a related topic of great importance in future virology research is emerging viruses. Emerging viruses are challenging as no therapeutics or vaccines exist to combat them, and historical examples of this include HIV and influenza. Emerging viruses could pose more challenges in the future due to the increasing world population and movement of people around the world [202]. As described, virus research has historically to large extent been focused on viruses that affect humans, domestic animals and plants, as well as those viruses that are easy handle in the laboratory, e.g. bacteriophages. The most current (2018b) release from the ICTV lists 5,561 different virus species [37], but new numbers on virus abundance and diversity in various environments are constantly being released, which greatly

exceed the official ICTV numbers [30], [203]–[208]. For example, a recent study showed that the oceans, which occupy the greatest abundance of viruses, host about 200,000 different DNA virus populations [204]. Virus ecology and the virosphere are areas where extensive efforts are likely in the future. As already touched upon in the introduction, the origin and evolution of viruses has been highly debated topic the last decade [20], [22], [23], [39, Ch. 11], [40]–[44], and will probably continue to be so.

Conventional X-ray crystallography has been the most powerful tool in structural biology and provided researchers with a deeper understanding of macromolecules and their functions. However, structural biology is currently in a boom where new methods are constantly being developed and refinements and varieties of the existing ones emerge. Cryo-EM has certainly made an impact during the last couple of years [209], and will advance further as new developments are being made on hardware and software [99], [210]–[217]. Virology is one of the fields that have benefitted the most. Electron diffraction has also gained increased attention lately [218], and was recently also demonstrated for serial electron crystallography [219]. XFEL based structural methods, having the ability to outrun most radiation damage, allows imaging of biological processes on fs timescales at room temperature. The XFELs impact on crystallography is obvious with the approximately 200 structures currently deposited in the PDB. They have enabled diffraction from smaller crystals than ever before [129], determination of novel proteins [220] and membrane protein [221] structures, and capturing of fast conformational changes in protein complexes [222]. Serial crystallography is nowadays also established at synchrotrons [223], [224]. New sample-delivery methods [225]–[228] and data-analysis algorithms are continuously being developed [142], [229]–[231]. However, many of the most interesting samples are difficult or impossible to crystallize and to image those samples on short timescales new methodology is required. Single-particle CDI has also made progress the last couple of years, but at a comparably slower pace since more challenges exist. Smaller samples [162] compared to the earliest experiments of giant viruses [135] and cells [149] have been imaged, work dedicated to sample delivery [153], [170] has been undertaken, and software has been developed [144]. Moreover, the first 3D reconstructions have been published [134], [156], [157]. A lot of work is owed to the SPI initiative collaboration [113] that has been managed by the LCLS (including **Paper II**). The first crystallography and single-particle experiments carried out at the European XFEL that started operating in September 2017, demonstrated the feasibility of the methods at megahertz repetition rate [27], [126], [127], [168], and it will be interesting to follow future developments that will enable the instruments full capacity. In terms of viruses, they have served as ideal reference samples for developing single-particle CDI due to their reproducibility, shape and large size. Virus crystallography

at XFELs is still rare [226], [232], [233], even though advantages may exist [226], [234].

Several studies suggest a toxic nature of anthropogenic NPs, where the effects on health of incidental NPs (such as pulmonary, cardiovascular and cancerogenic) have been the main subjects of investigation. This is justified since the greatest threat from anthropogenic particles on human health and environment is currently from the incidental NPs. Engineered NPs are still produced on a comparably small scale and in most consumer products the NPs are incorporated or attached to materials. Apart from combustion-derived NPs another increasing and current source of incidental particles are microplastics (including nanoplastics) [14], which was highlighted in a recent report from WWF claiming that we eat the equivalent of a credit card's worth of microplastics each week [15]. It has for example been shown that nanoplastics can travel through the food chain and alter the behaviour of the top consumer [235] and that long-term exposure reduces life-time [236]. Apart from microplastics, the risk of being exposed and affected by engineered NPs is currently probably low. However, the nanotechnology field is growing rapidly (Fig. 2.4) and a number of NP-based consumer products are constantly increasing [3]–[6]. Hence, the exposure risk of engineered NPs could increase in the future. Currently, the most common exposure route is dermal, but as the number of food and food packaging products containing NPs increases, the oral route can become an increased source of exposure [6]. The largest risk regarding engineered NPs is currently due to occupational exposure through the respiratory system by workers producing nanomaterial, where documented effects have already been reported. For that selected group of people, future efforts should be put into introducing regulatory-binding occupational exposure limits for engineered nanomaterials (currently non-existing) and to identifying biomarkers for exposure [74]. The toxicological studies have been criticised [79], [177], but they cannot be ignored. Surely, the experimental methods have the potential to improve and become standardised, and attempts in that direction have already been initiated [237].

Several future challenges related to NPs lie ahead. Reducing the amount of particles originating from industrial activities that are harmful for both humans and the environment is one example, preventing epidemics and pandemics is another, which due to the increasing world population and the ease of travelling anywhere in the world could have serious future consequences. However, the future also holds great promise for the many applications for engineered NPs and continuing method developments in structural biology will contribute to increase our understanding of the particles around us.

Author's contribution

Paper I
I took part in the data collection and performed most of the data analysis. I had a major role in writing the manuscript and prepared most of the figures.

Paper II
I was involved in the pre-characterisation tests performed on the candidate samples. I participated in the experiment at the LCLS where I was responsible for preparing the sample. I contributed to writing the paper and preparing figures.

Paper III
I performed all the experiments on *E. coli* and zebrafish embryos, wrote the manuscript and prepared all figures. The experiments were first carried out on *E.coli* alone, but I initiated and planned the tests on zebrafish embryos. I was involved in the characterisation of the NDs.

Populärvetenskaplig sammanfattning

Överallt, runtomkring oss finns mycket små partiklar som inte går att se med blotta ögat, men som har stor inverkan på vårt dagliga liv. Partiklarna kallas nanopartiklar och har en storlek på mindre än 100 nanometer. 1 nanometer är en miljarddels meter, vilket kan liknas med att om en nanopartikel vore stor som en fotboll, då skulle fotbollen vara stor som jordklotet. Det finns två typer av nanopartiklar – de som förekommer naturligt, t.ex. virus och vulkanaska, och de som skapats av oss människor. Den sistnämnda typen kan t.ex. bildas i förbrännings- och industriprocesser, men kan också tillverkas medvetet med särskilda egenskaper och kallas då tillverkade nanopartiklar. I media framhålls nanopartiklar ofta som något med en negativ inverkan på människor och vår omgivning, vilket är förståeligt med tanke på att t.ex. virus historiskt sett har orsakat några av de dödligaste pandemierna och skördat flera miljarder människoliv. Trots allt orsakar förmodligen de flesta virus ingen skada och det finns till och med virus som har en positiv påverkan på t.ex. människor och växter. De nanopartiklar som skapats av oss människor kan också påverka oss negativt, t.ex. de luftföroreningar i stadsmiljöer som vi inandas. Men det går också att tillverka nanopartiklar med positiva egenskaper, och vilka skulle kunna användas i flera medicinska tillämpningar, t.ex. inom kontraströntgen och för cancerbehandling.

Den här avhandlingen är baserad på tre delarbeten och i varje del beskrivs olika experiment som har gjorts på olika nanopartiklar. Gemensamt för **Delarbete I** och **II** är att virus har studerats med olika avbildningstekniker. För att avbilda något som inte går att se med blotta ögat måste man ta hjälp av speciella instrument. Ett optiskt mikroskop använder sig av det synliga ljuset och kan därför endast förstora föremål ungefär 1000 gånger, till exempelvis för att studera celler och deras uppbyggnad. Det synliga ljuset har relativt lång våglängd och därför syns inte mindre föremål. Elektroner (**Delarbete I**) och röntgenljus (**Delarbete II**) har däremot mycket kortare våglängd och kan användas för att se föremål som är tusentals gånger mindre än en cell, till exempelvis viruspartiklar.

I **Delarbete I** användes ett elektronmikroskop för att avbilda ett algvirus. Tekniken som används kallas kryoelektronmikroskopi och är en relativt välutvecklad metod, vilket resulterade i att en högupplöst bild av viruset kunde återskapas. Virus förekommer i olika former (t.ex. avlånga eller runda), men alla virus har som gemensamt att de är uppbyggda av genetiskt material/arvsmassa som är omslutet av ett proteinskal. Virus kan inte föröka sig på

egen hand utan behöver ta sig in i en värdcell, i detta fall en algcell. Cellen tillverkar då nya viruspartiklar som i sin tur kan infektera andra celler. Viruset som studerats i **Delarbete I** kallas CtenRNAV-II och är uppbyggt av ett runt proteinskal bestående av 180 proteiner. En av virusskalets funktioner är att binda till cellernas yta. Proteinerna i virusskalet utvecklas olika hos olika virus för att de ska kunna känna igen olika celltyper. CtenRNAV-II känner endast igen och infekterar encelliga alger, så kallade kiselalger, men är besläktad med andra virus som infekterar växter, ryggradslösa djur (t.ex. insekter) och ryggradsdjur (t.ex. människor). Poliovirus och hepatit A virus är exempel på välkända och besläktade virus som endast infekterar människor. Allt levande på jorden, t.ex. alger, insekter och djur, har ett gemensamt ursprung. De första levande organismerna som utvecklades var encelliga och de var troligen också värdar till de tidigaste virusen på jorden. Genom att jämföra proteinsskalet hos algviruset med proteinskalet hos de besläktade virusen som infekterar flercelliga organismer kunde vi därför kartlägga hur olika virus har förändrats och anpassats under livets utveckling för att kunna känna igen olika celltyper.

I **Delarbete II** användes en annan avbildningsmetod, vilken heter singelpartikel koherent avbildning med röntgendiffraktion (SP-CDI från engelskans ”single-particle coherent diffractive imaging”). Till skillnad från kryoelektronmikroskopi är SP-CDI mer outvecklad och man kan för närvarande därför inte erhålla högupplösta strukturer. En annan skillnad är att ingen direkt avbildning av viruset fås i SP-CDI, istället fås ett så kallat diffraktionsmönster som sedan måste omvandlas med hjälp av datorprogram till en bild av viruset. Instrumentet som används i SP-CDI kallas frielektronlaser, vilken krävs för att producera ett mycket starkt röntgenljus, upp till en miljard biljoner gånger starkare än det röntgenljus som används på sjukhuset för att undersöka benbrott. Förutom ljusets styrka är en annan viktig egenskap att röntgenljuset avges i form av extremt korta pulser. En puls är endast en miljondel av en miljarddels sekund lång. Detta gör det möjligt att få ett diffraktionsmönster innan viruset exploderar av det starka röntgenljuset. I **Delarbete II** användes metoden till att avbilda ett risvirus. Tidigare hade man lyckats avbilda små celler och stora virus, men här presenteras resultat som visar att även mindre virus är möjliga att se. Med ytterligare utveckling är förhoppningen att tekniken ska ge högupplösta bilder som i kryoelektronmikroskopi, och att den även ska kunna användas på enskilda proteiner och för att studera deras extremt snabba rörelser. Framtiden får utvisa om det också är experimentellt möjligt.

Virus är naturliga nanopartiklar. I **Delarbete III** studerades istället tillverkade nanopartiklar, specifikt nanodiamanter. Precis som stora diamanter består nanodiamanter till största delen av kolatomer och kan därför tillverkas genom att detonera kolrika sprängämnen, så som trinitrotoluen (TNT). Nanodiamanter har många attraktiva egenskaper och nuvarande användningsområden som t.ex. polering och plätering tar tillvara på nanodiamanternas mekaniska egenskaper. Nanodiamanter utvecklas för att i framtiden

också kunna användas inom den biomedicinska sektorn, t.ex. för att transportera läkemedel i kroppen och för att bygga implantat. För att nanodiamanter ska kunna användas i människor är det viktigt att säkerställa att de är ofarliga. I **Delarbete III** testades därför hur en rad olika nanodiamanter påverkar överlevnaden av bakterier och zebrafisk embryon. Resultaten visade att några nanodiamanter var giftiga och den negativa påverkan kunde härledas till olika egenskaper hos både kärnan och ytan hos nanodiamanterna. Dessutom pekade resultaten på att den nuvarande tillverkningsprocessen där sprängämnen detoneras är opålitlig eftersom slutprodukten varierar kraftigt mellan olika tillverkare, och till och med inom samma tillverkare. För att nanodiamanter i framtiden ska kunna användas inom den biomedicinska sektorn behöver därför den nuvarande tillverkningsprocessen förbättras eller nya metoder för att tillverka nanodiamanter utvecklas.

Acknowledgements

This thesis would not have been possible without the help and support from many persons.

I would especially like to acknowledge Marvin. Thank you for giving me the opportunity to do my PhD. I am grateful for all the opportunities you given me to work on many different projects and for all the traveling for beam-times, conferences and courses. Thank you for your kindness, for believing in me and for encouraging me to do things that I enjoy, but also things that are "good for me".

Kenta, thank you for giving me the opportunity to work on your projects and for sharing your knowledge on viruses and cryo-EM. Your hard work and engagement has been very encouraging.

To Inger, and Janos, thank you for your generosity, for sharing your life-long experience, and for creating a great atmosphere in the programme.

Karin, thank you for first introducing me to the interesting world of viruses, for your advice when I revisited your old PhD friend MS2, but also for the nice times during lunch and fika breaks.

Daniel L, I would like to thank you for your kindness, encouragement and for always taking time to answer my questions.

To my awesome roommate, Laura: your passion and hard work is inspiring! Thank you for just being there and for your kind words when I needed it.

Margareta, thank you for your support and management of the lab, and for your tireless attempts to keep order.

I am thankful to Dirk, Anna S-L and Gunilla for your help and advice in the wet lab.

I would like to thank the large and multidisciplinary "XFEL team": He-manth, Benedikt, Johan, Gjis, Max, Alberto, Carl, Jing, Tomas, Jonas, Ida,

Daniel W, Kerstin, Frederico, Martin, Filipe and Nic. Thank you everyone for all the fun during beamtimes and for everything that you taught me.

I would also like to thank Peter and group members, Ana, Sourav and Ricardo for bringing new life to the programme. It was great to see the empty offices and lab benches filled again and thank you for the nice conversations during fika and lunch breaks.

Han, Alfredo, August and Tej, it is likewise great to have you joined the programme. I wish you Han, Alfredo and August the best of luck with your PhD's!

This thesis would also not have been possible without the facilities SLAC, European XFEL and SciLifeLab, and their staff. I especially would like to thank Andy for you hard work in managing the SPI initiative, and Marta and Julian for you help with various cryo-EM projects.

Slutligen vill jag tacka min familj. Tack mamma och pappa för allt stöd under alla år. Mamma, jag beundrar din ihärdighet och hjälp i skolans tidigaste år, i allt från att traggla glosor till matteproblem. Och tack pappa för att du tidigt fick mig intresserad av naturvetenskap och teknik, och för att du stöttat och väglett mig i mina val. Astrid, du ger mig så mycket lycka varenda dag, tack för det. Och framför allt tack till Philip, för att du följde med mig till Uppsala, för att du stöttat mig när det varit jobbigt och för alla fina stunder utanför jobb.

References

[1] 'Cambridge Dictionary'. https://dictionary.cambridge.org/ (accessed Feb. 20, 2020).

[2] D. R. Boverhof *et al.*, 'Comparative assessment of nanomaterial definitions and safety evaluation considerations', *Regul. Toxicol. Pharmacol.*, vol. 73, no. 1, pp. 137–150, Oct. 2015, doi: 10.1016/j.yrtph.2015.06.001.

[3] 'Nanotechnology Consumer Products Inventory'. https://www.nanotechproject.org/cpi/ (accessed Feb. 24, 2020).

[4] 'StatNano'. https://statnano.com/nanomaterials (accessed Feb. 24, 2020).

[5] 'The Nanodatabase'. http://nanodb.dk/ (accessed Feb. 24, 2020).

[6] M. E. Vance *et al.*, 'Nanotechnology in the real world: Redeveloping the nanomaterial consumer products inventory', *Beilstein J. Nanotechnol.*, vol. 6, pp. 1769–1780, Aug. 2015, doi: 10.3762/bjnano.6.181.

[7] C. A. Suttle, 'Marine viruses — major players in the global ecosystem', *Nat. Rev. Microbiol.*, vol. 5, no. 10, pp. 801–812, Oct. 2007, doi: 10.1038/nrmicro1750.

[8] D. Enard, L. Cai, C. Gwennap, and D. A. Petrov, 'Viruses are a dominant driver of protein adaptation in mammals', *eLife*, vol. 5, p. e12469, May 2016, doi: 10.7554/eLife.12469.

[9] P. Manrique, B. Bolduc, S. T. Walk, J. van der Oost, W. M. de Vos, and M. J. Young, 'Healthy human gut phageome', *Proc. Natl. Acad. Sci.*, vol. 113, no. 37, pp. 10400–10405, Sep. 2016, doi: 10.1073/pnas.1601060113.

[10] M. J. Roossinck, 'The good viruses: viral mutualistic symbioses', *Nat. Rev. Microbiol.*, vol. 9, no. 2, pp. 99–108, Feb. 2011, doi: 10.1038/nrmicro2491.

[11] M. Yang, K. Sunderland, and C. Mao, 'Virus-Derived Peptides for Clinical Applications', *Chem. Rev.*, vol. 117, no. 15, pp. 10377–10402, Aug. 2017, doi: 10.1021/acs.chemrev.7b00100.

[12] D. M. Lin, B. Koskella, and H. C. Lin, 'Phage therapy: An alternative to antibiotics in the age of multi-drug resistance', *World J. Gastrointest. Pharmacol. Ther.*, vol. 8, no. 3, p. 162, 2017, doi: 10.4292/wjgpt.v8.i3.162.

[13] A. Munke *et al.*, 'Phage display and kinetic selection of antibodies that specifically inhibit amyloid self-replication', *Proc. Natl. Acad. Sci.*, vol. 114, no. 25, pp. 6444–6449, Jun. 2017, doi: 10.1073/pnas.1700407114.

[14] A. A. de Souza Machado, W. Kloas, C. Zarfl, S. Hempel, and M. C. Rillig, 'Microplastics as an emerging threat to terrestrial ecosystems', *Glob. Change Biol.*, vol. 24, no. 4, pp. 1405–1416, Apr. 2018, doi: 10.1111/gcb.14020.

[15] W. de Wit and N. Bigaud, 'No plastic in nature: assessing plastic ingestion from nature to people', WWF - World Wide Fund For nature, Jun. 2019.

[16] S. Thomas, *Industrial applications of nanomaterials*, 1st edition. Cambridge, CA: Elsevier, 2019.

[17] D. Ivanofsky, 'Concerning the mosaic disease of the tobacco plant', *St. Petersburg Acad. Imp. Sci. Bull*, vol. 35, pp. 67–70, 1892.

[18] M. W. Beijerinck, ‘Concerning a contagium vivum fluidum as a cause of the spot-disease of tobacco leaves’, *Verh. Akad. Wetensch., Amsterdam, II*, vol. 6, pp. 3–21, 1898.
[19] B. L. Scola, ‘A Giant Virus in Amoebae’, *Science*, vol. 299, no. 5615, pp. 2033–2033, Mar. 2003, doi: 10.1126/science.1081867.
[20] C. Abergel, M. Legendre, and J.-M. Claverie, ‘The rapidly expanding universe of giant viruses: Mimivirus, Pandoravirus, Pithovirus and Mollivirus’, *FEMS Microbiol. Rev.*, vol. 39, no. 6, pp. 779–796, Nov. 2015, doi: 10.1093/femsre/fuv037.
[21] D. Raoult and P. Forterre, ‘Redefining viruses: lessons from Mimivirus’, *Nat. Rev. Microbiol.*, vol. 6, no. 4, pp. 315–319, Apr. 2008, doi: 10.1038/nrmicro1858.
[22] D. Moreira and P. López-García, ‘Ten reasons to exclude viruses from the tree of life’, *Nat. Rev. Microbiol.*, vol. 7, no. 4, pp. 306–311, Apr. 2009, doi: 10.1038/nrmicro2108.
[23] M. Krupovic, V. V. Dolja, and E. V. Koonin, ‘Origin of viruses: primordial replicators recruiting capsids from hosts’, *Nat. Rev. Microbiol.*, vol. 17, no. 7, pp. 449–458, Jul. 2019, doi: 10.1038/s41579-019-0205-6.
[24] M. J. Roossinck and E. R. Bazán, ‘Symbiosis: Viruses as Intimate Partners’, *Annu. Rev. Virol.*, vol. 4, no. 1, pp. 123–139, Sep. 2017, doi: 10.1146/annurev-virology-110615-042323.
[25] E. V. Koonin, T. G. Senkevich, and V. V. Dolja, ‘The ancient Virus World and evolution of cells’, *Biol. Direct*, vol. 1, no. 1, p. 29, 2006, doi: 10.1186/1745-6150-1-29.
[26] R. J. Gifford, ‘Viral evolution in deep time: lentiviruses and mammals’, *Trends Genet.*, vol. 28, no. 2, pp. 89–100, Feb. 2012, doi: 10.1016/j.tig.2011.11.003.
[27] C. Gisriel *et al.*, ‘Membrane protein megahertz crystallography at the European XFEL’, *Nat. Commun.*, vol. 10, no. 1, p. 5021, Dec. 2019, doi: 10.1038/s41467-019-12955-3.
[28] H. S. Malik, ‘Retroviruses push the envelope for mammalian placentation’, *Proc. Natl. Acad. Sci.*, vol. 109, no. 7, pp. 2184–2185, Feb. 2012, doi: 10.1073/pnas.1121365109.
[29] J. A. Fuhrman, ‘Marine viruses and their biogeochemical and ecological effects’, *Nature*, vol. 399, no. 6736, pp. 541–548, Jun. 1999, doi: 10.1038/21119.
[30] R. W. Hendrix, M. C. M. Smith, R. N. Burns, M. E. Ford, and G. F. Hatfull, ‘Evolutionary relationships among diverse bacteriophages and prophages: All the world’s a phage’, *Proc. Natl. Acad. Sci.*, vol. 96, no. 5, pp. 2192–2197, Mar. 1999, doi: 10.1073/pnas.96.5.2192.
[31] B. R. Wasik and P. E. Turner, ‘On the Biological Success of Viruses’, *Annu. Rev. Microbiol.*, vol. 67, no. 1, pp. 519–541, Sep. 2013, doi: 10.1146/annurev-micro-090110-102833.
[32] M. Krupovic and D. H. Bamford, ‘Order to the Viral Universe’, *J. Virol.*, vol. 84, no. 24, pp. 12476–12479, Dec. 2010, doi: 10.1128/JVI.01489-10.
[33] A. Nasir and G. Caetano-Anollés, ‘Identification of Capsid/Coat Related Protein Folds and Their Utility for Virus Classification’, *Front. Microbiol.*, vol. 8, Mar. 2017, doi: 10.3389/fmicb.2017.00380.
[34] D. Baltimore, ‘Expression of animal virus genomes’, *Bacteriol. Rev.*, vol. 35, no. 3, pp. 235–241, Sep. 1971.

[35] E. V. Koonin, V. V. Dolja, and M. Krupovic, 'Origins and evolution of viruses of eukaryotes: The ultimate modularity', *Virology*, vol. 479–480, pp. 2–25, May 2015, doi: 10.1016/j.virol.2015.02.039.

[36] E. J. Lefkowitz, D. M. Dempsey, R. C. Hendrickson, R. J. Orton, S. G. Siddell, and D. B. Smith, 'Virus taxonomy: the database of the International Committee on Taxonomy of Viruses (ICTV)', *Nucleic Acids Res.*, vol. 46, no. D1, pp. D708–D717, Jan. 2018, doi: 10.1093/nar/gkx932.

[37] 'International Committee on Taxonomy of Viruses (ICTV)', *ICTV Virus Taxonomy: 2018b Release*, Jul. 2018. https://talk.ictvonline.org/taxonomy/ (accessed Nov. 07, 2019).

[38] M. Krupovic and E. V. Koonin, 'Multiple origins of viral capsid proteins from cellular ancestors', *Proc. Natl. Acad. Sci. U. S. A.*, vol. 114, no. 12, pp. E2401–E2410, 21 2017, doi: 10.1073/pnas.1621061114.

[39] D. M. Knipe and P. M. Howley, Eds., *Fields virology*, 6th ed. Philadelphia, PA: Wolters Kluwer/Lippincott Williams & Wilkins Health, 2013.

[40] J.-M. Claverie and C. Abergel, 'Mimivirus: the emerging paradox of quasi-autonomous viruses', *Trends Genet.*, vol. 26, no. 10, pp. 431–437, Oct. 2010, doi: 10.1016/j.tig.2010.07.003.

[41] D. Raoult, 'The 1.2-Megabase Genome Sequence of Mimivirus', *Science*, vol. 306, no. 5700, pp. 1344–1350, Nov. 2004, doi: 10.1126/science.1101485.

[42] N. Yutin, Y. I. Wolf, and E. V. Koonin, 'Origin of giant viruses from smaller DNA viruses not from a fourth domain of cellular life', *Virology*, vol. 466–467, pp. 38–52, Oct. 2014, doi: 10.1016/j.virol.2014.06.032.

[43] J. Durzyńska and A. Goździcka-Józefiak, 'Viruses and cells intertwined since the dawn of evolution', *Virol. J.*, vol. 12, no. 1, p. 169, Oct. 2015, doi: 10.1186/s12985-015-0400-7.

[44] G. Kostyrka, 'What roles for viruses in origin of life scenarios?', *Stud. Hist. Philos. Sci. Part C Stud. Hist. Philos. Biol. Biomed. Sci.*, vol. 59, pp. 135–144, Oct. 2016, doi: 10.1016/j.shpsc.2016.02.014.

[45] J. A. Gilbert, M. J. Blaser, J. G. Caporaso, J. K. Jansson, S. V. Lynch, and R. Knight, 'Current understanding of the human microbiome', *Nat. Med.*, vol. 24, no. 4, pp. 392–400, Apr. 2018, doi: 10.1038/nm.4517.

[46] J. J. Barr *et al.*, 'Bacteriophage adhering to mucus provide a non-host-derived immunity', *Proc. Natl. Acad. Sci.*, vol. 110, no. 26, pp. 10771–10776, Jun. 2013, doi: 10.1073/pnas.1305923110.

[47] M. J. Roossinck, 'Move Over, Bacteria! Viruses Make Their Mark as Mutualistic Microbial Symbionts', *J. Virol.*, vol. 89, no. 13, pp. 6532–6535, Jul. 2015, doi: 10.1128/JVI.02974-14.

[48] P. Xu, F. Chen, J. P. Mannas, T. Feldman, L. W. Sumner, and M. J. Roossinck, 'Virus infection improves drought tolerance', *New Phytol.*, vol. 180, no. 4, pp. 911–921, Dec. 2008, doi: 10.1111/j.1469-8137.2008.02627.x.

[49] E. V. Ryabov, G. Keane, N. Naish, C. Evered, and D. Winstanley, 'Densovirus induces winged morphs in asexual clones of the rosy apple aphid, Dysaphis plantaginea', *Proc. Natl. Acad. Sci.*, vol. 106, no. 21, pp. 8465–8470, May 2009, doi: 10.1073/pnas.0901389106.

[50] S. Heringlake *et al.*, 'GB virus C/hepatitis G virus infection: a favorable prognostic factor in human immunodeficiency virus-infected patients?', *J. Infect. Dis.*, vol. 177, no. 6, pp. 1723–1726, Jun. 1998, doi: 10.1086/517431.

[51] A. E. Zimmerman *et al.*, 'Metabolic and biogeochemical consequences of viral infection in aquatic ecosystems', *Nat. Rev. Microbiol.*, vol. 18, no. 1, pp. 21–34, Jan. 2020, doi: 10.1038/s41579-019-0270-x.

[52] M. Henry and L. Debarbieux, ‘Tools from viruses: Bacteriophage successes and beyond’, *Spec. Issue Viruses Microbes*, vol. 434, no. 2, pp. 151–161, Dec. 2012, doi: 10.1016/j.virol.2012.09.017.
[53] K. Lundstrom, ‘Viral Vectors in Gene Therapy’, *Dis. Basel Switz.*, vol. 6, no. 2, p. 42, May 2018, doi: 10.3390/diseases6020042.
[54] H. M. Babiker, I. B. Riaz, M. Husnain, and M. Borad, ‘Oncolytic virotherapy including Rigvir and standard therapies in malignant melanoma’, *Oncolytic Virotherapy*, vol. Volume 6, pp. 11–18, Feb. 2017, doi: 10.2147/OV.S100072.
[55] R. T. Schooley *et al.*, ‘Development and Use of Personalized Bacteriophage-Based Therapeutic Cocktails To Treat a Patient with a Disseminated Resistant Acinetobacter baumannii Infection’, *Antimicrob. Agents Chemother.*, vol. 61, no. 10, pp. e00954-17, /aac/61/10/e00954-17.atom, Oct. 2017, doi: 10.1128/AAC.00954-17.
[56] A. Wright, C. H. Hawkins, E. E. Änggård, and D. R. Harper, ‘A controlled clinical trial of a therapeutic bacteriophage preparation in chronic otitis due to antibiotic-resistant *Pseudomonas aeruginosa* ; a preliminary report of efficacy’, *Clin. Otolaryngol.*, vol. 34, no. 4, pp. 349–357, Aug. 2009, doi: 10.1111/j.1749-4486.2009.01973.x.
[57] M. Jalasvuori and J. K. H. Bamford, ‘Did the Ancient Crenarchaeal Viruses from the Dawn of Life Survive Exceptionally Well the Eons of Meteorite Bombardment?’, *Astrobiology*, vol. 9, no. 1, pp. 131–137, Jan. 2009, doi: 10.1089/ast.2007.0189.
[58] D. L. D. Caspar and A. Klug, ‘Physical Principles in the Construction of Regular Viruses’, *Cold Spring Harb. Symp. Quant. Biol.*, vol. 27, no. 0, pp. 1–24, Jan. 1962, doi: 10.1101/SQB.1962.027.001.005.
[59] N. G. A. Abrescia, D. H. Bamford, J. M. Grimes, and D. I. Stuart, ‘Structure Unifies the Viral Universe’, *Annu. Rev. Biochem.*, vol. 81, no. 1, pp. 795–822, Jul. 2012, doi: 10.1146/annurev-biochem-060910-095130.
[60] D. H. Bamford, J. M. Grimes, and D. I. Stuart, ‘What does structure tell us about virus evolution?’, *Curr. Opin. Struct. Biol.*, vol. 15, no. 6, pp. 655–663, Dec. 2005, doi: 10.1016/j.sbi.2005.10.012.
[61] M. Krupovic and D. H. Bamford, ‘Double-stranded DNA viruses: 20 families and only five different architectural principles for virion assembly’, *Virus Struct. Funct.*, vol. 1, no. 2, pp. 118–124, Aug. 2011, doi: 10.1016/j.coviro.2011.06.001.
[62] B. L. Nannenga, D. Shi, A. G. W. Leslie, and T. Gonen, ‘High-resolution structure determination by continuous-rotation data collection in MicroED’, *Nat. Methods*, vol. 11, no. 9, pp. 927–930, Sep. 2014, doi: 10.1038/nmeth.3043.
[63] I. Khan, K. Saeed, and I. Khan, ‘Nanoparticles: Properties, applications and toxicities’, *Arab. J. Chem.*, vol. 12, no. 7, pp. 908–931, Nov. 2019, doi: 10.1016/j.arabjc.2017.05.011.
[64] G. Oberdörster, E. Oberdörster, and J. Oberdörster, ‘Nanotoxicology: An Emerging Discipline Evolving from Studies of Ultrafine Particles’, *Environ. Health Perspect.*, vol. 113, no. 7, pp. 823–839, Jul. 2005, doi: 10.1289/ehp.7339.
[65] J. D’Silva, ‘What’s in a Name? – Defining a “Nanomaterial” for Regulatory Purposes in Europe’, *Eur. J. Risk Regul.*, vol. 2, no. 1, pp. 85–91, Mar. 2011, doi: 10.1017/S1867299X00000659.
[66] S. F. Hansen, ‘React now regarding nanomaterial regulation’, *Nat. Nanotechnol.*, vol. 12, no. 8, pp. 714–716, Aug. 2017, doi: 10.1038/nnano.2017.163.

[67] N. B. Hartmann *et al.*, 'Are We Speaking the Same Language? Recommendations for a Definition and Categorization Framework for Plastic Debris', *Environ. Sci. Technol.*, vol. 53, no. 3, pp. 1039–1047, Feb. 2019, doi: 10.1021/acs.est.8b05297.
[68] A. D. Maynard, 'Don't define nanomaterials', *Nature*, vol. 475, no. 7354, pp. 31–31, Jul. 2011, doi: 10.1038/475031a.
[69] M. Miernicki, T. Hofmann, I. Eisenberger, F. von der Kammer, and A. Praetorius, 'Legal and practical challenges in classifying nanomaterials according to regulatory definitions', *Nat. Nanotechnol.*, vol. 14, no. 3, pp. 208–216, Mar. 2019, doi: 10.1038/s41565-019-0396-z.
[70] H. Rauscher, K. Rasmussen, and B. Sokull-Klüttgen, 'Regulatory Aspects of Nanomaterials in the EU', *Chem. Ing. Tech.*, vol. 89, no. 3, pp. 224–231, Mar. 2017, doi: 10.1002/cite.201600076.
[71] H. Stamm, 'Nanomaterials should be defined', *Nature*, vol. 476, no. 7361, pp. 399–399, Aug. 2011, doi: 10.1038/476399c.
[72] Y. Pan *et al.*, 'Size-Dependent Cytotoxicity of Gold Nanoparticles', *Small*, vol. 3, no. 11, pp. 1941–1949, Nov. 2007, doi: 10.1002/smll.200700378.
[73] E. Fröhlich, 'The role of surface charge in cellular uptake and cytotoxicity of medical nanoparticles', *Int. J. Nanomedicine*, p. 5577, Nov. 2012, doi: 10.2147/IJN.S36111.
[74] A. Pietroiusti, H. Stockmann-Juvala, F. Lucaroni, and K. Savolainen, 'Nanomaterial exposure, toxicity, and impact on human health', *Wiley Interdiscip. Rev. Nanomed. Nanobiotechnol.*, vol. 10, no. 5, p. e1513, Sep. 2018, doi: 10.1002/wnan.1513.
[75] W. G. Kreyling *et al.*, 'Size dependence of the translocation of inhaled iridium and carbon nanoparticle aggregates from the lung of rats to the blood and secondary target organs', *Inhal. Toxicol.*, vol. 21, no. sup1, pp. 55–60, Jul. 2009, doi: 10.1080/08958370902942517.
[76] P. Kinaret *et al.*, 'Inhalation and Oropharyngeal Aspiration Exposure to Rod-Like Carbon Nanotubes Induce Similar Airway Inflammation and Biological Responses in Mouse Lungs', *ACS Nano*, vol. 11, no. 1, pp. 291–303, Jan. 2017, doi: 10.1021/acsnano.6b05652.
[77] J. P. Ryman-Rasmussen, E. W. Tewksbury, O. R. Moss, M. F. Cesta, B. A. Wong, and J. C. Bonner, 'Inhaled Multiwalled Carbon Nanotubes Potentiate Airway Fibrosis in Murine Allergic Asthma', *Am. J. Respir. Cell Mol. Biol.*, vol. 40, no. 3, pp. 349–358, Mar. 2009, doi: 10.1165/rcmb.2008-0276OC.
[78] N. A. Monteiro-Riviere and F. L. Filon, 'Skin', in *Adverse Effects of Engineered Nanomaterials*, Elsevier, 2017, pp. 357–380.
[79] H. F. Krug, 'Nanosafety Research-Are We on the Right Track?', *Angew. Chem. Int. Ed.*, p. n/a-n/a, 2014, doi: 10.1002/anie.201403367.
[80] A. C. Anselmo and S. Mitragotri, 'Nanoparticles in the clinic: An update', *Bioeng. Transl. Med.*, vol. 4, no. 3, Sep. 2019, doi: 10.1002/btm2.10143.
[81] B. Pelaz *et al.*, 'Diverse Applications of Nanomedicine', *ACS Nano*, vol. 11, no. 3, pp. 2313–2381, Mar. 2017, doi: 10.1021/acsnano.6b06040.
[82] S. Coy, E. Gann, H. Pound, S. Short, and S. Wilhelm, 'Viruses of Eukaryotic Algae: Diversity, Methods for Detection, and Future Directions', *Viruses*, vol. 10, no. 9, p. 487, Sep. 2018, doi: 10.3390/v10090487.
[83] D. Sahoo and J. Seckbach, Eds., *The Algae World*, vol. 26. Dordrecht: Springer Netherlands, 2015.

[84] K. Nagasaki, K. Tarutani, and M. Yamaguchi, ‘Growth Characteristics of Heterosigma akashiwo Virus and Its Possible Use as a Microbiological Agent for Red Tide Control’, *Appl. Environ. Microbiol.*, vol. 65, no. 3, p. 898, Mar. 1999.
[85] J. Seckbach and P. Kociolek, Eds., *The Diatom World*, vol. 19. Dordrecht: Springer Netherlands, 2011.
[86] L. Arsenieff *et al.*, ‘First Viruses Infecting the Marine Diatom Guinardia delicatula’, *Front. Microbiol.*, vol. 9, p. 3235, Jan. 2019, doi: 10.3389/fmicb.2018.03235.
[87] K. Kimura and Y. Tomaru, ‘Discovery of Two Novel Viruses Expands the Diversity of Single-Stranded DNA and Single-Stranded RNA Viruses Infecting a Cosmopolitan Marine Diatom’, *Appl. Environ. Microbiol.*, vol. 81, no. 3, pp. 1120–1131, Feb. 2015, doi: 10.1128/AEM.02380-14.
[88] K. Toyoda *et al.*, ‘Novel marine diatom ssRNA virus NitRevRNAV infecting Nitzschia reversa’, *Plant Ecol. Evol.*, vol. 152, no. 2, pp. 178–187, Jul. 2019, doi: 10.5091/plecevo.2019.1615.
[89] K. Toyoda, K. Kimura, N. Hata, N. Nakayama, K. Nagasaki, and Y. Tomaru, ‘Isolation and characterization of a single-stranded DNA virus infecting the marine planktonic diatom Chaetoceros sp. (strain TG07-C28)’, *Plankton Benthos Res.*, vol. 7, no. 1, pp. 20–28, 2012, doi: 10.3800/pbr.7.20.
[90] D. Schatz *et al.*, ‘Hijacking of an autophagy-like process is critical for the life cycle of a DNA virus infecting oceanic algal blooms’, *New Phytol.*, vol. 204, no. 4, pp. 854–863, Dec. 2014, doi: 10.1111/nph.13008.
[91] B. A. Wagstaff, M. Rejzek, and R. A. Field, ‘Identification of a Kdn biosynthesis pathway in the haptophyte *Prymnesium parvum* suggests widespread sialic acid biosynthesis among microalgae’, *J. Biol. Chem.*, vol. 293, no. 42, pp. 16277–16290, Oct. 2018, doi: 10.1074/jbc.RA118.004921.
[92] Y. Shirai, Y. Tomaru, Y. Takao, H. Suzuki, T. Nagumo, and K. Nagasaki, ‘Isolation and characterization of a single-stranded RNA virus infecting the marine planktonic diatom Chaetoceros tenuissimus Meunier’, *Appl. Environ. Microbiol.*, vol. 74, no. 13, pp. 4022–4027, Jul. 2008, doi: 10.1128/AEM.00509-08.
[93] Y. Tomaru, Y. Shirai, K. Toyoda, and K. Nagasaki, ‘Isolation and characterisation of a single-stranded DNA virus infecting the marine planktonic diatom Chaetoceros tenuissimus’, *Aquat. Microb. Ecol.*, vol. 64, no. 2, pp. 175–184, Sep. 2011, doi: 10.3354/ame01517.
[94] O. Le Gall *et al.*, ‘Picornavirales, a proposed order of positive-sense single-stranded RNA viruses with a pseudo-T = 3 virion architecture’, *Arch. Virol.*, vol. 153, no. 4, pp. 715–727, Apr. 2008, doi: 10.1007/s00705-008-0041-x.
[95] J. Tate, L. Liljas, P. Scotti, P. Christian, T. Lin, and J. E. Johnson, ‘The crystal structure of cricket paralysis virus: the first view of a new virus family’, *Nat. Struct. Biol.*, vol. 6, no. 8, pp. 765–774, Aug. 1999, doi: 10.1038/11543.
[96] S. Kalynych, A. Přidal, L. Pálková, Y. Levdansky, J. R. de Miranda, and P. Plevka, ‘Virion Structure of Iflavirus Slow Bee Paralysis Virus at 2.6-Angstrom Resolution’, *J. Virol.*, vol. 90, no. 16, pp. 7444–7455, Aug. 2016, doi: 10.1128/JVI.00680-16.
[97] X. Dai *et al.*, ‘In situ structures of the genome and genome-delivery apparatus in a single-stranded RNA virus’, *Nature*, vol. 541, no. 7635, pp. 112–116, Jan. 2017, doi: 10.1038/nature20589.
[98] S. L. Ilca *et al.*, ‘Multiple liquid crystalline geometries of highly compacted nucleic acid in a dsRNA virus’, *Nature*, vol. 570, no. 7760, pp. 252–256, Jun. 2019, doi: 10.1038/s41586-019-1229-9.

[99] J. Zivanov, T. Nakane, and S. H. W. Scheres, 'Estimation of High-Order Aberrations and Anisotropic Magnification from Cryo-EM Datasets in RELION-3.1', Biophysics, preprint, Oct. 2019. doi: 10.1101/798066.
[100] S. H. W. Scheres, 'RELION: Implementation of a Bayesian approach to cryo-EM structure determination', *J. Struct. Biol.*, vol. 180, no. 3, pp. 519–530, Dec. 2012, doi: 10.1016/j.jsb.2012.09.006.
[101] M. G. Rossmann, Y. He, and R. J. Kuhn, 'Picornavirus–receptor interactions', *Trends Microbiol.*, vol. 10, no. 7, pp. 324–331, Jul. 2002, doi: 10.1016/S0966-842X(02)02383-1.
[102] G. Zocher *et al.*, 'A Sialic Acid Binding Site in a Human Picornavirus', *PLoS Pathog.*, vol. 10, no. 10, p. e1004401, Oct. 2014, doi: 10.1371/journal.ppat.1004401.
[103] M. G. Rossmann, 'The canyon hypothesis. Hiding the host cell receptor attachment site on a viral surface from immune surveillance', *J. Biol. Chem.*, vol. 264, no. 25, pp. 14587–14590, Sep. 1989.
[104] X. Wang *et al.*, 'Hepatitis A virus and the origins of picornaviruses', *Nature*, vol. 517, no. 7532, pp. 85–88, Jan. 2015, doi: 10.1038/nature13806.
[105] D. Buchta *et al.*, 'Enterovirus particles expel capsid pentamers to enable genome release', *Nat. Commun.*, vol. 10, no. 1, Dec. 2019, doi: 10.1038/s41467-019-09132-x.
[106] J. Snijder *et al.*, 'Probing the biophysical interplay between a viral genome and its capsid', *Nat. Chem.*, vol. 5, p. 502, Apr. 2013.
[107] P. Danthi, M. Tosteson, Q. -h. Li, and M. Chow, 'Genome Delivery and Ion Channel Properties Are Altered in VP4 Mutants of Poliovirus', *J. Virol.*, vol. 77, no. 9, pp. 5266–5274, May 2003, doi: 10.1128/JVI.77.9.5266-5274.2003.
[108] R. Sánchez-Eugenia, J. Goikolea, D. Gil-Cartón, L. Sánchez-Magraner, and D. M. A. Guérin, 'Triatoma Virus Recombinant VP4 Protein Induces Membrane Permeability through Dynamic Pores', *J. Virol.*, vol. 89, no. 8, pp. 4645–4654, Apr. 2015, doi: 10.1128/JVI.00011-15.
[109] M. Zaitlin, 'The Discovery of the Causal Agent of the Tobacco Mosaic Disease', in *Discoveries in Plant Biology*, WORLD SCIENTIFIC, 1998, pp. 105–110.
[110] S. C. Harrison, A. J. Olson, C. E. Schutt, F. K. Winkler, and G. Bricogne, 'Tomato bushy stunt virus at 2.9 Å resolution', *Nature*, vol. 276, no. 5686, pp. 368–373, Nov. 1978, doi: 10.1038/276368a0.
[111] V. Nicaise, 'Crop immunity against viruses: outcomes and future challenges', *Front. Plant Sci.*, vol. 5, Nov. 2014, doi: 10.3389/fpls.2014.00660.
[112] R. Hull, *Plant Virology*. San Diego, UNITED STATES: Elsevier Science & Technology, 2013.
[113] A. Aquila *et al.*, 'The linac coherent light source single particle imaging road map', *Struct. Dyn.*, vol. 2, no. 4, p. 041701, Jul. 2015, doi: 10.1063/1.4918726.
[114] T. Wei *et al.*, 'The Spread of Rice Dwarf Virus among Cells of Its Insect Vector Exploits Virus-Induced Tubular Structures', *J. Virol.*, vol. 80, no. 17, pp. 8593–8602, Sep. 2006, doi: 10.1128/JVI.00537-06.
[115] F. Thomas, S. Adamo, and J. Moore, 'Parasitic manipulation: where are we and where should we go?', *Behav. Processes*, vol. 68, no. 3, pp. 185–199, Mar. 2005, doi: 10.1016/j.beproc.2004.06.010.
[116] Q. Wang *et al.*, 'Rice dwarf virus infection alters green rice leafhopper host preference and feeding behavior', *PLOS ONE*, vol. 13, no. 9, p. e0203364, Sep. 2018, doi: 10.1371/journal.pone.0203364.

[117] K. C. Ling, *The international rice research institute*. Los Banos, Philippines, 1972.
[118] T. Fukushi, E. Shikato, I. Kimura, and M. Nemoto, 'Electron microscopic studies on the rice dwarf virus', *Proc. Japan Acad.*, vol. 36, pp. 352–357, 1960.
[119] A. Nakagawa *et al.*, 'The atomic structure of rice dwarf virus reveals the self-assembly mechanism of component proteins', *Struct. Lond. Engl. 1993*, vol. 11, no. 10, pp. 1227–1238, Oct. 2003.
[120] N. Miyazaki *et al.*, 'Electron microscopic imaging revealed the flexible filamentous structure of the cell attachment protein P2 of *Rice dwarf virus* located around the icosahedral 5-fold axes', *J. Biochem. (Tokyo)*, vol. 159, no. 2, pp. 181–190, Feb. 2016, doi: 10.1093/jb/mvv092.
[121] K. Hagiwara, 'Assembly of single-shelled cores and double-shelled virus-like particles after baculovirus expression of major structural proteins P3, P7 and P8 of Rice dwarf virus', *J. Gen. Virol.*, vol. 84, no. 4, pp. 981–984, Apr. 2003, doi: 10.1099/vir.0.18904-0.
[122] A. Nakagawa, N. Miyazaki, and A. Higashiura, 'Hierarchical structure assembly model of rice dwarf virus particle formation', *Biophys. Rev.*, vol. 10, no. 2, pp. 659–665, Apr. 2018, doi: 10.1007/s12551-017-0375-2.
[123] Y. Nakamichi *et al.*, 'An Assembly Intermediate Structure of Rice Dwarf Virus Reveals a Hierarchical Outer Capsid Shell Assembly Mechanism', *Structure*, vol. 27, no. 3, pp. 439-448.e3, Mar. 2019, doi: 10.1016/j.str.2018.10.029.
[124] W. C. Rontgen, 'ON A NEW KIND OF RAYS', *Science*, vol. 3, no. 59, pp. 227–231, Feb. 1896, doi: 10.1126/science.3.59.227.
[125] F. R. Elder, A. M. Gurewitsch, R. V. Langmuir, and H. C. Pollock, 'Radiation from Electrons in a Synchrotron', *Phys. Rev.*, vol. 71, no. 11, pp. 829–830, Jun. 1947, doi: 10.1103/PhysRev.71.829.5.
[126] M. L. Grünbein *et al.*, 'Megahertz data collection from protein microcrystals at an X-ray free-electron laser', *Nat. Commun.*, vol. 9, no. 1, p. 3487, Dec. 2018, doi: 10.1038/s41467-018-05953-4.
[127] M. O. Wiedorn *et al.*, 'Megahertz serial crystallography', *Nat. Commun.*, vol. 9, no. 1, p. 4025, Oct. 2018, doi: 10.1038/s41467-018-06156-7.
[128] R. Neutze, R. Wouts, D. van der Spoel, E. Weckert, and J. Hajdu, 'Potential for biomolecular imaging with femtosecond X-ray pulses', *Nature*, vol. 406, no. 6797, pp. 752–757, Aug. 2000, doi: 10.1038/35021099.
[129] H. N. Chapman *et al.*, 'Femtosecond X-ray protein nanocrystallography', *Nature*, vol. 470, no. 7332, pp. 73–77, Feb. 2011, doi: 10.1038/nature09750.
[130] K. Pande *et al.*, 'Femtosecond structural dynamics drives the trans/cis isomerization in photoactive yellow protein', *Science*, vol. 352, no. 6286, pp. 725–729, May 2016, doi: 10.1126/science.aad5081.
[131] M. Suga *et al.*, 'Native structure of photosystem II at 1.95 Å resolution viewed by femtosecond X-ray pulses', *Nature*, vol. 517, no. 7532, pp. 99–103, Nov. 2014, doi: 10.1038/nature13991.
[132] G. Brändén *et al.*, 'Coherent diffractive imaging of microtubules using an X-ray laser', *Nat. Commun.*, vol. 10, no. 1, p. 2589, Dec. 2019, doi: 10.1038/s41467-019-10448-x.
[133] H. N. Chapman *et al.*, 'Femtosecond diffractive imaging with a soft-X-ray free-electron laser', *Nat Phys*, vol. 2, no. 12, pp. 839–843, Dec. 2006, doi: 10.1038/nphys461.

[134] R. P. Kurta *et al.*, 'Correlations in Scattered X-Ray Laser Pulses Reveal Nanoscale Structural Features of Viruses', *Phys. Rev. Lett.*, vol. 119, no. 15, Oct. 2017, doi: 10.1103/PhysRevLett.119.158102.
[135] M. M. Seibert *et al.*, 'Single mimivirus particles intercepted and imaged with an X-ray laser', *Nature*, vol. 470, no. 7332, pp. 78–81, Feb. 2011, doi: 10.1038/nature09748.
[136] G. van der Schot *et al.*, 'Imaging single cells in a beam of live cyanobacteria with an X-ray laser', *Nat. Commun.*, vol. 6, p. 5704, Feb. 2015, doi: 10.1038/ncomms6704.
[137] P. Nogly *et al.*, 'Retinal isomerization in bacteriorhodopsin captured by a femtosecond x-ray laser', *Science*, p. eaat0094, Jun. 2018, doi: 10.1126/science.aat0094.
[138] B. Davy *et al.*, 'Reducing sample consumption for serial crystallography using acoustic drop ejection', *J. Synchrotron Radiat.*, vol. 26, no. 5, pp. 1820–1825, Sep. 2019, doi: 10.1107/S1600577519009329.
[139] D. P. DePonte *et al.*, 'Gas dynamic virtual nozzle for generation of microscopic droplet streams', *J. Phys. Appl. Phys.*, vol. 41, no. 19, p. 195505, Oct. 2008, doi: 10.1088/0022-3727/41/19/195505.
[140] M. L. Grünbein and G. Nass Kovacs, 'Sample delivery for serial crystallography at free-electron lasers and synchrotrons', *Acta Crystallogr. Sect. Struct. Biol.*, vol. 75, no. 2, pp. 178–191, Feb. 2019, doi: 10.1107/S205979831801567X.
[141] M. L. Shelby *et al.*, 'A fixed-target platform for serial femtosecond crystallography in a hydrated environment', *IUCrJ*, vol. 7, no. 1, pp. 30–41, Jan. 2020, doi: 10.1107/S2052252519014003.
[142] A. Barty *et al.*, '*Cheetah* : software for high-throughput reduction and analysis of serial femtosecond X-ray diffraction data', *J. Appl. Crystallogr.*, vol. 47, no. 3, pp. 1118–1131, Jun. 2014, doi: 10.1107/S1600576714007626.
[143] K. Hirata *et al.*, '*ZOO* : an automatic data-collection system for high-throughput structure analysis in protein microcrystallography', *Acta Crystallogr. Sect. Struct. Biol.*, vol. 75, no. 2, pp. 138–150, Feb. 2019, doi: 10.1107/S2059798318017795.
[144] F. R. N. C. Maia, T. A. White, N. D. Loh, and J. Hajdu, 'CCP-FEL: a collection of computer programs for free-electron laser research', *J. Appl. Crystallogr.*, vol. 49, no. 4, pp. 1117–1120, Aug. 2016, doi: 10.1107/S1600576716011134.
[145] T. A. White *et al.*, 'Crystallographic data processing for free-electron laser sources', *Acta Crystallogr. D Biol. Crystallogr.*, vol. 69, no. 7, pp. 1231–1240, Jul. 2013, doi: 10.1107/S0907444913013620.
[146] J. M. Martin-Garcia *et al.*, 'Serial millisecond crystallography of membrane and soluble protein microcrystals using synchrotron radiation', *IUCrJ*, vol. 4, no. 4, pp. 439–454, Jul. 2017, doi: 10.1107/S205225251700570X.
[147] J. Miao, P. Charalambous, J. Kirz, and D. Sayre, 'Extending the methodology of X-ray crystallography to allow imaging of micrometre-sized non-crystalline specimens', *Nature*, vol. 400, no. 6742, pp. 342–344, Jul. 1999, doi: 10.1038/22498.
[148] J. Fan *et al.*, 'Single-pulse enhanced coherent diffraction imaging of bacteria with an X-ray free-electron laser', *Sci. Rep.*, vol. 6, no. 1, p. 34008, Sep. 2016, doi: 10.1038/srep34008.
[149] M. M. Seibert *et al.*, 'Femtosecond diffractive imaging of biological cells', *J. Phys. B At. Mol. Opt. Phys.*, vol. 43, no. 19, p. 194015, Oct. 2010, doi: 10.1088/0953-4075/43/19/194015.

[150] P. Hart *et al.*, 'The CSPAD megapixel x-ray camera at LCLS', Oct. 2012, p. 85040C, doi: 10.1117/12.930924.
[151] S. Herrmann *et al.*, 'CSPAD upgrades and CSPAD V1.5 at LCLS', *J. Phys. Conf. Ser.*, vol. 493, p. 012013, Mar. 2014, doi: 10.1088/1742-6596/493/1/012013.
[152] K. Mühlig, A. M. Gañán-Calvo, J. Andreasson, D. S. D. Larsson, J. Hajdu, and M. Svenda, 'Nanometre-sized droplets from a gas dynamic virtual nozzle', *J. Appl. Crystallogr.*, vol. 52, no. 4, pp. 800–808, Aug. 2019, doi: 10.1107/S1600576719008318.
[153] J. Bielecki *et al.*, 'Electrospray sample injection for single-particle imaging with x-ray lasers', *Sci. Adv.*, vol. 5, no. 5, p. eaav8801, May 2019, doi: 10.1126/sciadv.aav8801.
[154] B. J. Daurer *et al.*, 'Experimental strategies for imaging bioparticles with femtosecond hard X-ray pulses', *IUCrJ*, vol. 4, no. 3, pp. 251–262, May 2017, doi: 10.1107/S2052252517003591.
[155] M. F. Hantke *et al.*, 'High-throughput imaging of heterogeneous cell organelles with an X-ray laser', *Nat. Photonics*, vol. 8, no. 12, pp. 943–949, Nov. 2014, doi: 10.1038/nphoton.2014.270.
[156] T. Ekeberg *et al.*, 'Three-Dimensional Reconstruction of the Giant Mimivirus Particle with an X-Ray Free-Electron Laser', *Phys. Rev. Lett.*, vol. 114, no. 9, Mar. 2015, doi: 10.1103/PhysRevLett.114.098102.
[157] I. V. Lundholm *et al.*, 'Considerations for three-dimensional image reconstruction from experimental data in coherent diffractive imaging', *IUCrJ*, vol. 5, no. 5, pp. 531–541, Sep. 2018, doi: 10.1107/S2052252518010047.
[158] S. Boutet and G. J Williams, 'The Coherent X-ray Imaging (CXI) instrument at the Linac Coherent Light Source (LCLS)', *New J. Phys.*, vol. 12, no. 3, p. 035024, Mar. 2010, doi: 10.1088/1367-2630/12/3/035024.
[159] M. Liang *et al.*, 'The Coherent X-ray Imaging instrument at the Linac Coherent Light Source', *J. Synchrotron Radiat.*, vol. 22, no. 3, pp. 514–519, May 2015, doi: 10.1107/S160057751500449X.
[160] F. R. N. C. Maia, 'The Coherent X-ray Imaging Data Bank', *Nat. Methods*, vol. 9, no. 9, pp. 854–855, Aug. 2012, doi: 10.1038/nmeth.2110.
[161] A. Munke *et al.*, 'Coherent diffraction of single Rice Dwarf Virus particles using soft X-rays at the Linac Coherent Light Source', *Nature Scientific Data*, 2018.
[162] H. K. N. Reddy *et al.*, 'Coherent soft X-ray diffraction imaging of coliphage PR772 at the Linac coherent light source', *Sci. Data*, vol. 4, p. 170079, Jun. 2017.
[163] A. Hosseinizadeh *et al.*, 'Conformational landscape of a virus by single-particle X-ray scattering', *Nat. Methods*, vol. 14, no. 9, pp. 877–881, Sep. 2017, doi: 10.1038/nmeth.4395.
[164] M. Rose *et al.*, 'Single-particle imaging without symmetry constraints at an X-ray free-electron laser', *IUCrJ*, vol. 5, no. 6, pp. 727–736, Nov. 2018, doi: 10.1107/S205225251801120X.
[165] B. J. Daurer, M. F. Hantke, C. Nettelblad, and F. R. N. C. Maia, 'Hummingbird: monitoring and analyzing flash X-ray imaging experiments in real time', *J. Appl. Crystallogr.*, vol. 49, no. Pt 3, pp. 1042–1047, Jun. 2016, doi: 10.1107/S1600576716005926.
[166] M. F. Hantke, T. Ekeberg, and F. R. N. C. Maia, '*Condor* : a simulation tool for flash X-ray imaging', *J. Appl. Crystallogr.*, vol. 49, no. 4, pp. 1356–1362, Aug. 2016, doi: 10.1107/S1600576716009213.

[167] O. Yefanov *et al.*, 'Evaluation of serial crystallographic structure determination within megahertz pulse trains', *Struct. Dyn.*, vol. 6, no. 6, p. 064702, Nov. 2019, doi: 10.1063/1.5124387.
[168] E. Sobolev *et al.*, 'Megahertz single-particle imaging at the European XFEL', *ArXiv191210796 Phys.*, Dec. 2019, Accessed: Feb. 18, 2020. [Online]. Available: http://arxiv.org/abs/1912.10796.
[169] C. Uetrecht *et al.*, 'Native mass spectrometry provides sufficient ion flux for XFEL single-particle imaging', *J. Synchrotron Radiat.*, vol. 26, no. 3, pp. 653–659, May 2019, doi: 10.1107/S1600577519002686.
[170] M. F. Hantke *et al.*, 'Rayleigh-scattering microscopy for tracking and sizing nanoparticles in focused aerosol beams', *IUCrJ*, vol. 5, no. 6, pp. 673–680, Nov. 2018, doi: 10.1107/S2052252518010837.
[171] V. N. Mochalin, O. Shenderova, D. Ho, and Y. Gogotsi, 'The properties and applications of nanodiamonds', *Nat. Nanotechnol.*, vol. 7, no. 1, pp. 11–23, Dec. 2011, doi: 10.1038/nnano.2011.209.
[172] E. Anders and E. Zinner, 'Interstellar Grains in Primitive Meteorites: Diamond, Silicon Carbide, and Graphite', *Meteoritics*, vol. 28, no. 4, pp. 490–514, Sep. 1993, doi: 10.1111/j.1945-5100.1993.tb00274.x.
[173] M. Goto *et al.*, 'SPATIALLY RESOLVED 3 μm SPECTROSCOPY OF ELIAS 1: ORIGIN OF DIAMONDS IN PROTOPLANETARY DISKS', *Astrophys. J.*, vol. 693, no. 1, pp. 610–616, Mar. 2009, doi: 10.1088/0004-637x/693/1/610.
[174] V. V. Danilenko, 'On the history of the discovery of nanodiamond synthesis', *Phys. Solid State*, vol. 46, no. 4, pp. 595–599, Apr. 2004, doi: 10.1134/1.1711431.
[175] *Nanodiamonds*. Elsevier, 2017.
[176] V. Y. Dolmatov, 'Detonation-synthesis nanodiamonds: synthesis, structure, properties and applications', *Russ. Chem. Rev.*, vol. 76, no. 4, pp. 339–360, Apr. 2007, doi: 10.1070/RC2007v076n04ABEH003643.
[177] K. Turcheniuk and V. N. Mochalin, 'Biomedical applications of nanodiamond (Review)', *Nanotechnology*, vol. 28, no. 25, p. 252001, Jun. 2017, doi: 10.1088/1361-6528/aa6ae4.
[178] S. Chauhan, N. Jain, and U. Nagaich, 'Nanodiamonds with powerful ability for drug delivery and biomedical applications: Recent updates on in vivo study and patents', *J. Pharm. Anal.*, vol. 10, no. 1, pp. 1–12, Feb. 2020, doi: 10.1016/j.jpha.2019.09.003.
[179] D. P. Mitev, A. T. Townsend, B. Paull, and P. N. Nesterenko, 'Screening of elemental impurities in commercial detonation nanodiamond using sector field inductively coupled plasma-mass spectrometry', *J. Mater. Sci.*, vol. 49, no. 10, pp. 3573–3591, May 2014, doi: 10.1007/s10853-014-8036-3.
[180] N. Dworak, M. Wnuk, J. Zebrowski, G. Bartosz, and A. Lewinska, 'Genotoxic and mutagenic activity of diamond nanoparticles in human peripheral lymphocytes in vitro', *Carbon*, vol. 68, pp. 763–776, Mar. 2014, doi: 10.1016/j.carbon.2013.11.067.
[181] A. P. Puzyr, D. A. Neshumayev, S. V. Tarskikh, G. V. Makarskaya, V. Yu. Dolmatov, and V. S. Bondar, 'Destruction of human blood cells in interaction with detonation nanodiamonds in experiments in vitro', *Diam. Relat. Mater.*, vol. 13, no. 11–12, pp. 2020–2023, Nov. 2004, doi: 10.1016/j.diamond.2004.06.003.
[182] A. M. Schrand *et al.*, 'Are Diamond Nanoparticles Cytotoxic?', *J. Phys. Chem. B*, vol. 111, no. 1, pp. 2–7, Jan. 2007, doi: 10.1021/jp066387v.

[183] J. Beranová *et al.*, 'Sensitivity of bacteria to diamond nanoparticles of various size differs in gram-positive and gram-negative cells', *FEMS Microbiol. Lett.*, vol. 351, no. 2, pp. 179–186, Feb. 2014, doi: 10.1111/1574-6968.12373.
[184] J. Wehling, R. Dringen, R. N. Zare, M. Maas, and K. Rezwan, 'Bactericidal Activity of Partially Oxidized Nanodiamonds', *ACS Nano*, vol. 8, no. 6, pp. 6475–6483, Jun. 2014, doi: 10.1021/nn502230m.
[185] L. Marcon, F. Riquet, D. Vicogne, S. Szunerits, J.-F. Bodart, and R. Boukherroub, 'Cellular and in vivo toxicity of functionalized nanodiamond in Xenopus embryos', *J. Mater. Chem.*, vol. 20, no. 37, p. 8064, 2010, doi: 10.1039/c0jm01570a.
[186] N. Mohan, C.-S. Chen, H.-H. Hsieh, Y.-C. Wu, and H.-C. Chang, 'In Vivo Imaging and Toxicity Assessments of Fluorescent Nanodiamonds in *Caenorhabditis elegans*', *Nano Lett.*, vol. 10, no. 9, pp. 3692–3699, Sep. 2010, doi: 10.1021/nl1021909.
[187] Y. Yuan *et al.*, 'Pulmonary toxicity and translocation of nanodiamonds in mice', *Diam. Relat. Mater.*, vol. 19, no. 4, pp. 291–299, Apr. 2010, doi: 10.1016/j.diamond.2009.11.022.
[188] X. Zhang *et al.*, 'Biodistribution and toxicity of nanodiamonds in mice after intratracheal instillation', *Toxicol. Lett.*, vol. 198, no. 2, pp. 237–243, Oct. 2010, doi: 10.1016/j.toxlet.2010.07.001.
[189] A. Cid *et al.*, 'Oxidative stress and histological changes following exposure to diamond nanoparticles in the freshwater Asian clam Corbicula fluminea (Müller, 1774)', *J. Hazard. Mater.*, vol. 284, pp. 27–34, Mar. 2015, doi: 10.1016/j.jhazmat.2014.10.055.
[190] Y. Yuan, Y. Chen, J.-H. Liu, H. Wang, and Y. Liu, 'Biodistribution and fate of nanodiamonds in vivo', *Diam. Relat. Mater.*, vol. 18, no. 1, pp. 95–100, Jan. 2009, doi: 10.1016/j.diamond.2008.10.031.
[191] D. Zupančič, M. E. Kreft, M. Grdadolnik, D. Mitev, A. Iglič, and P. Veranič, 'Detonation nanodiamonds are promising nontoxic delivery system for urothelial cells', *Protoplasma*, vol. 255, no. 1, pp. 419–423, Jan. 2018, doi: 10.1007/s00709-017-1146-4.
[192] H. Tinwala and S. Wairkar, 'Production, surface modification and biomedical applications of nanodiamonds: A sparkling tool for theranostics', *Mater. Sci. Eng. C*, vol. 97, pp. 913–931, Apr. 2019, doi: 10.1016/j.msec.2018.12.073.
[193] D.-K. Lee *et al.*, 'Nanodiamond–Gutta Percha Composite Biomaterials for Root Canal Therapy', *ACS Nano*, vol. 9, no. 11, pp. 11490–11501, Nov. 2015, doi: 10.1021/acsnano.5b05718.
[194] 'Nanodiamond-Gutta Percha Composite Biomaterials for Root Canal Therapy (NDGX)', *ClinicalTrials.gov*. https://clinicaltrials.gov/ct2/show/NCT03376984 (accessed Mar. 18, 2020).
[195] D.-K. Lee *et al.*, 'Clinical validation of a nanodiamond-embedded thermoplastic biomaterial', *Proc. Natl. Acad. Sci.*, vol. 114, no. 45, pp. E9445–E9454, Nov. 2017, doi: 10.1073/pnas.1711924114.
[196] M. I. Setyawati, V. N. Mochalin, and D. T. Leong, 'Tuning Endothelial Permeability with Functionalized Nanodiamonds', *ACS Nano*, vol. 10, no. 1, pp. 1170–1181, Jan. 2016, doi: 10.1021/acsnano.5b06487.
[197] B. J. M. Etzold, I. Neitzel, M. Kett, F. Strobl, V. N. Mochalin, and Y. Gogotsi, 'Layer-by-Layer Oxidation for Decreasing the Size of Detonation Nanodiamond', *Chem. Mater.*, vol. 26, no. 11, pp. 3479–3484, Jun. 2014, doi: 10.1021/cm500937r.

[198] C. Corbo, R. Molinaro, A. Parodi, N. E. Toledano Furman, F. Salvatore, and E. Tasciotti, 'The impact of nanoparticle protein corona on cytotoxicity, immunotoxicity and target drug delivery', *Nanomed.*, vol. 11, no. 1, pp. 81–100, Jan. 2016, doi: 10.2217/nnm.15.188.
[199] D. Howell, C. J. O'Neill, K. J. Grant, W. L. Griffin, N. J. Pearson, and S. Y. O'Reilly, 'μ-FTIR mapping: Distribution of impurities in different types of diamond growth', *Diam. Relat. Mater.*, vol. 29, pp. 29–36, Sep. 2012, doi: 10.1016/j.diamond.2012.06.003.
[200] V. Yu. Dolmatov, I. I. Kulakova, V. Myllymäki, A. Vehanen, A. N. Panova, and A. A. Voznyakovskii, 'IR spectra of detonation nanodiamonds modified during the synthesis', *J. Superhard Mater.*, vol. 36, no. 5, pp. 344–357, Sep. 2014, doi: 10.3103/S1063457614050086.
[201] L. W. Enquist and for the Editors of the Journal of Virology, 'Virology in the 21st Century', *J. Virol.*, vol. 83, no. 11, pp. 5296–5308, Jun. 2009, doi: 10.1128/JVI.00151-09.
[202] F. Wu *et al.*, 'A new coronavirus associated with human respiratory disease in China', *Nature*, vol. 579, no. 7798, pp. 265–269, Mar. 2020, doi: 10.1038/s41586-020-2008-3.
[203] S. J. Anthony *et al.*, 'A Strategy To Estimate Unknown Viral Diversity in Mammals', *mBio*, vol. 4, no. 5, pp. e00598-13-e00598-13, Sep. 2013, doi: 10.1128/mBio.00598-13.
[204] A. C. Gregory *et al.*, 'Marine DNA Viral Macro- and Microdiversity from Pole to Pole', *Cell*, vol. 177, no. 5, pp. 1109-1123.e14, May 2019, doi: 10.1016/j.cell.2019.03.040.
[205] 'Microbiology by numbers', *Nat. Rev. Microbiol.*, vol. 9, no. 9, pp. 628–628, Sep. 2011, doi: 10.1038/nrmicro2644.
[206] C. A. Suttle, 'Viruses in the sea', *Nature*, vol. 437, no. 7057, pp. 356–361, Sep. 2005, doi: 10.1038/nature04160.
[207] I. Reche, G. D'Orta, N. Mladenov, D. M. Winget, and C. A. Suttle, 'Deposition rates of viruses and bacteria above the atmospheric boundary layer', *ISME J.*, vol. 12, no. 4, pp. 1154–1162, Apr. 2018, doi: 10.1038/s41396-017-0042-4.
[208] A. G. Cobián Güemes, M. Youle, V. A. Cantú, B. Felts, J. Nulton, and F. Rohwer, 'Viruses as Winners in the Game of Life', *Annu. Rev. Virol.*, vol. 3, no. 1, pp. 197–214, Sep. 2016, doi: 10.1146/annurev-virology-100114-054952.
[209] E. Callaway, 'Revolutionary cryo-EM is taking over structural biology', *Nature*, vol. 578, no. 7794, pp. 201–201, Feb. 2020, doi: 10.1038/d41586-020-00341-9.
[210] T. Moriya *et al.*, 'High-resolution Single Particle Analysis from Electron Cryo-microscopy Images Using SPHIRE', *J. Vis. Exp.*, no. 123, p. 55448, May 2017, doi: 10.3791/55448.
[211] A. Punjani, J. L. Rubinstein, D. J. Fleet, and M. A. Brubaker, 'cryoSPARC: algorithms for rapid unsupervised cryo-EM structure determination', *Nat. Methods*, vol. 14, no. 3, pp. 290–296, Mar. 2017, doi: 10.1038/nmeth.4169.
[212] D. Kimanius, B. O. Forsberg, S. H. Scheres, and E. Lindahl, 'Accelerated cryo-EM structure determination with parallelisation using GPUs in RELION-2', *eLife*, vol. 5, p. e18722, Nov. 2016, doi: 10.7554/eLife.18722.
[213] Y. Z. Tan, A. Cheng, C. S. Potter, and B. Carragher, 'Automated data collection in single particle electron microscopy', *Microscopy*, vol. 65, no. 1, pp. 43–56, Feb. 2016, doi: 10.1093/jmicro/dfv369.

[214] M. A. Cianfrocco and A. E. Leschziner, 'Low cost, high performance processing of single particle cryo-electron microscopy data in the cloud', *eLife*, vol. 4, p. e06664, May 2015, doi: 10.7554/eLife.06664.
[215] M. Khoshouei, M. Radjainia, W. Baumeister, and R. Danev, 'Cryo-EM structure of haemoglobin at 3.2 Å determined with the Volta phase plate', *Nat. Commun.*, vol. 8, no. 1, p. 16099, Dec. 2017, doi: 10.1038/ncomms16099.
[216] T. O. Yeates, M. P. Agdanowski, and Y. Liu, 'Development of imaging scaffolds for cryo-electron microscopy', *Curr. Opin. Struct. Biol.*, vol. 60, pp. 142–149, Feb. 2020, doi: 10.1016/j.sbi.2020.01.012.
[217] A. D. Schenk, S. Cavadini, N. H. Thomä, and C. Genoud, 'Live analysis and reconstruction of single-particle cryo-electron microscopy data with CryoFLARE', Biophysics, preprint, Dec. 2019. doi: 10.1101/861740.
[218] B. L. Nannenga and T. Gonen, 'The cryo-EM method microcrystal electron diffraction (MicroED)', *Nat. Methods*, vol. 16, no. 5, pp. 369–379, May 2019, doi: 10.1038/s41592-019-0395-x.
[219] R. Bücker *et al.*, 'Serial protein crystallography in an electron microscope', *Nat. Commun.*, vol. 11, no. 1, p. 996, Dec. 2020, doi: 10.1038/s41467-020-14793-0.
[220] R. Koopmann *et al.*, 'In vivo protein crystallization opens new routes in structural biology', *Nat. Methods*, vol. 9, no. 3, pp. 259–262, Mar. 2012, doi: 10.1038/nmeth.1859.
[221] W. Liu *et al.*, 'Serial Femtosecond Crystallography of G Protein-Coupled Receptors', *Science*, vol. 342, no. 6165, pp. 1521–1524, Dec. 2013, doi: 10.1126/science.1244142.
[222] J. Tenboer *et al.*, 'Time-resolved serial crystallography captures high-resolution intermediates of photoactive yellow protein', *Science*, vol. 346, no. 6214, pp. 1242–1246, Dec. 2014, doi: 10.1126/science.1259357.
[223] P. Nogly *et al.*, 'Lipidic cubic phase serial millisecond crystallography using synchrotron radiation', *IUCrJ*, vol. 2, no. 2, pp. 168–176, Mar. 2015, doi: 10.1107/S2052252514026487.
[224] R. L. Owen *et al.*, 'Low-dose fixed-target serial synchrotron crystallography', *Acta Crystallogr. Sect. Struct. Biol.*, vol. 73, no. 4, pp. 373–378, Apr. 2017, doi: 10.1107/S2059798317002996.
[225] G. D. Calvey, A. M. Katz, C. B. Schaffer, and L. Pollack, 'Mixing injector enables time-resolved crystallography with high hit rate at X-ray free electron lasers', *Struct. Dyn.*, vol. 3, no. 5, p. 054301, Sep. 2016, doi: 10.1063/1.4961971.
[226] P. Roedig *et al.*, 'High-speed fixed-target serial virus crystallography', *Nat. Methods*, vol. 14, no. 8, pp. 805–810, Aug. 2017, doi: 10.1038/nmeth.4335.
[227] U. Weierstall *et al.*, 'Lipidic cubic phase injector facilitates membrane protein serial femtosecond crystallography', *Nat. Commun.*, vol. 5, Feb. 2014, doi: 10.1038/ncomms4309.
[228] J. Knoška *et al.*, 'Ultracompact 3D microfluidics for time-resolved structural biology', *Nat. Commun.*, vol. 11, no. 1, p. 657, Dec. 2020, doi: 10.1038/s41467-020-14434-6.
[229] Y. Gevorkov *et al.*, '*XGANDALF* – extended gradient descent algorithm for lattice finding', *Acta Crystallogr. Sect. Found. Adv.*, vol. 75, no. 5, pp. 694–704, Sep. 2019, doi: 10.1107/S2053273319010593.
[230] T. A. White *et al.*, 'Recent developments in *CrystFEL*', *J. Appl. Crystallogr.*, vol. 49, no. 2, pp. 680–689, Apr. 2016, doi: 10.1107/S1600576716004751.

[231] A. J. Morgan *et al.*, '*Ab initio* phasing of the diffraction of crystals with translational disorder', *Acta Crystallogr. Sect. Found. Adv.*, vol. 75, no. 1, pp. 25–40, Jan. 2019, doi: 10.1107/S2053273318015395.

[232] C. Gati *et al.*, 'Atomic structure of granulin determined from native nanocrystalline granulovirus using an X-ray free-electron laser', *Proc. Natl. Acad. Sci.*, vol. 114, no. 9, pp. 2247–2252, Feb. 2017, doi: 10.1073/pnas.1609243114.

[233] R. M. Lawrence *et al.*, 'Serial femtosecond X-ray diffraction of enveloped virus microcrystals', *Struct. Dyn.*, vol. 2, no. 4, p. 041720, Jul. 2015, doi: 10.1063/1.4929410.

[234] A. Meents and M. O. Wiedorn, 'Virus Structures by X-Ray Free-Electron Lasers', *Annu. Rev. Virol.*, vol. 6, no. 1, pp. 161–176, Sep. 2019, doi: 10.1146/annurev-virology-092818-015724.

[235] K. Mattsson, E. V. Johnson, A. Malmendal, S. Linse, L.-A. Hansson, and T. Cedervall, 'Brain damage and behavioural disorders in fish induced by plastic nanoparticles delivered through the food chain', *Sci. Rep.*, vol. 7, no. 1, p. 11452, Dec. 2017, doi: 10.1038/s41598-017-10813-0.

[236] E. Kelpsiene, O. Torstensson, M. T. Ekvall, L.-A. Hansson, and T. Cedervall, 'Long-term exposure to nanoplastics reduces life-time in Daphnia magna', *Sci. Rep.*, vol. 10, no. 1, p. 5979, Dec. 2020, doi: 10.1038/s41598-020-63028-1.

[237] K. Rasmussen, H. Rauscher, P. Kearns, M. González, and J. Riego Sintes, 'Developing OECD test guidelines for regulatory testing of nanomaterials to ensure mutual acceptance of test data', *Regul. Toxicol. Pharmacol.*, vol. 104, pp. 74–83, Jun. 2019, doi: 10.1016/j.yrtph.2019.02.008.

Acta Universitatis Upsaliensis

Digital Comprehensive Summaries of Uppsala Dissertations from the Faculty of Science and Technology 1929

Editor: The Dean of the Faculty of Science and Technology

A doctoral dissertation from the Faculty of Science and Technology, Uppsala University, is usually a summary of a number of papers. A few copies of the complete dissertation are kept at major Swedish research libraries, while the summary alone is distributed internationally through the series Digital Comprehensive Summaries of Uppsala Dissertations from the Faculty of Science and Technology. (Prior to January, 2005, the series was published under the title "Comprehensive Summaries of Uppsala Dissertations from the Faculty of Science and Technology".)

Distribution: publications.uu.se
urn:nbn:se:uu:diva-406705

ACTA
UNIVERSITATIS
UPSALIENSIS
UPPSALA
2020